National Library of Canada
Bibliothèque nationale du Canada

Canadian Theses Service
Service des thèses canadiennes

Ottawa, Canada
K1A 0N4

NOTICE

The quality of this microform is heavily dependent upon the quality of the original thesis submitted for microfilming. Every effort has been made to ensure the highest quality of reproduction possible.

If pages are missing, contact the university which granted the degree.

Some pages may have indistinct print especially if the original pages were typed with a poor typewriter ribbon or if the university sent us an inferior photocopy.

Previously copyrighted materials (journal articles, published tests, etc.) are not filmed.

Reproduction in full or in part of this microform is governed by the Canadian Copyright Act, R.S.C. 1970, c. C-30.

AVIS

La qualité de cette microforme dépend grandement de la qualité de la thèse soumise au microfilmage. Nous avons tout fait pour assurer une qualité supérieure de reproduction.

S'il manque des pages, veuillez communiquer avec l'université qui a conféré le grade.

La qualité d'impression de certaines pages peut laisser à désirer, surtout si les pages originales ont été dactylographiées à l'aide d'un ruban usé ou si l'université nous a fait parvenir une photocopie de qualité inférieure.

Les documents qui font déjà l'objet d'un droit d'auteur (articles de revue, tests publiés, etc.) ne sont pas microfilmés.

La reproduction, même partielle, de cette microforme est soumise à la Loi canadienne sur le droit d'auteur, SRC 1970, c. C-30.

NL-339 (r. 88/04)

Canada

THE UNIVERSITY OF ALBERTA

A DIAGNOSTIC MODEL FOR MIXING HEIGHTS APPLICABLE TO NOCTURNAL RADIATION INVERSIONS

by

PANAGIOTIS KLIVOKIOTIS

A THESIS

SUBMITTED TO THE FACULTY OF GRADUATE STUDIES AND RESEARCH

IN PARTIAL FULFILMENT OF THE REQUIREMENTS FOR THE DEGREE

OF MASTER OF SCIENCE

IN

METEOROLOGY

DEPARTMENT OF GEOGRAPHY

EDMONTON, ALBERTA

FALL, 1988

Permission has been granted to the National Library of Canada to microfilm this thesis and to lend or sell copies of the film.

The author (copyright owner) has reserved other publication rights, and neither the thesis nor extensive extracts from it may be printed or otherwise reproduced without his/her written permission.

L'autorisation a été accordée à la Bibliothèque nationale du Canada de microfilmer cette thèse et de prêter ou de vendre des exemplaires du film.

L'auteur (titulaire du droit d'auteur) se réserve les autres droits de publication; ni la thèse ni de longs extraits de celle-ci ne doivent être imprimés ou autrement reproduits sans son autorisation écrite.

ISBN 0-315-45673-6

THE UNIVERSITY OF ALBERTA

RELEASE FORM

NAME OF AUTHOR PANAGIOTIS KLIVOKIOTIS

TITLE OF THESIS A DIAGNOSTIC MODEL FOR MIXING HEIGHTS APPLICABLE TO NOCTURNAL RADIATION INVERSIONS

DEGREE FOR WHICH THESIS WAS PRESENTED MASTER OF SCIENCE

YEAR THIS DEGREE GRANTED FALL, 1988

Permission is hereby granted to THE UNIVERSITY OF ALBERTA LIBRARY to reproduce single copies of this thesis and to lend or sell such copies for private, scholarly or scientific research purposes only.

The author reserves other publication rights, and neither the thesis nor extensive extracts from it may be printed or otherwise reproduced without the author's written permission.

(SIGNED) Klivokiotis

PERMANENT ADDRESS:

Agon Didaskalou 32

Alimos, Athens, Greece

DATED August 16, 1988

THE UNIVERSITY OF ALBERTA

FACULTY OF GRADUATE STUDIES AND RESEARCH

The undersigned certify that they have read, and recommend to the Faculty of Graduate Studies and Research, for acceptance, a thesis entitled A DIAGNOSTIC MODEL FOR MIXING HEIGHTS APPLICABLE TO NOCTURNAL RADIATION INVERSIONS submitted by PANAGIOTIS KLIVOKIOTIS in partial fulfilment of the requirements for the degree of MASTER OF SCIENCE in METEOROLOGY.

.....

Supervisor

.....

.....

Date.....

To

Christine and Nicholas,

"ΤΗΝ ΕΤΔΑΙΜΟΝΙΑΝ ΟΤΚ ΕΝ ΤΩ
ΠΟΛΛΑ ΚΕΚΤΗΣΘΑΙ ΓΙΓΝΕΣΘΑΙ,
ΑΛΛ' ΕΝ ΤΩ ΤΗ ΨΤΧΗ ΕΤ ΔΙΑ-
ΚΕΙΣΘΑΙ."

Aristotle

for they stood by me in hunger and diet till this work to be completed. Yet they proved that happiness may exist even where money do not.

Acknowledgments

The author would like to express his sincere appreciation to Dr. K.D. Hage for the supervision and the positive guidance in the many areas needed in this work. The author would like as well to express his deep respects to Dr. E.R. Reinelt for his encouragement and most of all for the financial support needed during the course of this work. The Institute of Earth and Planetary Physics, the University of Alberta and the Atmospheric Environment Service (Scientific Department) covered partly, by providing part-time employment, the overall financing.

Many thanks are due to the Air Pollution Control Division, Alberta Environment and specifically to Mr. R. Angle for permission to use facilities and equipment for the experimental work. The author owes special thanks to Mr. Joe Godin,technician of Alberta Environment, whose experience and good will helped to complete the experiment on schedule.

Last but not least the author thanks Dr. R.B. Charlton, Division of Meteorology, University of Alberta and Dr. D.J. Wilson, Mechanical Engineering, University of Alberta for review, corrections and challenging arguments as members of the examining committee.

Abstract

Two diagnostic models are used to estimate the time changes of mixed layer height on clear mornings after sunrise. Both begin with the nocturnal inversion temperature profile predicted by Brunt's radiational cooling with remodifications by Anfossi and others. The first model is a simple practical one which assumes a dry adiabatic mixed layer. The second model utilizes Deardorff's steady-state entrainment by convection for the temperature profile in the upper portion of the mixed layer. Both models require estimates of the morning minimum temperature, the maximum temperature of the previous day, the time span between these two temperatures, the height of the top of the nocturnal inversion at the time of minimum temperature, and the surface temperature at times for which the mixing heights are calculated.

The second model also requires an estimate of the ratio of the vertical temperature gradient within the nocturnal inversion at the top of the mixed layer to the vertical temperature gradient within the upper portion of the mixed layer. The models are tested using minisonde temperature profile and supplementary observations on seven mornings. Some difficulties were encountered in the identification of both the entrainment layer and the mixed layer using minisonde data. The models fail in the presence of strong thermal advection but may be useful on mornings with clear skies and light winds. The best results are found for low

mixing heights within the first few hours following the time of minimum temperature.

Table of Contents

Chapter — Page

1. INTRODUCTION 1

1.1 Diurnal development of the boundary layer 1

1.2 Convective boundary layer 5

1.3 Height of the mixed layer 7

1.4 Methods of measuring mixing heights 14

1.5 Radiational contribution in determining the height of the mixed layer 17

1.6 General approach 19

2. THEORETICAL ANALYSIS AND MODELS 21

2.1 Background 21

2.2 Brunt's simplified radiation model 24

2.3 Theory of the entrainment model 42

2.3.1 The turbulent kinetic energy and the thermodynamic energy equations 42

2.3.2 The mixed layer model 52

3. Experiment 69

3.1 Introduction 69

3.2 Topography of the area 69

3.3 Climatology of Edmonton 72

3.4 Scheduling of observations. Experimental program. 74

3.5 Observation periods 77

3.5.1 First general observation period 77

3.5.1.1 Summary of synoptic conditions 77

3.5.1.2 Relevant data 77

3.5.2 Second general observation period 82

3.5.2.1 Summary of synoptic conditions. ...82

3.5.2.2 Relevant data 84

3.5.3 Third general observation period 87

3.5.3.1 Summary of synoptic coditions. 87

3.5.3.2 Relevant data 89

3.5.4 Fourth general observation period 93

3.5.4.1 Summary of synoptic conditions. ...93

3.5.4.2 Relevant data 93

4. Mixing Height models 97

4.1 Introduction 97

4.2 Basic assumptions 98

4.3 No capping inversion-encroachment 99

4.4 General structure entrainment model: Steady state case 103

4.5 Input data and results 106

4.6 Estimation of the nocturnal inversion height and RMSE of the models. 128

5. Summary, Conclusions and Recommendations 135

Bibliography 142

Appendix I 147

Appendix II 148

List of Tables

Table		Page
2.1	Rate of change of the irradiance with respect to the temperature as a function of the temperature T	28
3.1	Instruments and priority of measured quantities	75
3.2	Summary of measurements and data	78
3.3	Wind measurements at 10m	80
3.4	Minisonde temperature data based on an assumed rate of ascent of 3m/s	80
3.5	Temperature, pressure and humidity at the surface at the onset of the minisonde releases	82
3.6	Wind data at 10m height	84
3.7	Minisonde data based on an assumed rate of ascent 3m/s	86
3.8	Surface temperature, relative humidity and pressure during the minisonde releases	87
3.9	Wind measurements at 10m	89
3.10	Temperature, pressure and humidity at the surface on the onset of the minisonde releases	89
3.11	Minisonde temperature data based on an assumed rate of ascent of 3m/s	91
3.12	Wind measurements at 10m	95
3.13	Temperature, humidity and pressure at the surface during the onset of the minisonde releases.	95
3.14	Minisonde temperature data based on an assumed rate of ascent 3m/s	96
4.1	Input data to estimate the mixing heights	118
4.2	Estimation of the nocturnal inversion height	130
4.3	Estimation of the RMSE for the Encroachment model	132

Table Page

4.4 Estimation of the RMSE for the GSE-s.s. model 132

4.5 Average observed mixing heights estimated by the indicated methods 133

List of Figures

Figure		Page
1.1	An idealized depiction of a mature mixed layer developed by convection	4
1.2	A schematic representation of the mean profiles of potential temperature, wind speed and specific humidity in the convective PBL (The Planetary Boundary Layer, WMO Techn. No 165)	6
1.3	A nomogram for estimating the height of the mixed layer assuming no marked advective effects and no basic changes in weather conditions. (Atmospheric Diffusion, Pasquill, 1984)	9
1.4	An artistic depiction of the convective PBL. Near the surface are convective plumes. At the top, the capping inversion layer is entrained by the large eddies. (WMO, Tech. Note 165)	10
1.5	Representation of the effects which control the entrainment process in a convectively developed PBL under a capping nonturbulent stable layer. (Advances in Geophysics v.18A, Carson & Smith)	12
2.1	Radiative processes in a plane parallel atmosphere for Brunt's model.	25
2.2	A schematic description of the model used by Brunt to derive the equation of radiative transfer of heat	28
2.3	Distribution of potential temperature and turbulent heat flux according to (a) Ball, (b)Lilly and (c)Betts and Carson	53
2.4	Distribution of potential temperature and turbulent heat flux according to Betts(1974)	54
2.5	Distribution of potential temperature and turbulent heat flux according to Deardorff (1979).	55
3.1	Array of surface and air sampling equipments at the field site.	70

Figure Page

3.2 Topographical and physical features and location of climatological stations in the Edmonton area. The area where the experiment was executed is depicted by the letter S, Olsen(1985). 71

3.3 A more detailed description of the area where the experiment was executed. S is the location of the station. 73

3.4 Autumn winds (From "The climate of Edmonton" Olsen (1985)) 74

3.5 Autumn Temperatures (From "The climate of Edmonton"; Olsen (1985)) 76

3.6 Synoptic surface conditions on October 2, 1987 at 1200Z. 79

3.7 Radiosonde of Stony Plain (WSE) on October 2, 1987 at 1200Z (temperature history T_H is valid at 0000Z) 81

3.8 Synoptic surface conditions on October 3, 1987 valid at 1200Z 83

3.9 Radiosonde of Stony Plain (WSE) on October 3, 1987 valid at 1200Z (temperature history T_H is valid at 0000Z) 85

3.10 Synoptic surface conditions over Alberta on October 6, 1987 valid at 1200Z 88

3.11 Radiosonde of Stony Plain (WSE) on October 6, 1987 valid at 1200Z (Temperature history T_H valid at 0000Z) 90

3.12 Synoptic surface conditions over Alberta on October 12, 1987 valid at 1200Z 92

3.13 Radiosonde of Stony Plain (WSE) on October 12, 1987 valid at 1200Z 94

4.1 Two ideal temperature profiles before and after sunrise. 97

4.2 Ideal temperature profile with no capping inversion. 99

4.3 Potential temperature and heat flux vs. height for the General Structure Entrainment model. 103

Figure Page

4.4 Temperature profiles at indicated times on November 22, 1974 at rural area, Edmonton, Alberta 107

4.5 Temperature profiles at indicated times on November 23, 1974 at rural area, Edmonton, Alberta 108

4.6 Temperature profiles at indicated times on November 27, 1974 at rural area, Edmonton, Alberta 109

4.7 Temperature profiles at indicated times on October 2, 1987 at Ellerslie, Edmonton, Alberta 110

4.8 Temperature profiles at indicated times on October 2, 1987 at Ellerslie, Edmonton, Alberta 111

4.9 Temperature profiles at indicated times on October 3, 1987 at Ellerslie, Edmonton, Alberta 112

4.10 Temperature profiles at indicated times on October 3, 1987 at Ellerslie, Edmonton, Alberta 113

4.11 Temperature profiles at indicated times on October 6, 1987 at Ellerslie, Edmonton, Alberta 114

4.12 Temperature profiles at indicated times on October 6, 1987 at Ellerslie, Edmonton, Alberta 115

4.13 Temperature profiles at indicated times on October 12, 1987 at Ellerslie, Edmonton, Alberta 116

4.14 Temperature profiles at indicated times on October 12, 1987 at Ellerslie, Edmonton, Alberta 117

4.15 Observed vs. calculated mixing heights with the encroachment model valid for November 22, 1974 119

4.16 Observed vs. calculated mixing heights with the encroachment model valid for November 23,1974 120

Figure Page

4.17 Observed vs. calculated mixing heights with the encroachment model valid for November 27,1974 120

4.18 Observed vs. calculated mixing heights with the encroachment model valid for October 2,1987 121

4.19 Observed vs. calculated mixing heights with the encroachment model valid for October 3,1987 122

4.20 Observed vs. calculated mixing heights with the encroachment model valid for October 6,1987 122

4.21 Observed vs. calculated mixing heights with the encroachment model valid for October 12,1987 123

4.22 Observed vs. calculated mixing heights with the G.S.E.-s.s. model valid for November 22,1974 124

4.23 Observed vs. calculated mixing heights with the G.S.E.-s.s. model valid for November 23,1974 124

4.24 Observed vs. calculated mixing heights with the G.S.E.-s.s. model valid for November 27,1974 125

4.25 Observed vs. calculated mixing heights with the G.S.E.-s.s. model valid for October 2,1987 126

4.26 Observed vs. calculated mixing heights with the G.S.E.-s.s. model valid for October 3,1987 126

4.27 Observed vs. calculated mixing heights with the G.S.E.-s.s. model valid for October 6,1987 127

4.28 Observed vs. calculated mixing heights with the G.S.E.-s.s. model valid for October 12,1987 128

4.29 Observed vs. estimated inversion height with K_n=0.34m^3/sec 129

Figure Page

4.30 Relation between estimated inversion heights with the methods (b) K_R=0.11m²/sec and (c) 130

1. INTRODUCTION

1.1 Diurnal development of the boundary layer

It is widely known to meteorologists that under favorable weather conditions, a temperature inversion is formed within the first two kilometers, above ground level. Such inversions limit the transport of the kinetic and thermodynamic energy in the vertical direction. Conduction, radiation and convection are the main processes to play decisive roles in the creation and destruction of this temperature inversion. Many special experiments as well as observations of the soundings at many meteorological upper air stations verify that this inversion starts at the surface of the earth and with the onset of the solar heatingits base is elevated to higher altitudes with time.
The diurnal changes of solar and terrestrial radiation set up a cycle of cooling and heating of the planetary boundary layer which is strongly related with the wind field.

In my view an excellent description of the diurnal events that take place with respect to the development and destruction of the temperature inversion can be found in Aerodynamic Characteristics of the Atmospheric Boundary Layer (Plate,1971) and quoted herein:

1. "Before sunrise, the stratification of the air layer is stable because the ground is cooler than the air mass above".
2. "With the rising of the sun, on a clear day, solar

radiation heats up the ground much faster than the overlying air. Heat moves from the ground to the air layer in contact with the ground. The warm air expands and becomes lighter than the air above it. Parcels of heated air tend to move up into the cooler air above, while cooler air moves down, i.e. the air layer is unstable. Since there is no instantaneous mixing with the warmer parcels moving at the new level, the heating of the air lags behind the heating of the ground and the layer cannot acquire the same, constant potential temperature, as that at the ground. Because the air velocity, directly at the ground, is zero, the transfer of heat from the ground takes place by molecular conduction and a very strong vertical temperature gradient develops.

The molecular conduction layer is very thin. This layer changes with height into the forced-convection layer in which heat is transported by turbulence that is almost entirely caused by mechanical action, i.e. wind shear.

At large distances from the ground, the gradients in temperature and velocity decrease. The temperature distribution remains superadiabatic. But with increasing height less turbulence is maintained by wind shear and an increasing amount of turbulence is buoyancy induced. The forced-convection layer changes gradually into a free-convection layer. Out of the superadiabatic layer, turbulent parcels of warmer air rise into colder regions aloft and mix with the surroundings in the free-convection layer, which is vigorously agitated because the warmer

thermal plumes or thermals have significant vertical uplift velocities and the mass transport associated with them creates a downward motion of colder, but also, turbulent air. The result is a mixing of the air which is so strong that in the free-convection layer, the potential temperature is almost constant."

3. "In the course of the day, the ground gets warmer, the air above heats up, and the convective layer increases in thickness at a rate that is determined by the heat flux from the ground, which in turn depends on the temperature gradient across the superadiabatic layer.
In the afternoon, an instant of quasi-equilibrium is reached and the ground is at nearly the same temperature as the layer above it (superadiabatic and convective). The conductive heat flux ceases to exist when the vertical temperature gradient vanishes and in the absence of fluxes, all temperature fluctuations must die out, so that the neutral stratified boundary layer is asymptotically free of fluctuating temperature everywhere."

4. "Later in the afternoon the temperature of the air exceeds that of the ground.The mixing layer loses heat and gradually cools. The height at which the upper inversion occurs, i.e. the mixing height, is lowered while a ground based inversion builds up, particularly after sunset.
If the conditions for cooling of the surface persist long enough, then eventually the upper and lower inversions merge and the constant potential temperature layer between them

disappears. Further cooling increases the vertical temperature gradient until the next morning, when the cycle starts again."

The convective layer is capped by an inversion, i.e. by the stably stratified air aloft, which begins near the elevation where the undisturbed stable potential temperature is equal to the mean potential temperature of the convective layer (see Fig. 1.1). This is valid during the encroachment stage whereas usually an entrainment layer is developed with a lapse rate in between those of the convective layer and the stable layer aloft.

Short and long wave radiation contribute to the cycle in a major way. In the mixing layer, gases important for their contribution to the net radiation heat fluxes are water vapor and carbon dioxide. Water vapor, however, is the major contributor because it is a strong absorber and emitter of infrared radiation.

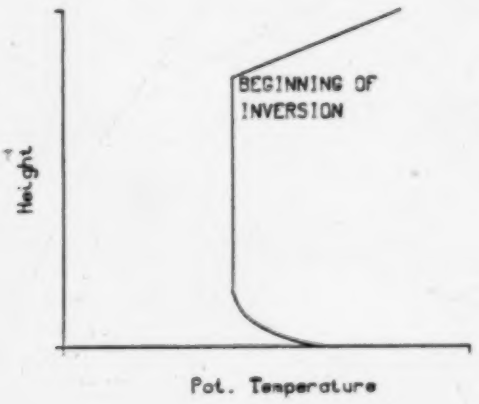

Fig. 1.1 An idealized depiction of a mature mixed layer developed by convection

1.2 Convective boundary layer

The convective boundary layer is regarded as the layer in which turbulence is enhanced by buoyancy production through most of its depth. The structure of the convective boundary layer differs from land to sea mainly near the surface where roughness and conduction differ. We shall constrain ourselves to the case of a convective boundary layer over land. In this case, depending on the parameters considered relevant to the turbulence, the convective boundary layer may be separated into four main layers:

I)The surface layer, where wind shear plays a dominant role.

II) The free-convection layer, where the surface stress $\tau_0=\rho u_*^2$ no longer plays an important role. The energy budget becomes:

$$\frac{\partial}{\partial z}(\overline{wq})=\frac{g}{\Theta}(\overline{w\theta}) \qquad q=\frac{1}{2}(\overline{u^2+v^2+w^2})$$

where (u,v,w) are the wind component fluctuations, Θ is the average potential temperature and θ is the potential temperature fluctuation.

III) The mixed layer, where the structure of turbulence is insensitive to the height z as well as to the surface stress τ_0. The boundary layer depth h emerges as the controlling length scale. Within this region, an approximate energy budget for the turbulence above the surface layer is:

$$\frac{g}{\Theta}(\overline{w\theta})\simeq\epsilon \qquad \epsilon\text{:dissipation}$$

(Tennekes and Lumley, 1972)

The scaling velocity and temperature are given by:

$w_* = [h\frac{g}{\theta}(\overline{w\theta})]^{\frac{1}{3}}$ and $T_* = \frac{1}{w_*}(\overline{w\theta})$ (Nieuwstadt and van Dop, 1982).

IV) The entrainment interfacial layer which varies between 0.8h and 1.2h, whereas the free-convection layer is limited to 0.1h. The turbulence structure in this layer may be dominated by entrainment effects, the characteristics of the capping inversion and the stable atmosphere aloft. This description applies best over land for $\frac{h}{|L|} \simeq 50\text{-}100$ and over a marine surface for $\frac{h}{|L|} \simeq 10$, indicating the fact that surface-induced mechanical turbulence cannot be neglected at higher levels. Here |L| is the Obhukov length.

The structure of turbulence in the mixed layer and entrainment layer are of concern to us in determining the height of the mixed layer. Fig. 1.2 depicts the characteristic regions of the convective boundary layer.

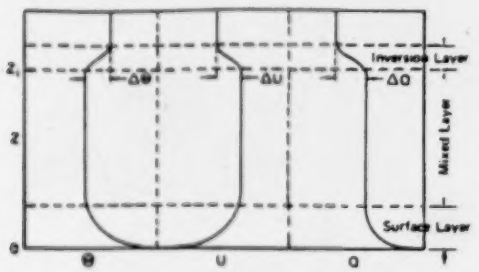

Fig. 1.2 A schematic representation of the mean profiles of potential temperature, wind speed and specific humidity in the convective PBL (The Planetary Boundary Layer, WMO Techn. No 165)

1.3 Height of the mixed layer

As our society becomes more technologically advanced, more detailed descriptions of energy exchanges in nature are needed. Computer technology and atmospheric sciences have worked in parallel to provide short range weather forecasts with promises of long range weather forecasts in the future. Global circulation models must incorporate boundary layer processes in order to have any degree of accuracy in long range forecasting. An accurate estimate of the height of the mixed layer is necessary, in order to parameterize these boundary layer processes(Hanna et al.,1980).

The numerical models of mesoscale circulations assume that the mixing property of convective turbulence is important as well. In that context the mixing height is also important for parameterization.

Another important topic for which the height of the mixed layer is significant is air pollution meteorology (Plate,1982). The height of the mixed layer determines the volume of air over which the pollutants, emitted at the surface of the earth, are dispersed. For the plumes rising off the stacks, the height of the mixing layer may be important for predicting fumigation which can bring high concentrations of the effluent to the ground. Under calm conditions and with large temperature difference strength in the interfacial layer, the concentration of the effluent at the ground is increased and the effective ventilation, i.e.the ratio of the rate of the emitted pollutants to the

ground concentration, is decreased(Briggs, 1969). The height of the mixed layer has been used in a number of diffusion models for determining the maximum concentration at the ground and its distance downwind from a source(Sun and Chang, 1986). It plays an active role in the determination of the standard deviation σ_y of the concentration distribution in the horizontal crosswind direction, under unstable (daytime) stratification,

$$\frac{\sigma_y}{z_i}=f[(\frac{w_*}{U})(\frac{x}{z_i})],\ w_*=[z_i\frac{g}{\theta}(\overline{w\theta})]^{\gamma}$$

where U≡ mean velocity for the mixed layer as a whole. It also plays an active role in the determination of the vertical spread of a passive material, σ_z, and especially in the determination of the stability and its effect on σ_z (Hanna et al.,1977). In this context, the height of the mixed layer determines also the maximum plume thickness, under moderate or strong stratification.

In using the Gaussian model for a uniform vertical distribution, the mixing height z_i is inserted as

$$\chi(x,y)=(2\pi)^{-\frac{1}{2}}\frac{Q}{\sigma_y z_i u}\exp(-\frac{y^2}{2\sigma_y^2})$$

where u is the average horizontal wind through the depth z_i of the convective layer.

Depending on the cloud cover, the time of the day and the wind speed a nomogram can be developed, showing the mixing

height as in Fig. 1.3 (Pasquill, 1984).

Other applications may include the role of the height of the mixed layer in explaining the daytime urban thermal anomaly since an increased inversion-level entrainment occurs over urban areas (Hildebrand and Ackerman, 1984).

Another application is the calculation of the refractive index for estimating the ability of the boundary layer to attenuate the electromagnetic waves passing through it.

Besides the day-to-day requirements of determining the height of the mixed layer, long-term planning for industrialization may have to take into consideration the air pollution potential of an area selected for development. Estimates of mixing heights, wind speeds and ventilation

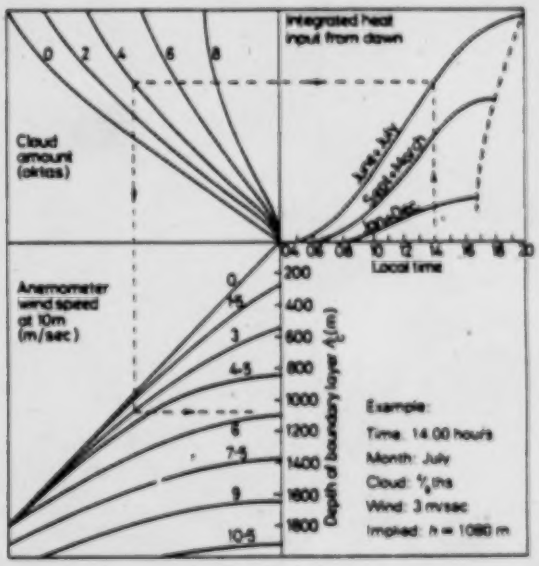

Fig. 1.3 A nomogram for estimating the height of the mixed layer assuming no marked advective effects and no basic changes in weather conditions. (Atmospheric Diffusion, Pasquill, 1984)

coefficients should be provided. In that respect climatological values have been calculated for most of North America (Portelli, 1977). Fig. 1.4 shows an artist's conception of the convective boundary layer. A more articulated description of the mixing of stable warmer air with cooler convective air is depicted in Fig. 1.5 . In practice the height of the same mixed layer determined by different methods is different. R. Dobbins defines the mixing height as " the height in meters to which relatively vigorous mixing occurs "(Dobbins, 1979).
According to G.Holzworth (Holzworth 1967,1971,1972) the morning mixing depth is intended to be " an estimate of the height of the mixed layer at the hour of peak morning

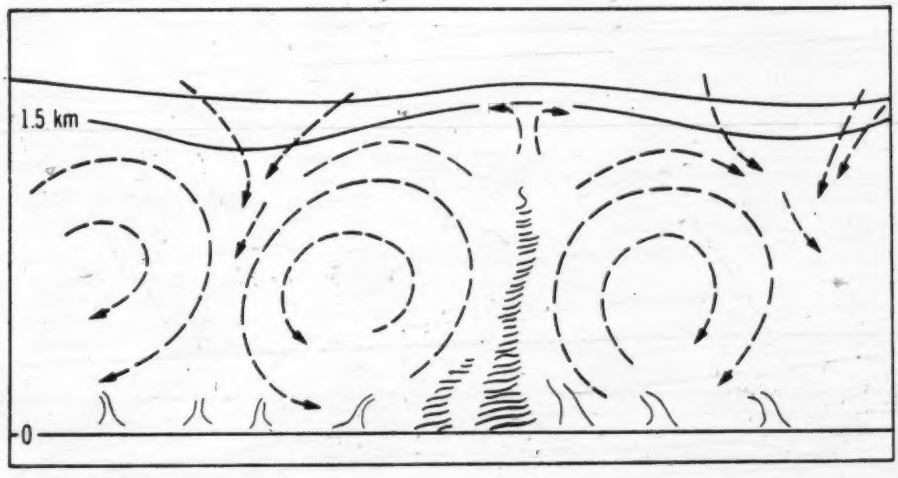

Fig. 1.4 An artistic depiction of the convective PBL. Near the surface are convective plumes. At the top, the capping inversion layer is entrained by the large eddies. (WMO, Tech. Note 165)

traffic activity " and it is calculated with the knowledge of the minimum surface temperature T_{min} observed between 0200 and 0600 local standard time and the profile of the temperature versus altitude from the 1200GMT sounding. The intersection of the sounding with an adiabatic temperature profile drawn from a surface temperature which is 5°C greater than T_{min} defines the morning mixing height.

The afternoon mixing height is defined by Holzworth as " the altitude at which the profile T(z) determined by the 1200GMT sounding is intersected by an adiabatic profile drawn from the maximum air temperature observed near the ground between 1200 and 1600 local standard time".

However,R.Aron(1983) criticizing this method states in his paper:"The standard calculation (that is the Holzworth's method) of mixing height may not give an accurate estimation of the height to which pollutants actually disperse. Many meteorological variables have a higher correlation to air pollution concentrations than mixing height. Therefore, if mixing height is to be used to estimate potential air pollution concentrations in a given area, significant correlation with pollution levels for the area and the period being considered must be shown."

Definitions vary within a wide range, from qualitative to specific quantitative, practical and simple measures.

Another contributor to the uncertainty of the height of the mixed layer is the instrument or procedure used for measuring it, since each instrument uses a different

physical principle to define the mixing height (or depth) :

1. On a thermodynamic diagram, the mixing height is defined where the potential temperature starts to increase with height.
2. The mixing height is defined by lidar as the level at which there is a sudden decrease in the suspended particulate concentration.
3. The sodar trace will show a variety of echo regions with the mixing height corresponding to the bottom of the echo region during the daytime and under clear conditions.

In general,estimates of the daytime mixing height show a greater accuracy than those of the nighttime mixing height.

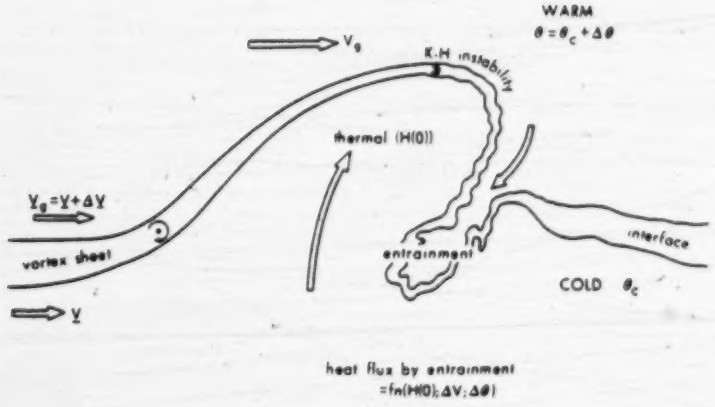

Fig. 1.5 Representation of the effects which control the entrainment process in a convectively developed PBL under a capping nonturbulent stable layer. (Advances in Geophysics v.18A, Carson & Smith)

Hanna's statistics, however, indicate that the majority of the daytime mixing height observations and predictions are within 40% of each other (Hanna, 1980).

The approach for defining the height of the mixed layer or the mixing height becomes complicated during the nighttime period: "It has been defined by various authors as the height at which turbulence decreases to zero, the height of the nocturnal low-level jet, the top of the surface-based inversion and the height where the local Richardson number first exceeds 0.25. Of course the acoustic sounder and lidar also will indicate a mixing height which will not necessarily agree with any of the above definitions." (Hanna, 1980).

In my opinion the height of the mixed layer is clearly of theoretical interest but of debatable definition. If the height of the mixed layer is determined as the one corresponding to the layer having constant mean potential temperature (Lilly,1968;Betts,1973), which in the wide sense may include the contribution of all the relevant processes, or as the height at which the turbulent heat flux becomes zero (Businger,1972; Deardorff,1979), its practical usefulness depends on the ability to determine in an accurate fashion the mathematical expressions of the processes involved. However, the determination of the mixing height can be simply a matter of practical utility which is immediately correlated with the purpose it serves. In this case we are referring to the mixing height (or depth) and

not to the height of the mixed layer. The close relation of the traditional need to determine the height of the mixed layer and its usefulness for the study of the dispersion of pollutants, may be indicated by Hanna's statement (Hanna,1980):"Because the lidar directly measures the height to which aerosol pollutants are mixed, it may thus be considered a "true" indicator of the mixed height".

1.4 Methods of measuring mixing heights

As we pointed out earlier a variety of instruments have been used to determine the mixing height. The theoretical approach is not necessarily correlated with the appropriate instrument(s), but rather with what is available to the researcher. Remote sensing techniques are not always compatible in their results. A multi-sensor experiment involving an acoustic sounder, an FM-CW radar, a high power narrow beam radar and an instrumented aircraft, supports the view that different techniques emphasize different microstructural details of the convective boundary layer (Richter et al.,1974). Research has shown that the acoustic sounder is able to "see" any atmospheric structure having associated fine-scale turbulence producing signficant temperature and humidity fluctuations on a length scale approximately equal to that of the transmitted sound half-wavelength (Crease et al.,1977). As the turbulent heat flux decreases with height so do the temperature fluctuations up to the height at which the effect of the entrainment of air from

the stable layer becomes noticeable by increasing the temperature fluctuations again(Kaimal et al.,1976). This means that a monostatic acoustic sounder will significantly underestimate the upper limit of convection in deep boundary layers and may provide more accurate measurements under the encroachment stage of development of the convective boundary layer(Crease et al., 1977).

A number of shortcomings, however, can cause inaccurate results to the degree that acoustic or electromagnetic waves are affected by the stability of the boundary layer overnight and during convective conditions.

Excess attenuation of the beam due to broadening by turbulence or bending by the wind or anisotropy of the temperature field and variations in the significance of this with height, as the case may be with local Kelvin-Helmholtz wave breakdown (Moulsley et al.,1981), may also provide inaccurate measurements. Direct and acoustically measured values of atmospheric parameters may vary due to the different sampled volumes of air (Cole et al.,1980). Balloon-borne measurements and acoustic measurements give more compatible results after corrections are made by time-averaging statistics and avoiding spurious reflections. Such corrections are not needed for tower measurements. A less expensive method for measuring the mixing height is a direct measurement, by a tethered balloon (also called Balthum sonde) of temperature and humidity with or without wind profiles supplemented by surface measurements of

sensible heat flux. The latter can be measured by turbulence probe, or using the residual technique, or by constructing sensible heat-flux profiles by downward summation of the flux divergences over 5-mb layers (Chorley et al.,1975).

A number of models and nomograms provide estimates of the mixing height under various weather conditions. Besides Holzworth's method D.J.Carson(1973) has suggested a model determining the mixing height:

$$\frac{dz_i^2}{dt} - 2\beta z_i^2 = \frac{2[1+2A]Q_H(0,t)}{\rho c_p \gamma(t)}$$

where z_i is the mixing depth, $Q_H(0,t)$ is the surface heat flux, A is the ratio of the sensible heat fluxes at the height of the mixed layer and the surface, i.e. $Q_H(z_i,t)=-AQ_H(0,t)$, β: is a constant convergence parameter determining the vertical velocity field $w(z)=-\beta z$ and $\gamma(t)=\gamma(0)\exp(\beta t)$.

A simplified expression of the model, with $\beta=0$, is

$$\frac{dz_i^2}{dt} = \frac{2[1+2A]Q_H(0,t)}{\rho c_p \gamma}$$

and A takes values about 0.2 to 0.5 (Betts,1973).

A test of this model, with A=0 shows consistent results under conditions of steadily "warming out" of a nocturnal inversion (Chorley et al., 1975). However, the order of disagreement increases beyond limits of tolerance as the conditions become complicated (low-level inversion beneath a

higher capping inversion, cloud cover, vertical motion, advection). In addition difficulties arise with respect to the lapse rate of the stable layer as to how it is measured and over what layer, as well as from uncertainties in the value of A.

A more general approach has been taken by Pasquill(1983). He provided a nomogram for z_i valid for the United Kingdom assuming no strong advection or basic changes in weather. Inputs of month, hour, cloud cover and wind speed at 10m height are used to determine the mixing height (Fig. 1.3).

Observational methods for estimating mixing heights have also been suggested (Hanna,1982).
Other models will be analysed in the following chapter.

1.5 Radiational contribution in determining the height of the mixed layer

Solar radiation or short-wave radiation has negligible effect as a source of direct heating of the atmosphere. Long-wave radiation or terrestrial radiation, however, plays a significant role in the thermodynamic balance within the boundary layer. The diurnal cycle of the oscillation of the boundary layer may develop stable conditions with an inversion starting at the surface due to the radiational cooling of the ground. Radiational cooling occurs within the boundary layer if divergence of radiation takes place, mainly due to the absence of adequate amounts of water

vapor, the most significant constituent to absorb terrestrial radiation, which otherwise is lost into the space.

A theoretical approach to determine the heating rate

$$c_p \rho \frac{dT}{dt}$$

involves the calculation of the average transmission of the atmosphere, from individual spectral lines and bands, a method which encounters numerous difficulties for all practical purposes.Radiative charts may be used instead and some micrometeorologists have followed that avenue especially for cloud-topped convective boundary layers(Zdunkowski,1965; Deardorff,1974a). Other micrometeorologists have attempted to parameterize the radiative flux (i.e. Lacis and Hansen,1974; Yamamoto et al,1970; for references see Deardorff,1976).

A semiempirical approach was initiated by Simpson and advanced by Brunt(Sutton,1953; Brunt,1939) and Anfossi et al.(1976). Brunt showed that the radiative transfer of heat in the vertical can be modelled approximately as a simple diffusion process, conforming to the equation

$$\frac{\partial T}{\partial t} = K_R \frac{\partial^2 T}{\partial z^2}$$

where K_R is an exchange coefficient, constant for all practical purposes, called the radiative diffusivity.

Brunt following Simpson, assumed an unsaturated lower atmosphere(clear nights) with light winds and layers, containing water vapor, of thickness necessary for complete absorption of the incoming long-wave radiation. Under the

assumption that a column of air with 0.3mm precipitable water will qualify for complete absorption, Brunt determined the magnitude of K_R to be $0.16 m^2 sec^{-1}$.

Anfossi et al.(1976) provided more realistic profiles of T(z,t) by modifying Brunt's equation in two main ways:

1. By considering the lower portion of the atmosphere as a slab instead of an semi-infinite medium.
2. By replacing the thermal diffusivity of the soil with the radiative coefficient, a characteristic parameter of the air. In this case, the thrmal diffusivity of the soil does not affect directly the temperature profile but only the radiative coefficient.

In taking into consideration Anfossi's boundary conditions we may incorporate this radiative transfer of heat in the thermodynamic equation as we attempt to evaluate the height of the mixed layer.

1.6 General approach

The usual approach to determine the height of the mixed layer of the convective boundary layer neglects the radiational term under clear conditions and light winds. However the radiative heat transfer may cause the vertical turbulent heat flux to vary, may influence the mean temperature profile and the resulting stability, and may reduce the magnitude of local and temporal buoyancy forces, through attenuation of the turbulent temperature fluctuations(Brutseart, 1972).

Our objective is to employ convective boundary layer models like those of Lilly's (1968), Betts(1973) and Deardorff's (1979) in an attempt to derive a simple equation for the height of the mixed layer assuming that a surface-based inversion has occured overnight and that its profile follows Anfossi's temperature profile equation. Since all the convective models assume the lapse rate of the free atmosphere constant Anfossi's equation not only will provide this lapse rate but it will be considered also as a boundary condition for the temperature profile within the convective boundary layer.

2. THEORETICAL ANALYSIS AND MODELS

2.1 Background

The traditional treatment of heat transfer based on the continuum point of view, defines three distinct mechanisms, i.e. conduction, convection and radiation.
The classical theory of the conduction of heat has been described by Fourier for an isotropic solid as:

$$q=-k\nabla T$$

T is the temperature, q is the heat flux (heat per unit time and unit area)in [Joule $sec^{-1}m^{-2}$], and k is the thermal conductivity in [Joule sec^{-3} deg^{-2} m^{-1}] (Sutton, 1953). The rise in temperature that this heat will produce, will vary with the specific heat c and the density ρ. The constant $\kappa=\frac{k}{c\rho}$ has been termed the thermal diffusivity by Kelvin or the thermometric conductivity by Maxwell.
Fourier's law of heat conductivity is:

$$\frac{\partial T}{\partial t}=\kappa\nabla^2 T$$

$$\text{where } \nabla^2 T=\frac{\partial^2 T}{\partial x^2}+\frac{\partial^2 T}{\partial y^2}+\frac{\partial^2 T}{\partial z^2}$$

and κ is the thermal diffusivity in [m^2sec^{-1}]
In the general case where k varies from point to point, the corresponding equation becomes:

$$\frac{\partial T}{\partial t}=\frac{1}{c\rho}\left[\frac{\partial}{\partial x}\left(k\frac{\partial T}{\partial x}\right)+\frac{\partial}{\partial y}\left(k\frac{\partial T}{\partial y}\right)+\frac{\partial}{\partial z}\left(k\frac{\partial T}{\partial z}\right)\right]$$

(Ingersoll, 1948)

Assuming horizontal homogeneity (k:constant) for air at 0°C and 1Atm:

$$\frac{\partial T}{\partial t}=\frac{0.055\ 10^{-3}\text{cal sec}^{-1}\text{ cm}^{-1}\text{ deg}^{-1}}{0.24\text{cal gr}^{-1}\text{ deg}^{-1}\,0.00129\text{ gr cm}^{-3}}\left(\frac{\partial^2 T}{\partial z^2}\right)$$

$$=0.178\ 10^{-4}\text{m}^2\text{sec}^{-1}\ \frac{\partial^2 T}{\partial z^2}$$

Still air is a very good thermal insulator with a thermal diffusivity of the order of $10^{-5}\text{m}^2/\text{sec}$.

In the case of fluids, the corresponding equation for heat conduction is:

$$c_p\rho\frac{dT}{dt}-A\frac{dp}{dt}=k\left(\frac{\partial^2 T}{\partial x^2}+\frac{\partial^2 T}{\partial y^2}+\frac{\partial^2 T}{\partial z^2}\right)+A\Phi$$

where c_p is the specific heat at constant pressure, A is the reciprocal of the mechanical equivalent of heat and Φ is the dissipation function,

$$\Phi=\mu\left[-\frac{2}{3}\left(\frac{\partial u}{\partial x}+\frac{\partial v}{\partial y}+\frac{\partial w}{\partial z}\right)^2+2\left(\frac{\partial u}{\partial x}\right)^2+2\left(\frac{\partial v}{\partial y}\right)^2+2\left(\frac{\partial w}{\partial z}\right)^2+\left(\frac{\partial w}{\partial y}+\frac{\partial v}{\partial z}\right)^2+\left(\frac{\partial w}{\partial x}+\frac{\partial u}{\partial z}\right)^2+\left(\frac{\partial u}{\partial y}+\frac{\partial v}{\partial x}\right)^2\right]$$

In micrometeorology we may neglect the pressure change in many applications. If we neglect dissipation the conduction equation is:

$$\frac{dT}{dt}=\kappa\nabla^2T \qquad \text{(Sutton, 1953)}$$

The problem of thermal diffusion was approached by Taylor who derived a similar equation:

$$\frac{dT}{dt}=-\frac{\partial}{\partial x}(K_{H_x}\frac{\partial T}{\partial x})+\frac{\partial}{\partial y}(K_{H_y}\frac{\partial T}{\partial y})+\frac{\partial}{\partial z}(K_{H_z}\frac{\partial T}{\partial z})$$

where K_H is the turbulent diffusion coefficient. The transfer of heat, for K_H constant for an isotropic fluid and with horizontal homogeneity of the temperature, is called Fickian diffusion and is given by:

$$\frac{dT}{dt}=K_H(\frac{\partial^2T}{\partial z^2})$$

or

$$\frac{\partial T}{\partial t}+ w(\frac{\partial T}{\partial z})=K_H(\frac{\partial^2T}{\partial z^2})$$

or

$$\frac{\partial T}{\partial t}=K_H(\frac{\partial^2T}{\partial z^2})$$

for w=0, if the air is not isothermal.

The problem of thermal radiation has been analysed by Brunt in a way that led him to derive a formula similar to the diffusion equation, namely:

$$\frac{\partial T}{\partial t}=K_R(\frac{\partial^2T}{\partial z^2})$$

where K_R: radiative diffusivity

2.2 Brunt's simplified radiation model

The most important process contributing to the temperature change of the troposphere, among at least five responsible for the depletion of the incoming solar radiation, is absorption by water vapor. Other processes like absorption by other constituents of dry air, scattering by molecules of dry air and water vapor in the troposphere are unimportant while scattering and diffuse reflection and absorption by solid and liquid particles are highly variable in time and space.

To avoid complications of the last processes, Brunt(1939) applied his model when only infrared radiation is present, namely,during nighttime under cloudless conditions. In addition calm conditions are imposed in order to eliminate temperature advection. In that respect only terrestrial radiation need be considered in the vertical, and horizontal homogeneity becomes a valid assumption.

As far as radiative effects are concerned, Brunt assumed that the water vapor in the atmosphere is the exclusive constituent of the atmosphere, and the contribution of the dry air is considered negligible.

To derive Brunt's equation of radiative transfer of heat, we consider, based on the above arguments, a plane parallel atmosphere, uniform in the horizontal (Fig. 2.1). Then we consider the absorption along the vertical coordinate z. Lambert's law states that the absorption is proportional to the mass of absorber $\rho_v dz$ in unit cross-section of a slab of

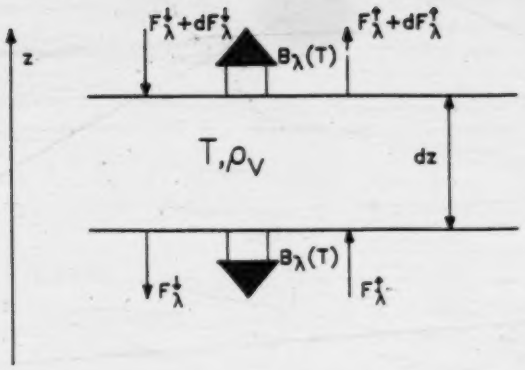

Fig. 2.1 Radiative processes in a plane parallel atmosphere for Brunt's model.

atmosphere of thickness dz (ρ_v being the density of the absorber). It is also proportional to the incident intensity of radiation:

$$dI_{\lambda}=-I_{\lambda}\eta_{\lambda}\rho_v dz$$

where η_{λ} is the absorption coefficient and I_{λ} is the intensity of radiation (radiance) in [Watts m^{-2} $sr^{-1}\mu m^{-1}$]

By integration:

$$I=I_o\exp(-_z\int^{\infty}\eta_{\lambda}\rho_v dz)$$

where $\exp(-_z\int^{\infty}\eta_{\lambda}\rho_v dz)\equiv\tau_{\lambda}$ is the fractional transmission of the path, whereas the expression $_z\int^{\infty}\rho_v dz\equiv\chi_{\lambda}$ is the optical path (or optical thickness) and $\sec\phi\,_z\int^{\infty}\eta_{\lambda}\rho_v dz=\sigma_{\lambda}$ is the optical depth for the incoming solar radiation as a source of reference. Here $\phi=0$.

The flux is

$$F=_{2\pi}\int I(\phi)\cos\phi d\omega$$

and the heating rate

$$h=-\nabla.F=-divF=c_p\rho(\frac{dT}{dt}) \qquad (2-1)$$

Assuming the net flux exists in the vertical only,

$$\frac{dF(z)}{dz}=div\ F(z)$$

and consequently

$$\frac{dF(z)}{dz}=-c_p\rho(\frac{dT}{dt})$$

Let us assume that the slab is at temperature T with corresponding black body radiance $B'_\lambda(T)$ or irradiance $B_\lambda=\pi B'_\lambda(T)$. Then $\eta_\lambda\rho_v dz$ is the absorptivity of this slab and by Kirchhoff's law the emissivity as well. For the upwelling flux:

$$dF^{\uparrow}_\lambda=\eta_\lambda\rho_v dzF^{\uparrow}_\lambda-\eta_\lambda\rho_v dz\,B_\lambda(T)$$

and for the downwelling flux :

$$dF^{\downarrow}_\lambda=-[\eta_\lambda\rho_v dzF^{\downarrow}_\lambda-\eta_\lambda\rho_v dzB_\lambda(T)]$$

Since $d\chi\equiv\rho_v dz$ we get:

$$\frac{dF^{\uparrow}_\lambda}{d\chi}=\eta_\lambda[F^{\uparrow}_\lambda-B_\lambda(T)] \qquad \text{and} \qquad \frac{dF^{\downarrow}_\lambda}{d\chi}=-\eta_\lambda[F^{\downarrow}_\lambda-B_\lambda(T)]$$

The sum of the two defines the total amount of radiation gained or lost from the slab. Therefore, the heating rate

is:

$$\frac{dF_\lambda^\uparrow}{dx}+\frac{dF_\lambda^\downarrow}{dx}=\eta_\lambda(F_\lambda^\uparrow-F_\lambda^\downarrow) \text{ or } \frac{dF}{dz}=\eta_\lambda\rho_v(F_\lambda^\uparrow-F_\lambda^\downarrow)=-\{c_p\rho\}\frac{dT}{dt}$$

As noted in the introduction, the rise of temperature that the radiative heat will produce, depends on the specific heat and density of the interactive medium and therefore $[c_p\rho]$ represents the moist air in the slab and when $\frac{dT}{dt}=0$ then $F_\lambda^\uparrow=F_\lambda^\downarrow$. The model assumes that the incoming flux is absorbed completely. This may happen if we consider a slab of thickness Δz such that the contained vapor is able to absorb the whole amount of the incident longwave radiation. In that case the layer shall transfer upwards and downwards the same amount of radiation. But Δz will not be constant, since the vapor density decreases with height and therefore the thickness should increase with height in order to contain the necessary amount of vapor for complete absorption. The net upwelling flux of radiation across AB is $\Delta E_r^{r+1}=E_r-E_{r+1}$. Similarly, across CD the net flux is $\Delta E_{r-1}^{r}=E_{r-1}-E_r$ (Fig. 2.2). Therefore the cooling or warming of the rth slab is taking place if $\Delta E_{r+1}^{r}-\Delta E_{r-1}^{r}$ is positive or negative. Since the incident terrestrial radiation is absorbed completely, the emitted E_r depends on the mean temperature of the slab $\bar{T}_r$ and

$$\Delta E_r^{r+1}=\frac{\Delta E_r^{r+1}}{\Delta T_r^{r+1}}(\bar{T}_r-\bar{T}_{r+1}) \text{ also } \Delta E_{r-1}^{r}=\frac{\Delta E_{r-1}^{r}}{\Delta T_{r-1}^{r}}(\bar{T}_{r-1}-\bar{T}_r)$$

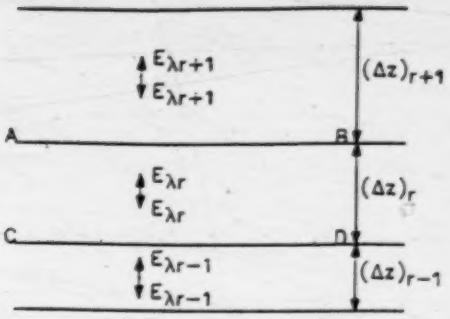

Fig. 2.2 A schematic description of the model used by Brunt to derive the equation of radiative transfer of heat

Let

$$\Delta F_r = \Delta E^r_{r-1} - \Delta E^{r+1}_r = \frac{\Delta E^r_{r-1}}{\Delta T^r_{r-1}}(\overline{T}_{r-1} - \overline{T}_r) - \frac{\Delta E^{r+1}_r}{\Delta T^{r+1}_r}(\overline{T}_r - \overline{T}_{r+1})$$

$$= \frac{\Delta E^r_{r-1}}{\Delta T^r_{r-1}}(\overline{T}_{r-1} - \overline{T}_r) - \frac{\Delta E^{r+1}_r}{\Delta T^{r+1}_r}(\overline{T}_{r+1} - \overline{T}_r) \qquad (2\text{-}2)$$

E_r is the irradiance in the opaque bands of the water vapor absorption spectrum (Sutton, 1953 p. 226).

Simpson(Brunt 1939 p. 131) derived a linear relation between $\frac{\partial E}{\partial T}$ and temperature T as $\frac{\partial E}{\partial T} = [3.0 + 0.02(T-270)]10^{-3}$ within a range of temperatures 200°-295°K:

Table 2.1 Rate of change of the irradiance w.r.t. the temperature as a function of T

T /°K	200	220	270	295
$\partial E/\partial T$ [Watts $m^{-2}deg^{-1}$]	1.12	1.40	2.09	2.44

The table indicates the slow rate of change of $\frac{\partial E}{\partial T}$ with temperature T. Therefore, from (2-2) we may get

$$\Delta F_r = -\frac{\Delta E_r^{r-1}}{\Delta T_r^{r-1}} (\bar{T}_r - \bar{T}_{r-1}) + \frac{\Delta E_{r+1}^{r}}{\Delta T_{r+1}^{r}} (\bar{T}_{r+1} - \bar{T}_r)$$

In the limit, as the slab thickness approaches zero, the approximation becomes

$$\frac{\Delta E_{r+1}^{r}}{\Delta T_{r+1}^{r}} = \frac{\Delta E_r^{r-1}}{\Delta T_r^{r-1}} = \frac{\partial E}{\partial T}$$

and

$$\Delta F_r = -\frac{\partial E}{\partial T}(\bar{T}_r - \bar{T}_{r-1}) - [-\frac{\partial E}{\partial T}(\bar{T}_{r+1} - \bar{T}_r] = -\frac{\partial E}{\partial T}(\Delta T_r^{r-1} - \Delta T_{r+1}^{r})$$

or

$$\Delta F_r = -\frac{\partial E}{\partial T}(\frac{\Delta T_r^{r-1}}{\Delta z_{r-1}} \Delta z_{r-1} - \frac{\Delta T_{r+1}^{r}}{\Delta z_r} \Delta z_r) \qquad (2\text{-}3)$$

where Δz_r depends on the precipitable water able to absorb long wave radiation completely. The vapor pressure of the slab is given by the equation of state as

$$e = \rho_v R_v \bar{T}_r$$

where ρ_v is the vapor density at $\bar{T}_r$, $R_v = 461.5 \frac{\text{Joules}}{\text{kg deg}}$ is the gas constant for water vapor, and $\bar{T}$ is the average temperature of the slab r. The vapor density is

$$\rho_v = \frac{\text{mass}}{\text{volume}} = \frac{\text{mass}}{\text{Area} \times \Delta z_r}$$

therefore

$$\Delta z_r \rho_v = \frac{\text{mass of vapor}}{\text{Area}} = \rho_{vs}$$

hence

$$\Delta z_r\left(\frac{e}{R_v \bar{T}_r}\right)=\rho_{vs}$$

or

$$\Delta z_r=\rho_{vs}\left(\frac{R_v \bar{T}_r}{e}\right)$$

Given that the mass of water either in liquid or vapor form is the same

$$\rho_w l_{pw}=\frac{\text{mass of vapor}}{\text{Area}}=\rho_{vs}$$

where ρ_w is the density of water at $\bar{T}_r$ and l_{pw} is the length of column of precipitable water for complete absorption.
Then

$$\Delta z_r=l_{pw}\rho_w\left(\frac{R_v \bar{T}_r}{e}\right)$$

Assuming $\rho_w=1000\frac{kg}{m^3}$ $\qquad$ $\Delta z_r=461.5\ 10^3\frac{\bar{T}_r}{e}\ l_{pw}$

According to Simpson $l_{pw}=0.3mm$.
However Randall et al.(Sutton, 1953 p.171) advocated that considerably more water vapor is needed for complete absorption. An amount of the order of 1mm appears to be more convincing for their smaller absorption coefficients.
For the previous mentioned value of $l_{pw}=0.3mm$ we get

$$\Delta z_r=138.5\frac{\bar{T}_r}{e}$$

Given that the boundary layer extends up to about 1Km and that the present application is limited to the early morning

hours with the mixed layer extending to 500m or less, we may argue that Δz_r is subject to small changes:

1.Because, according to Hann(Brunt, 1939 p.131), the vapor pressure varies by less than 20% between the ground and 500m.

2.Because the variation of the temperature with height within the mixed layer(i.e. excluding the change within the surface layer) is of the order of 10 deg. Therefore ΔT_r^{r-1} may be considered small.

In (2-3) we may approximate $\Delta z_{r-1} = \Delta z_r = dz$ and $(\overline{T}_r - \overline{T}_{r-1}) - (\overline{T}_{r+1} - \overline{T}_r) = 2\overline{T}_r - (\overline{T}_{r-1} + \overline{T}_{r+1}) \simeq (\Delta T)^2$ Then (2-3) may be written as:

$$\Delta F = -138.5 \frac{T}{e} \frac{\partial E}{\partial T} \frac{(\Delta T)^2}{\Delta z}$$

or in the limit,

$$\frac{\partial F}{\partial z} = -j \frac{\partial}{\partial z}\left(\frac{\partial T}{\partial z}\right) \quad , \quad j\text{:constant}$$

Since the heating rate is $h = -\mathrm{div}F = -\frac{\partial F}{\partial z}$, it is implied that $h = j\frac{\partial}{\partial z}\left(\frac{\partial T}{\partial z}\right)$.

Then, from (2-1)

$$c_p \rho \left(\frac{\partial T}{\partial t}\right) = j \frac{\partial^2 T}{\partial z^2}$$

or

$$\frac{\partial T}{\partial t} = \frac{j}{c_p \rho} \frac{\partial^2 T}{\partial z^2}$$

And the equation of radiative transfer of heat may be written

$$\frac{\partial T}{\partial t} = K_R \left(\frac{\partial^2 T}{\partial z^2}\right)$$

In SI-units,we assume:

$l_{pw}=3\times10^{-4}m$, $T=295°K$, $e=500$ Pa, $\frac{\partial E}{\partial T}=2.44\frac{\text{Joules}}{m^2 sec\ deg}$,

$\rho=1.25\frac{kg}{m^3}$, $c_p=1004$ Joules $deg^{-1}kg^{-1}$

Then

$$K_R=0.16m^2sec^{-1}$$

Compared with the thermal diffusivity $k=1.78\ 10^{-5}m^2sec^{-1}$ the radiative transfer is much more important with $K_R=0.16m^2sec^{-1}$ and as a result, conduction can be neglected. Brunt analyzed the effects of radiation on the distribution of temperature based on Simpson's work related with the absorption of long wave radiation by water vapor. The main assumptions for the equation of the radiative transfer of heat are:

1. Water vapor completely absorbs all radiation of wavelengths between 5.5 and 7μm and greater than 14μm (called W-radiation by Brunt).
2. The atmosphere allows any radiation below 4μm and between 8.5μm and 11μm to pass through unaffected.
3. Neglect partial absorption between 4μm and 5.5μm and 11μm and 14μm.
4. Assumptions 1 to 3 above are most nearly satisfied by atmospheric conditions of middle latitude.
5. Layers containing water vapor corresponding to 0.3mm of precipitable water behave as if they were black bodies at temperature T for the absorbed wavelengths, where T is the uniform temperature of the layer or for all practical

purposes, its mean temperature. The thickness of the layers depends on the temperature and vapor pressure.

6. The radiation emitted by a layer cannot be less than that of a black body at a temperature corresponding that of its outer boundary.

7. Clear skies or only high clouds.

8. Absence of wind.

9. No scattering or diffusion of the radiation occurs. Radiation is treated as parallel beams in the vertical.

10. The earth behaves as a black body at temperature T measured at close-cut grass height independent of the surface cover. The mean deviation is ±½°C. The error on the calculated black body radiation does not exceed ±5 Watts m^{-2} (Sutton, 1953, p.175).

A number of limitations encountered in this analysis of the radiative transfer as described by Brunt are:

1. Practical inability of determining accurate measurements of the distribution of water vapor with height, since water vapor varies irregularly with time.

2. Radiation is not a parallel beam.

3. The absorption coefficient η_λ being a complex function of the wavelength, is not capable of representation by any simple mathematical approximation.

4. The depth of the layer cannot be allowed to increase unconditionally, since uniform temperature and vapor pressure equal to the mean values can no longer be representative of the temperature and vapor pressure changes

within the layers. An acceptable thickness of 40m may determine a ratio $\frac{T}{e}=\frac{40}{1.39}=30$ with T in °K and e in mb.

5. The method gives no information about the lowest layers, say below 50m. (Sutton,1953 p.227)

The equation applied by Brunt(1939) in Paris shows that radiation has a negligible effect on the diurnal variation of temperature at a height of 300m.

To derive an analytical solution of the radiative transfer of heat equation in order to predict the night minimum temperature of the soil, resulting from nocturnal radiative cooling of ground surface, Brunt(1939) assumed that the earth surface is the outer border of a semi-infinite medium with steady flow at constant temperature T_s. If κ_g is the thermal diffusivity of the ground, then the flux of heat from the ground is:

$$q_s=\kappa_g \rho_g c_g \left(\frac{\partial T}{\partial z}\right)_{z=o}$$

Then, he assumed that the net outgoing (longwave) radiation

$$R_N=R^{\uparrow}_{surf}-R^{\downarrow}_{atm}$$

may be expressed as

$$R_N=\sigma T^4(1-a-b\sqrt{e}).$$

Since the vapor pressure e remains practically constant and the temperature change during the night has no essential effect on R_N, the net outgoing radiation is assumed constant over night. The formula $R_N=\sigma T^4(1-a-b\sqrt{e})$ is an empirical equation derived by Brunt with a=0.6 and b=0.042. By

eliminating the conduction, which we have seen is of no practical importance, and convection processes, since we assumed that calm conditions prevail and they do not favor forced convection from the air to the surface, the continuity of the heat flux across z=0 gives

$$R_N = k_g \left(\frac{\partial T}{\partial z}\right)_{z=o} = \kappa_g \rho_g c_g \left(\frac{\partial T}{\partial z}\right)_{z=o} = q_s \qquad (2\text{-}4)$$

This is a condition for the prescribed flux. In this case $\left(\frac{\partial T}{\partial z}\right)_{z=o}$ is constant since R_N is assumed constant.
We have seen that the conduction of heat through the ground is described by

$$\frac{\partial T}{\partial t} = \kappa_g \left(\frac{\partial^2 T}{\partial z^2}\right) \qquad (2\text{-}5)$$

By differentiating the conduction equation (2-5) with respect to z, we get

$$\frac{\partial}{\partial z}\left(\frac{\partial T}{\partial t}\right) = \kappa_g \left[\frac{\partial}{\partial z}\left(\frac{\partial^2 T}{\partial z^2}\right)\right]$$

In general, for any depth z,

$$\frac{\partial q}{\partial t} = k_g \left[\frac{\partial}{\partial t}\left(\frac{\partial T}{\partial z}\right)\right] = k_g \left[\frac{\partial}{\partial z}\left(\frac{\partial T}{\partial t}\right)\right]$$

and

$$\frac{\partial q}{\partial z} = k_g \left(\frac{\partial^2 T}{\partial z^2}\right) \qquad \text{or} \qquad \frac{\partial^2 q}{\partial z^2} = k_g \left[\frac{\partial}{\partial z}\left(\frac{\partial^2 T}{\partial z^2}\right)\right]$$

Therefore the heat flux satisfies the same differential equation as T:

$$\frac{1}{k_g}\left(\frac{\partial q}{\partial t}\right) = \kappa_g \left[\frac{1}{k_g}\left(\frac{\partial^2 q}{\partial z^2}\right)\right]$$

Hence

$$\frac{\partial q}{\partial t}=\kappa_g\left(\frac{\partial^2 q}{\partial z^2}\right) \qquad (2\text{-}6)$$

By dimensional analysis $q=q(\kappa_g,t,z)=q\left[\frac{z}{\sqrt{(\kappa_g t)}}\right]$

If $\lambda=\frac{z}{2\sqrt{(\kappa_g t)}}$ then

$$\frac{\partial q(\lambda)}{\partial t}=\frac{\partial q(\lambda)}{\partial \lambda}\frac{\partial \lambda}{\partial t}=-\frac{\lambda}{2t}\frac{\partial q(\lambda)}{\partial \lambda}$$

also

$$\frac{\partial^2 q(\lambda)}{\partial z^2}=\frac{1}{4\kappa_g t}\frac{\partial^2 q(\lambda)}{\partial \lambda^2}$$

From (2-6) we get

$$-\frac{\lambda}{2t}\left(\frac{\partial q(\lambda)}{\partial \lambda}\right)=\frac{\kappa_q}{4\kappa_g t}\left(\frac{\partial^2 q(\lambda)}{\partial \lambda^2}\right)$$

or

$$\frac{\partial q}{\partial \lambda}=-\frac{1}{2\lambda}\left(\frac{\partial^2 q}{\partial \lambda^2}\right)$$

or

$$\frac{\frac{\partial}{\partial \lambda}\left(\frac{\partial q}{\partial \lambda}\right)}{\frac{\partial q}{\partial \lambda}}=-2\lambda$$

or

$$\ln\frac{\partial q(\lambda)}{\partial \lambda}=-\lambda^2+C' \quad \text{or} \quad \frac{\partial q(\lambda)}{\partial \lambda}=C\exp(-\lambda^2)+D'$$

and

$$q(\lambda)=C\int_{\lambda}^{\infty} e^{-s^2}ds+D \quad \text{and} \quad \lambda=\frac{z}{2\sqrt{\kappa_s t}}$$

The constants C and D are determined by requiring the flux at $z=\infty$ be negligibly small so that the temperature be unaffected by conduction. Therefore the boundary conditions should be,

at $z=0$ $q=q_s=R_N$

at $z=\infty$ $q=0$

But

$$\operatorname{erfc}(\lambda)=\frac{2}{\sqrt{\pi}}\int_{\lambda}^{\infty} e^{-s^2}ds$$

or

$$\int_{\lambda}^{\infty} e^{-s^2}ds=\frac{\sqrt{\pi}}{2}\operatorname{erfc}(\lambda)$$

and

$$q=C\,\frac{\sqrt{\pi}}{2}\operatorname{erfc}\left[\frac{z}{(4\kappa_g t)^{1/2}}\right]+D \qquad (2\text{-}7)$$

For fixed time t at z=0 $q=C\,\frac{\sqrt{\pi}}{2}+D$, erfc(0)=1

For $z=\infty$ erfc(∞)=0 and q=D. Therefore D=0

Thus $q=C\,\frac{\sqrt{\pi}}{2}$ at z=0

and from (2-4) $C\,\frac{\sqrt{\pi}}{2}=R_N=q_s$ or $C=\frac{2}{\sqrt{\pi}}R_N=\frac{2}{\sqrt{\pi}}q_s$

whereas from (2-7) the heat flux equation is:

$$q=R_N\operatorname{erfc}\left[\frac{z}{(4\kappa_g t)^{1/2}}\right] \qquad (2\text{-}8)$$

From (2-4), at z=0

$$q_s=\kappa_g\rho_g c_g\left(\frac{\partial T}{\partial z}\right)_{z=0}$$

In general, for any z

$$q=\kappa_g\rho_g c_g\left(\frac{\partial T}{\partial z}\right) \qquad (2\text{-}9)$$

Then

$$\kappa_g\rho_g c_g\left(\frac{\partial T}{\partial z}\right)=\frac{2}{\sqrt{\pi}}R_N\int_{\lambda}^{\infty} e^{-s^2}ds$$

From(2-8) and (2-9)

$$\frac{\partial T}{\partial z}=\frac{2}{\sqrt{\pi}}\,\frac{R_N}{\kappa_g\rho_g c_g}\int_{\lambda}^{\infty} e^{-s^2}ds \qquad (2\text{-}10)$$

or

$$\frac{\partial T}{\partial z}=\frac{R_N}{\kappa_g\rho_g c_g}\operatorname{erfc}\left(\frac{z}{\sqrt{4\kappa_g t}}\right) \qquad (2\text{-}11)$$

Brunt integrates (2-11):

$$T(z,t)-T(0,t)=-\frac{R_N}{\kappa_g\rho_g c_g}\int_z^\infty \operatorname{erfc}\left(\frac{z}{2\sqrt{\kappa_g t}}\right)dz$$

$$=-2\sqrt{(\kappa_g t)}\frac{R_N}{\kappa_g\rho_g c_g}\int_{\frac{z}{\sqrt{(4\kappa_g t)}}}^\infty \operatorname{erfc}\left(\frac{z}{\sqrt{(4\kappa_g t)}}\right)d\left(\frac{z}{\sqrt{(4\kappa_g t)}}\right)$$

and since

$$i^n\operatorname{erfc}(x)=\int_x^\infty i^{n-1}\operatorname{erfc}(\xi)d\xi \quad ,n=1,2,\ldots$$

we get for n=1:

$$i\operatorname{erfc}_x=\int_x^\infty \operatorname{erf}(\xi)d\xi=\frac{1}{\sqrt{\pi}}e^{-x^2}-x\operatorname{erfc}(x)$$

(Carlslaw and Jaeger ,1959)

Brunt derives the equation:

$$T(z,t)=T(0,0)-\frac{2R_N\sqrt{(\kappa_g t)}}{\kappa_g\rho_g c_g}\left[\frac{1}{\sqrt{\pi}}\exp\left(-\frac{z^2}{4\kappa_g t}\right)-\frac{z}{2\sqrt{(\kappa_g t)}}\operatorname{erfc}\left(\frac{z}{2\sqrt{(\kappa_g t)}}\right)\right] \qquad (2\text{-}12a)$$

At z=0 the temperature of the surface is:

$$T(0,t)=T(0,0)-\frac{2R_N}{\kappa_g\rho_g c_g}\sqrt{\left(\frac{\kappa_g t}{\pi}\right)} \qquad (2\text{-}12b)$$

Sutton(1951, p.131) assumes T(0,0)=0, a relative value for temperature at time t_o=0, and derives the solution for the fall of the temperature at the surface as:

$$T(0,t)=\frac{2R_N}{\kappa_g\rho_g c_g}\left(\frac{\kappa_g t}{\pi}\right)^{1/2}$$

Anfossi et al(1976) assume that Brunt's equation:

$$T(z,t)-T(0,0)=-\frac{2R_N}{\kappa_g\rho_g c_g}\left\{\left(\frac{\kappa_g t}{\pi}\right)^{1/2}\exp\left(-\frac{z^2}{4\kappa_g t}\right)-\frac{z}{2}\operatorname{erfc}\left(\frac{z}{2\sqrt{(\kappa_g t)}}\right)\right\}$$

is valid for the diffusion of heat in air due to long wave radiation on replacing the thermal diffusivity by the radiative diffusivity:

$$T(z,t)-T(0,0)=-\frac{2R_N}{K_R\rho_a c_p}\left(\frac{K_R t}{\pi}\right)^{1/2}\left\{\exp\left(-\frac{z^2}{4K_R t}\right)-\frac{z}{2}\left(\frac{\pi}{K_R t}\right)^{1/2}\operatorname{erfc}\left(\frac{z}{2\sqrt{(K_R t)}}\right)\right\}$$

and from (2-12b):

$$T(z,t)-T(0,0)=[T(0,t)-T(0,0)]\left\{\exp\left(-\frac{z^2}{4K_R t}-\frac{z}{2}\left(\frac{\pi}{K_R t}\right)^{1/2}\right.\right.$$
$$\left.\left.\operatorname{erfc}\left(\frac{z}{2\sqrt{(K_R t)}}\right)\right\}\right. \qquad (2\text{-}13a)$$

This modification is accompanied by a number of boundary conditions that more closely resemble reality. These are:

1. The starting time of the process is made to coincide with the moment at which the temperature (near the surface) becomes maximum (T_{max}).
Then $\frac{\partial T}{\partial z}$=const. and $T(z,0)=C_1 z+C_2$

2. The top of the stable layer $h_i=a(t)^{1/2}$ follows a parabolic law with time, with a=70 when h_i is in meters and t is in hrs.

3. Above h_i turbulent processes are dominant and the effect of radiation becomes negligible. It is, therefore, likely, that $\left(\frac{\partial T}{\partial z}\right)_{h_i}\simeq 0$ and $[R_N]_{h_i}=0$

4. The radiative diffusivity is constant and poorly correlated to wind speed.

5. $T(h_i,t)-T(0,t)=\frac{1}{2}[T(0,0)-T(0,t)]$

6. When water vapor condensation near the ground does not occur, the fall of temperature on the earth's surface after sunset up to dawn is described by

$$T(0,t)=\frac{2R_N}{\kappa_g\rho_g c_g}\left(\frac{\kappa_g t}{\pi}\right)^{1/2}$$

7. Stable stratification persists till dawn when wind speed does not exceed 7 m/s at 120m, and with thin overcast.

8. The depth of the layer influenced by the surface is given by $z^2=4K_H t$ and in our circumstance $h_i=(4K_R t)^{1/2}$. K_H is a virtual eddy conductivity of heat, constant in magnitude, described by Taylor (Sutton, 1953 p.212)

In light of the new boundary conditions:

$$q(0,t)=R_N$$

$$q(h_i,t)=0$$

$$h_i=(4K_R t)^{1/2}$$

equation (2-6) modified as $\frac{\partial q}{\partial t}=K_R\frac{\partial^2 q}{\partial z^2}$ may be integrated and gives:

$$q(z,t)=\frac{R_N}{1-\mathrm{erfc}(1)}\left[\mathrm{erfc}\left(\frac{z}{h_i}\right)-\mathrm{erfc}(1)\right] \qquad (2\text{-}13b)$$

(Anfossi et al., 1976 p.177)

and

$$T(z,t)=T(0,0)-[T(0,0)-T(0,t)]\left\{\exp\left[-\left(\frac{z}{h_i}\right)^2\right]-\frac{z}{h_i}\pi^{1/2}\mathrm{erfc}\left(\frac{z}{h_i}\right)+0.278\left(\frac{z}{h_i}\right)\right\}$$

$$h_i=(4K_R t)^{1/2}=70t^{1/2}$$

and at z=0

$$T(0,0)-T(0,t)=\frac{2R_N}{K_R[1-\mathrm{erfc}(1)]}\left(\frac{K_R t}{\pi}\right)^{1/2}, \quad \sqrt{\pi}[\mathrm{erfc}(1)]=0.278$$

The model described by Brunt(1939) and modified by Anfossi et al.(1976) appears to work best with relatively high surface temperatures.A better approximation is achieved if the atmosphere is modelled not as a semi-infinite medium but rather as a medium with a lower and upper boundary. The upper boundary is characterized by $\frac{\partial T}{\partial z}=0$ and is variable in time. Observations and model predictions agree with a significant accuracy up to 120m. Beyond that height no observations were available in Anfossi's analysis and no comparison for accuracy is available. The errors of temperature predictions and predicted inversion heights were within the range of 10% to 20% under ideal conditions. The error increased when condensation was formed at the ground and when winds were greater than 4 m/s at 120 m height.

A final note concerns the rate at which changes may be expected to occur. The time constant appropriate to radiative processes will depend on the scale of the phenomenon under consideration and the density of the air as well as on the details of the process itself. Houghton(1980) proposes that $\Delta t=\frac{c_p \rho h}{8\sigma T^3}$ where ρ is the uniform density of the medium of thickness h, and T the temperature at which the slab radiates as a black body.

If $O(h)\text{-}10^3$, $O(\rho)\text{-}10^0$, $O(T)\text{-}10^3$, $c_p=1004$ J deg^{-1} kg^{-1}, $\sigma=5.7\times10^{-8}$ W m^{-2} deg^{-4}

Then

$$\Delta t=\frac{1004\ \text{J/(deg kg)}\times 1.2\ \text{kg/m}^3\times 3\times10^3\ \text{m}}{8\times5.7\times10^{-8}\ \text{W/(m}^3\text{deg}^4)\times(2.8\times10^3)^3\ \text{deg}^3}$$

$$\simeq \frac{1.004 \times 1.2 \times 3 \times 10^{3}}{8 \times 5.7 \times 21.95 \times 10^{-3}} \text{sec} \simeq 3.6 \times 10^{4} \simeq 10 \text{hr}$$

Therefore for a slab of thickness $\Delta z \simeq 300$m, estimated by Brunt, it will take approximately ten hours for changes to occur due to radiational energy exchanges. As a result, our experi- ments with a time delay between runs of 45 minutes for a period of time of six hours allows us to assume that the temperature profile is conserved within the stable layer while the convective layer is developed after sunrise.

2.3 Theory of the entrainment model

2.3.1 The turbulent kinetic energy and the thermodynamic energy equations

Boundary layer processes are a consequence of the interaction between the atmosphere and the earth's surface and take place mainly in a layer about 1km in depth. In this planetary boundary layer the fluxes are mainly a consequence of small scale turbulence and convection.

During the daytime, solar radiation heats the surface of the earth and the air in contact becomes convectively unstable. This condition causes warm air to rise and mix with upper cooler air strata creating a mixed layer above which convection comes to a stop due to the loss of buoyancy. The height of the mixed layer increases with time as more solar energy is absorbed by the surface of the earth, warms the

adjacent stratum of air and increases the mixing at the lower levels of the atmosphere.

In general the atmosphere is treated for many practical purposes as a compressible viscous fluid in a rotating system, obeying the continuity equation. In our particular case it is assumed to be horizontally homogeneous. Then the Navier-Stokes (N-S) equations become:

$$\frac{\partial u}{\partial t}+w\frac{\partial u}{\partial z}=-\frac{1}{\rho}\frac{\partial p}{\partial x}+\nu\frac{\partial^2 u}{\partial z^2}+fv$$

$$\frac{\partial v}{\partial t}+w\frac{\partial v}{\partial z}=-\frac{1}{\rho}\frac{\partial p}{\partial y}+\nu\frac{\partial^2 v}{\partial z^2}-fu$$

$$\frac{\partial w}{\partial t}+w\frac{\partial w}{\partial z}=-\frac{1}{\rho}\frac{\partial p}{\partial z}+\nu\frac{\partial^2 w}{\partial z^2}-g$$

and $\nu=\frac{\mu}{\rho}$ (Nieuwstadt and van Dop, 1982)

I. To derive the the turbulent kinetic energy equation which will eventually determine the dissipation contributing to the thermodynamic balance at the top of the mixed layer we consider the following steps:

1.Assume a neutral reference state (ρ_R, T_R, p_R) such that

$$\frac{\partial T_R}{\partial z}=-\frac{g}{c_p},\ \frac{\partial}{\partial z}p_R=-g\rho_R\ ,p_R=\rho_R R T_R$$

2.Assume shallow convection (h<< scale height H≈8km) , such that, any temperature, density, or pressure (T,ρ,p) obeys the Boussinesq approximations:

$T=T_R+\Delta T$ and $|\frac{\Delta T}{T_R}|<<1$, $p=p_R+\Delta p$ and $|\frac{\Delta p}{p_R}|<<1$, $\rho=\rho_R+\Delta\rho$ and $|\frac{\Delta\rho}{\rho_R}|<<1$

3. Assume that density variations are affected by temperature but not by pressure variations: $(\rho_R+\Delta\rho)=\frac{p_R}{R(T_R+\Delta T)}$

Then if $x_i=(x_1,x_2,x_3)\equiv(x,y,z)$:

$$-\frac{1}{\rho}\frac{\partial p}{\partial x_i}=-\frac{1}{\rho}\frac{\partial}{\partial x_i}(p_R+\Delta p)=-\frac{1}{\rho_R}\left(\frac{\partial p_R}{\partial x_i}+\frac{\partial(\Delta p)}{\partial x_i}\right)\left(1+\frac{\Delta\rho}{\rho_R}\right)^{-1}$$

Taylor's expansion gives $(1+\frac{\Delta\rho}{\rho_R})^{-1}=1-\frac{\Delta\rho}{\rho_R}+\ldots$ and

$\frac{1}{\rho}\frac{\partial p}{\partial x_i}=\frac{1}{\rho_R}\frac{\partial p_R}{\partial x_i}+\frac{1}{\rho_R}\frac{\partial(\Delta p)}{\partial x_i}-\frac{\Delta\rho}{\rho_R^2}\left(\frac{\partial}{\partial x_i}p_R\right)$. Since $p_R=\rho_R R T_R$ and

$$\frac{p_R}{\rho_R+\Delta\rho}=R(T_R+\Delta T) \text{ or } R(\Delta T)=-\frac{p_R\Delta\rho}{\rho_R^2} \text{ or } \Delta\rho=-\frac{R(\Delta T)}{p_R}\rho_R^2=-\frac{\Delta T}{T_R}\rho_R$$

or

$$\frac{\Delta\rho}{\rho_R^2}\frac{\partial}{\partial x_i}p_R=-\frac{R(\Delta T)}{p_R}\frac{\partial}{\partial x_i}p_R=-\frac{\Delta T}{\rho_R T_R}\frac{\partial}{\partial x_i}p_R=-\frac{\Delta T}{\rho_R T_R}(-g\rho_R\delta_{3i})=g\frac{\Delta T}{T_R}\delta_{3i}$$

since $\Delta\rho$ is considered signficant only when multiplied by gravity g. The N-S equations become, recalling that $\frac{\partial}{\partial x}p_R=\frac{\partial}{\partial y}p_R=0$:

$$\frac{\partial u}{\partial t}+w\frac{\partial u}{\partial z}=-\frac{1}{\rho_R}\frac{\partial\Delta p}{\partial x}+\nu\frac{\partial^2 u}{\partial z^2}+fv \qquad \text{and} \qquad \nu=\frac{\mu}{\rho_R}$$

$$\frac{\partial v}{\partial t}+w\frac{\partial v}{\partial z}=-\frac{1}{\rho_R}\frac{\partial\Delta p}{\partial y}+\nu\frac{\partial^2 v}{\partial z^2}-fu$$

$$\frac{\partial w}{\partial t}+w\frac{\partial w}{\partial z}=-\frac{1}{\rho_R}\frac{\partial}{\partial z}p_R-\frac{1}{\rho_R}\frac{\partial(\Delta p)}{\partial z}+g\frac{\Delta T}{T_R}+\nu\frac{\partial^2 w}{\partial z^2}-g$$

$$=-\frac{1}{\rho_R}(-g\rho_R)-\frac{1}{\rho_R}\frac{\partial(\Delta p)}{\partial z}+g\frac{\Delta T}{T_R}+\nu\frac{\partial^2 w}{\partial z^2}-g$$

$$=-\frac{1}{\rho_R}\frac{\partial(\Delta p)}{\partial z}+g\frac{\Delta T}{T_R}+\nu\frac{\partial^2 w}{\partial z^2}$$

4. Apply the Reynold's convention:

$$u=\bar{u}+u', \quad \overline{u'}=0$$

$$v=\bar{v}+v', \quad \overline{v'}=0$$

$$w=\bar{w}+w' \quad ,\overline{w'}=0$$

$$\Delta T=\bar{T}+T' \quad ,\overline{T'}=0$$

$$\Delta p=\bar{p}+p' \quad ,\overline{p'}=0$$

and the N-S equations become:

$$\frac{\partial}{\partial t}(\bar{u}+u')+(\bar{w}+w')\frac{\partial}{\partial z}(\bar{u}+u')=-\frac{1}{\rho_R}\frac{\partial}{\partial x}(\bar{p}+p')+\nu\frac{\partial^2}{\partial z^2}(\bar{u}+u')+f(\bar{v}+v')$$

$$\frac{\partial}{\partial t}(\bar{v}+v')+(\bar{w}+w')\frac{\partial}{\partial z}(\bar{v}+v')=-\frac{1}{\rho_R}\frac{\partial}{\partial y}(\bar{p}+p') +\nu\frac{\partial^2}{\partial z^2}(\bar{v}+v')-f(\bar{u}+u')$$

$$\frac{\partial}{\partial t}(\bar{w}+w')+(\bar{w}+w')\frac{\partial}{\partial z}(\bar{w}+w')=-\frac{1}{\rho_R}\frac{\partial}{\partial z}(\bar{p}+p')+g(\frac{\bar{T}+T'}{T_R})+\nu\frac{\partial^2}{\partial z^2}(\bar{w}+w')$$

5. Ensemble average the equations in step 4:

$$\frac{\partial}{\partial t}\bar{u}+\bar{w}\frac{\partial}{\partial z}\bar{u}+\overline{w'\frac{\partial u'}{\partial z}}=-\frac{1}{\rho_R}\frac{\partial}{\partial x}\bar{p}+\nu\frac{\partial^2}{\partial z^2}\bar{u}+f\bar{v}$$

$$\frac{\partial}{\partial t}\bar{v}+\bar{w}\frac{\partial}{\partial z}\bar{v}+\overline{w'\frac{\partial v'}{\partial z}}=-\frac{1}{\rho_R}\frac{\partial}{\partial y}\bar{p}+\nu\frac{\partial^2}{\partial z^2}\bar{v}-f\bar{u}$$

$$\frac{\partial}{\partial t}\bar{w}+\bar{w}\frac{\partial}{\partial z}\bar{w}+\overline{w'\frac{\partial w'}{\partial z}}=-\frac{1}{\rho_R}\frac{\partial}{\partial z}\bar{p}+g\frac{\bar{T}}{T_R}+\nu\frac{\partial^2}{\partial z^2}\bar{w}$$

6. We subtract the averaged equations of step 5 from the complete analytical N-S equations in step 4 and get :

$$\frac{\partial u'}{\partial t}+\bar{w}\frac{\partial u'}{\partial z}+w'\frac{\partial \bar{u}}{\partial z}+w'\frac{\partial u'}{\partial z}-\overline{w'\frac{\partial u'}{\partial z}}=-\frac{1}{\rho_R}\frac{\partial p'}{\partial x}+\nu\frac{\partial^2 u'}{\partial z^2}+fv'$$

$$\frac{\partial v'}{\partial t}+\bar{w}\frac{\partial v'}{\partial z}+w'\frac{\partial \bar{v}}{\partial z}+w'\frac{\partial v'}{\partial z}-\overline{w'\frac{\partial v'}{\partial z}}=-\frac{1}{\rho_R}\frac{\partial p'}{\partial y}+\nu\frac{\partial^2 v'}{\partial z^2}-fu'$$

$$\frac{\partial w'}{\partial t}+\bar{w}\frac{\partial w'}{\partial z}+w'\frac{\partial \bar{w}}{\partial z}+w'\frac{\partial w'}{\partial z}-\overline{w'\frac{\partial w'}{\partial z}}=-\frac{1}{\rho_R}\frac{\partial p'}{\partial z}+g\frac{T'}{T_R}+\nu\frac{\partial^2 w'}{\partial z^2}$$

7. Multiply each of the equations in step 6 by u′, v′, w′, respectively:

$$u'\frac{\partial u'}{\partial t}+u'\bar{w}\frac{\partial u'}{\partial z}+u'w'\frac{\partial \bar{u}}{\partial z}+u'w'\frac{\partial u'}{\partial z}-u'\overline{w'\frac{\partial u'}{\partial z}}=-\frac{1}{\rho_R}u'\frac{\partial p'}{\partial x}+\nu u'\frac{\partial^2 u'}{\partial z^2}+fu'v'$$

$$v'\frac{\partial v'}{\partial t}+v'\bar{w}\frac{\partial v'}{\partial z}+v'w'\frac{\partial \bar{v}}{\partial z}+v'w'\frac{\partial v'}{\partial z}-v'\overline{w'\frac{\partial v'}{\partial z}}=-\frac{1}{\rho_R}v'\frac{\partial p'}{\partial y}+\nu v'\frac{\partial^2 v'}{\partial z^2}-fu'v'$$

$$w'\frac{\partial w'}{\partial t}+w'\bar{w}\frac{\partial w'}{\partial z}+w'w'\frac{\partial \bar{w}}{\partial z}+w'w'\frac{\partial w'}{\partial z}-w'\overline{w'\frac{\partial w'}{\partial z}}=-\frac{1}{\rho_R}w'\frac{\partial p'}{\partial z}+\nu w'\frac{\partial^2 w'}{\partial z^2}+g\frac{w'T'}{T_R}$$

8. Rewrite some of the terms in step 7 and average:

$$\frac{\partial}{\partial t}\left(\frac{\overline{u'^2}}{2}\right)+\bar{w}\frac{\partial}{\partial z}\left(\frac{\overline{u'^2}}{2}\right)+\overline{u'w'}\frac{\partial \bar{u}}{\partial z}+\overline{u'w'\frac{\partial u'}{\partial z}}=-\overline{\frac{u'}{\rho_R}\frac{\partial p'}{\partial x}}+\overline{u'\nu\frac{\partial^2 u'}{\partial z^2}}+f(\overline{u'v'})$$

$$\frac{\partial}{\partial t}\left(\frac{\overline{v'^2}}{2}\right)+\bar{w}\frac{\partial}{\partial z}\left(\frac{\overline{v'^2}}{2}\right)+\overline{v'w'}\frac{\partial \bar{v}}{\partial z}+\overline{v'w'\frac{\partial v'}{\partial z}}=-\overline{\frac{v'}{\rho_R}\frac{\partial p'}{\partial y}}+\overline{v'\nu\frac{\partial^2 v'}{\partial z^2}}-f(\overline{u'v'})$$

$$\frac{\partial}{\partial t}\left(\frac{\overline{w'^2}}{2}\right)+\bar{w}\frac{\partial}{\partial z}\left(\frac{\overline{w'^2}}{2}\right)+\overline{w'w'}\frac{\partial \bar{w}}{\partial z}+\overline{w'w'\frac{\partial w'}{\partial z}}=-\overline{\frac{w'}{\rho_R}\frac{\partial p'}{\partial z}}+\overline{w'\nu\frac{\partial^2 w'}{\partial z^2}}+\frac{g}{T_R}(\overline{w'T'})$$

Consider separately $\bar{w}\frac{\partial}{\partial z}\left(\frac{\overline{u'^2}}{2}\right)+\overline{u'w'\frac{\partial u'}{\partial z}}$:

$$\frac{\partial}{\partial z}\left(\bar{w}\frac{\overline{u'^2}}{2}\right)=\bar{w}\frac{\partial}{\partial z}\left(\frac{\overline{u'^2}}{2}\right)+\frac{\overline{u'^2}}{2}\frac{\partial \bar{w}}{\partial z}=\bar{w}\overline{u'\frac{\partial u'}{\partial z}}+\frac{\overline{u'^2}}{2}\frac{\partial \bar{w}}{\partial z} \qquad (2\text{-}14a)$$

$$\frac{\partial}{\partial z}\left(\overline{w'\frac{u'^2}{2}}\right)=\overline{\frac{u'^2}{2}\frac{\partial w'}{\partial z}+u'w'\frac{\partial u'}{\partial z}} \qquad (2\text{-}14b)$$

From (2-14a) and (2-14b) we get:

$$\bar{w}\frac{\partial}{\partial z}\left(\frac{\overline{u'^2}}{2}\right)+\overline{u'w'\frac{\partial u'}{\partial z}}=\frac{\partial}{\partial z}\left(\bar{w}\frac{\overline{u'^2}}{2}\right)-\frac{\overline{u'^2}}{2}\frac{\partial \bar{w}}{\partial z}+\frac{\partial}{\partial z}\left(\overline{w'\frac{u'^2}{2}}\right)-\overline{\frac{u'^2}{2}\frac{\partial w'}{\partial z}}$$

Similarly:

$$\bar{w}\frac{\partial}{\partial z}\left(\frac{\overline{v'^2}}{2}\right)+\overline{v'w'\frac{\partial v'}{\partial z}}=\frac{\partial}{\partial z}\left(\bar{w}\frac{\overline{v'^2}}{2}\right)-\frac{\overline{v'^2}\,\partial\bar{w}}{2\ \partial z}+\frac{\partial}{\partial z}\left(\overline{w'\frac{v'^2}{2}}\right)-\frac{\overline{v'^2\partial w'}}{2\ \partial z}$$

and

$$\bar{w}\frac{\partial}{\partial z}\left(\frac{\overline{w'^2}}{2}\right)+\overline{w'w'\frac{\partial w'}{\partial z}}=\frac{\partial}{\partial z}\left(\bar{w}\frac{\overline{w'^2}}{2}\right)-\frac{\overline{w'^2}\,\partial\bar{w}}{2\ \partial z}+\frac{\partial}{\partial z}\left(\overline{w'\frac{w'^2}{2}}\right)-\frac{\overline{w'^2\partial w'}}{2\ \partial z}$$

Also consider separately $\overline{u'\nu\frac{\partial^2 u'}{\partial z^2}}$:

$$\nu\frac{\partial^2}{\partial z^2}\left(\frac{\overline{u'^2}}{2}\right)=\nu\frac{\partial}{\partial z}\left(\overline{u'\frac{\partial u'}{\partial z}}\right)=\nu\overline{u'\frac{\partial^2 u'}{\partial z^2}}+\nu\overline{\frac{\partial u'}{\partial z}\ \frac{\partial u'}{\partial z}} \qquad (2\text{-}14c)$$

and

$$\nu\frac{\partial}{\partial z}\left(\overline{u'\frac{\partial w'}{\partial x}}\right)=\nu\overline{\frac{\partial u'}{\partial z}\ \frac{\partial w'}{\partial x}}+\ \nu\overline{u'\frac{\partial}{\partial x}\ \frac{\partial w'}{\partial z}} \qquad (2\text{-}14d)$$

We add (2-14c) and (2-14d) and get:

$$\nu\left(\overline{u'\frac{\partial^2 u'}{\partial z^2}}\right)=\ \nu\frac{\partial^2}{\partial z^2}\left(\frac{\overline{u'^2}}{2}\right)+\ \nu\frac{\partial}{\partial z}\left(\overline{u'\frac{\partial w'}{\partial x}}\right)-\nu\overline{\frac{\partial u'}{\partial z}\ \frac{\partial u'}{\partial z}}-\nu\overline{\frac{\partial u'}{\partial z}\ \frac{\partial w'}{\partial x}}-\nu\overline{u'\frac{\partial}{\partial x}\ \frac{\partial w'}{\partial z}}$$

Similarly

$$\nu\left(\overline{v'\frac{\partial^2 v'}{\partial z^2}}\right)=\ \nu\frac{\partial^2}{\partial z^2}\left(\frac{\overline{v'^2}}{2}\right)+\ \nu\frac{\partial}{\partial z}\left(\overline{v'\frac{\partial w'}{\partial y}}\right)-\nu\overline{\frac{\partial v'}{\partial z}\ \frac{\partial v'}{\partial z}}-\nu\overline{\frac{\partial v'}{\partial z}\ \frac{\partial w'}{\partial y}}-\nu\overline{v'\frac{\partial}{\partial y}\ \frac{\partial w'}{\partial z}}$$

$$\nu\left(\overline{w'\frac{\partial^2 w'}{\partial z^2}}\right)=\ \nu\frac{\partial^2}{\partial z^2}\left(\frac{\overline{w'^2}}{2}\right)+\ \nu\frac{\partial}{\partial z}\left(\overline{w'\frac{\partial w'}{\partial z}}\right)-\nu\overline{\frac{\partial w'}{\partial z}\ \frac{\partial w'}{\partial z}}-\nu\overline{\frac{\partial w'}{\partial z}\ \frac{\partial w'}{\partial z}}-\nu\overline{w'\frac{\partial}{\partial z}\ \frac{\partial w'}{\partial z}}$$

9. Add to form the average turbulent kinetic energy equation using $\bar{e}=\frac{1}{2}(\overline{u'^2}+\overline{v'^2}+\overline{w'^2})$ and the continuity equation

$$\frac{\partial\bar{u}}{\partial x}+\frac{\partial\bar{v}}{\partial y}+\frac{\partial\bar{w}}{\partial z}=\frac{\partial u'}{\partial x}+\frac{\partial v'}{\partial y}+\frac{\partial w'}{\partial z}=0$$

Since horizontal homogeneity implies $\frac{\partial}{\partial x}=\frac{\partial}{\partial y}=0$ then $\frac{\partial \bar{w}}{\partial z}=\frac{\partial w'}{\partial z}=0$

and

$$\frac{\partial \bar{e}}{\partial t}=-\overline{u'w'}\frac{\partial \bar{u}}{\partial z}-\overline{v'w'}\frac{\partial \bar{v}}{\partial z}-\overline{w'w'}\frac{\partial \bar{w}}{\partial z}-\frac{\overline{u'\partial p'}}{\rho_R \partial x}-\frac{\overline{v'\partial p'}}{\rho_R \partial y}-\frac{\overline{w'\partial p'}}{\rho_R \partial z}+\frac{g}{T_R}(\overline{w'T'})$$

$$-\bar{w}\frac{\partial}{\partial z}\left(\frac{\overline{u'^2}}{2}+\frac{\overline{v'^2}}{2}+\frac{\overline{w'^2}}{2}\right)-\left(\overline{u'w'\frac{\partial u'}{\partial z}}+\overline{v'w'\frac{\partial v'}{\partial z}}+\overline{w'w'\frac{\partial w'}{\partial z}}\right)$$

$$+\nu\left(\overline{u'\frac{\partial^2 u'}{\partial z^2}}+\overline{v'\frac{\partial^2 v'}{\partial z^2}}+\overline{w'\frac{\partial^2 w'}{\partial z^2}}\right)$$

or

$$\frac{\partial \bar{e}}{\partial t}=-\left(\overline{u'w'}\frac{\partial \bar{u}}{\partial z}+\overline{v'w'}\frac{\partial \bar{v}}{\partial z}+\overline{w'w'}\frac{\partial \bar{w}}{\partial z}\right)-\frac{\overline{w'\partial p'}}{\rho_R \partial z}+\frac{g}{T_R}(\overline{w'T'})-\nu\left[\overline{\frac{\partial u'}{\partial z}\left(\frac{\partial u'}{\partial z}+\frac{\partial w'}{\partial x}\right)}\right.$$

$$\left.+\overline{\frac{\partial v'}{\partial z}\left(\frac{\partial v'}{\partial z}+\frac{\partial w'}{\partial y}\right)}+\overline{\frac{\partial w'}{\partial z}\left(\frac{\partial w'}{\partial z}+\frac{\partial w'}{\partial z}\right)}\right]-\frac{\partial}{\partial z}\left[\bar{w}\frac{\overline{u'^2}}{2}+\bar{w}\frac{\overline{v'^2}}{2}+\bar{w}\frac{\overline{w'^2}}{2}\right]$$

$$-\frac{\partial}{\partial z}\left(\frac{\overline{w'u'^2}}{2}+\frac{\overline{w'v'^2}}{2}+\frac{\overline{w'w'^2}}{2}\right)+\left[\frac{\overline{u'^2}\partial \bar{w}}{2\ \partial z}+\frac{\overline{v'^2}\partial \bar{w}}{2\ \partial z}+\frac{\overline{w'^2}\partial \bar{w}}{2\ \partial z}\right]$$

$$+\left[\frac{\overline{u'^2\partial w'}}{2\ \partial z}+\frac{\overline{v'^2\partial w'}}{2\ \partial z}+\frac{\overline{w'^2\partial w'}}{2\ \partial z}\right]$$

$$-\nu\left[\overline{u'\frac{\partial}{\partial z}\frac{\partial w'}{\partial x}}+\overline{v'\frac{\partial}{\partial z}\frac{\partial w'}{\partial y}}+\overline{w'\frac{\partial}{\partial z}\frac{\partial w'}{\partial z}}\right]+\nu\frac{\partial}{\partial z}\left[\frac{\partial \overline{u'^2}}{\partial z\ 2}+\frac{\partial \overline{v'^2}}{\partial z\ 2}+\frac{\partial \overline{w'^2}}{\partial z\ 2}\right]$$

$$+\nu\left[\overline{u'\frac{\partial w'}{\partial x}}+\overline{v'\frac{\partial w'}{\partial y}}+\overline{w'\frac{\partial w'}{\partial z}}\right]$$

or

$$\frac{\partial \bar{e}}{\partial t}=-\left(\overline{u'w'}\frac{\partial \bar{u}}{\partial z}+\overline{v'w'}\frac{\partial \bar{v}}{\partial z}\right)-\frac{1}{\rho_R}\overline{w'\frac{\partial p'}{\partial z}}+\frac{g}{T_R}(\overline{w'T'})-\nu\left[\overline{\frac{\partial u'}{\partial z}\left(\frac{\partial u'}{\partial z}\frac{\partial w'}{\partial x}\right)}\right.$$

$$\left.+\overline{\frac{\partial v'}{\partial z}\left(\frac{\partial v'}{\partial z}\frac{\partial w'}{\partial y}\right)}+\overline{\frac{\partial w'}{\partial z}\left(\frac{\partial w'}{\partial z}\frac{\partial w'}{\partial z}\right)}\right]+\nu\frac{\partial}{\partial z}\left(\overline{u'\frac{\partial w'}{\partial x}}+\overline{v'\frac{\partial w'}{\partial y}}+\overline{w'\frac{\partial w'}{\partial z}}\right)$$

$$+\nu\frac{\partial}{\partial z}\left(\overline{u'\frac{\partial u'}{\partial z}}+\overline{v'\frac{\partial v'}{\partial z}}+\overline{w'\frac{\partial w'}{\partial z}}\right)-\frac{\partial}{\partial z}[\overline{we}]-\frac{\partial}{\partial z}\left[\frac{1}{2}\left(\overline{w'u'^2}+\overline{w'v'^2}+\overline{w'w'^2}\right)\right]$$

$$+\bar{e}\frac{\partial \bar{w}}{\partial z}+\overline{e\frac{\partial w'}{\partial z}}$$

or

$$\frac{\partial \bar{e}}{\partial t}=-(\overline{u'w'}\frac{\partial \bar{u}}{\partial z}+\overline{v'w'}\frac{\partial \bar{v}}{\partial z})-\frac{1}{\rho_R}\overline{w'\frac{\partial p'}{\partial z}}+\frac{g}{T_R}(\overline{w'T'})$$

$$-2\nu[\overline{\frac{\partial u'}{\partial z}s_{uw}}+\overline{\frac{\partial v'}{\partial z}s_{vw}}+\overline{\frac{\partial w'}{\partial z}s_{ww}}]+\nu\frac{\partial}{\partial z}(\overline{u'\frac{\partial w'}{\partial x}}+\overline{v'\frac{\partial w'}{\partial y}}+\overline{w'\frac{\partial w'}{\partial z}})$$

$$+\nu\frac{\partial}{\partial z}(\overline{u'\frac{\partial u'}{\partial z}}+\overline{v'\frac{\partial v'}{\partial z}}+\overline{w'\frac{\partial w'}{\partial z}})\ -\bar{w}\frac{\partial \bar{e}}{\partial z}$$

$$-\overline{w'[\frac{\partial}{\partial z}(\frac{u'^2}{2})+\frac{\partial}{\partial z}(\frac{v'^2}{2})+\frac{\partial}{\partial z}(\frac{w'^2}{2})]}\qquad ,s_{ij}=\frac{1}{2}(\frac{\partial u_i}{\partial x_j}+\frac{\partial u_j}{\partial x_i})$$

or

$$\frac{\partial \bar{e}}{\partial t}=\frac{g}{T_R}(\overline{w'T'})-\frac{1}{\rho_R}\overline{w'\frac{\partial p'}{\partial z}}\ -(\overline{u'w'}\frac{\partial \bar{u}}{\partial z}+\overline{v'w'}\frac{\partial \bar{v}}{\partial z})$$

$$-2\nu[\overline{\frac{\partial u'}{\partial z}s_{uw}}+\overline{\frac{\partial v'}{\partial z}s_{vw}}+\overline{\frac{\partial w'}{\partial z}s_{ww}}]$$

$$-\bar{w}(\frac{\partial \overline{u'^2}}{\partial z\ 2}+\frac{\partial \overline{v'^2}}{\partial z\ 2}+\frac{\partial \overline{w'^2}}{\partial z\ 2}]\ -\overline{w'\frac{\partial e}{\partial z}}\ +\nu\frac{\partial}{\partial z}(\frac{\partial}{\partial z}\bar{e})$$

or

$$\frac{\partial \bar{e}}{\partial t}=\frac{g}{T_R}(\overline{w'T'})-\frac{1}{\rho_R}\overline{w'\frac{\partial p'}{\partial z}}\ -(\overline{u'w'}\frac{\partial \bar{u}}{\partial z}+\overline{v'w'}\frac{\partial \bar{v}}{\partial z})-\epsilon-\bar{w}\frac{\partial}{\partial z}\bar{e}\overline{w'\frac{\partial}{\partial z}e}\ +\nu\frac{\partial}{\partial z}\frac{\partial}{\partial z}\bar{e}$$

or, assuming $\frac{\partial \bar{e}}{\partial z}=0$, we get:

$$\frac{\partial \bar{e}}{\partial t}=\frac{g}{T_R}(\overline{w'T'})-\frac{\partial}{\partial z}[\overline{w'e}+\frac{(\overline{w'p'})}{\rho_R}]\ -(\overline{u'w'}\frac{\partial \bar{u}}{\partial z}+\overline{v'w'}\frac{\partial \bar{v}}{\partial z})-\epsilon \qquad (2\text{-}15a)$$

where e is the turbulent kinetic energy, $\frac{1}{2}(u'^2+v'^2+w'^2)$, assumed constant with height.

T_R is the temperature of the reference state, $T_o-\frac{g}{c_p}z_R$, and T_o is the ground temperature, $T'=T-T_R$ is the temperature

fluctuation, ρ_R is the density of air at the reference state, and ϵ is the average energy dissipation rate of work against viscous forces.

Assuming days with calm conditions, the turbulent mean kinetic energy equation (2-15a) becomes:

$$\frac{\partial \bar{e}}{\partial t}=\frac{g}{T_R}(\overline{w'T'})-\frac{\partial}{\partial z}[\overline{w'e'}+\frac{(\overline{w'p'})}{\rho_R}]-\epsilon \qquad (2\text{-}15b)$$

II. The thermodynamic energy equation

1. Consider the first law of thermodynamics $\frac{d}{dt}(\rho c_p T)=\sum_i C_{ei}$, where C_{ei} represents sources and sinks of specific heat fluxes, and $\sum_i C_{ei}= k\frac{\partial^2 T}{\partial x^2}+\epsilon+(-\frac{\partial Q_{Ni}}{\partial x_i})$ for dry air where k is the thermal conductivity, Q_N is the net irradiance and we have neglected evaporation.

2. We replace T with the potential temperature $\Theta= T(\frac{p_o}{p})^{R/c_p}$

or

$$\ln\Theta=\ln T+\frac{R}{c_p}(\ln p_o-\ln p) \text{ or } \frac{1}{\Theta}\frac{\partial\Theta}{\partial t}=\frac{1}{T}\frac{\partial T}{\partial t}+\frac{R}{c_p}(\frac{1}{p_o}\frac{\partial p_o}{\partial t}-\frac{1}{p}\frac{\partial p}{\partial t})$$

Assume that the sampling time is short (usually <1 hr) compared to the time scale of pressure changes and therefore $\frac{\partial p_o}{\partial t}=\frac{\partial p}{\partial t}=0$.

Therefore

$$\frac{1}{\Theta}\frac{\partial\Theta}{\partial t}=-\frac{1}{T}\frac{\partial T}{\partial t} \text{ or } \frac{\partial T}{\partial t}=\frac{T}{\Theta}\frac{\partial\Theta}{\partial t}$$

Also,

$$\frac{1}{\Theta}\frac{\partial\Theta}{\partial z}=\frac{1}{T}\frac{\partial T}{\partial z}+\frac{R}{c_p}(-\frac{1}{p}\frac{\partial p}{\partial z})=\frac{1}{T}\frac{\partial T}{\partial z}+\frac{R}{c_p}(\frac{\rho g}{p})=\frac{1}{T}\frac{\partial T}{\partial z}+\frac{R}{c_p}(\frac{\rho g}{\rho RT})$$

or

$$\frac{1}{\Theta}\frac{\partial\Theta}{\partial z}=\frac{1}{T}(\frac{\partial T}{\partial z}+\frac{g}{c_p}) \text{ and } \frac{\partial T}{\partial z}=\frac{T}{\Theta}\frac{\partial\Theta}{\partial z}-\frac{g}{c_p}$$

3. Given the first law of thermodynamics and assuming horizontal homogeneity, then

$$\frac{d}{dt}(\rho c_p T)=k\frac{\partial^2 T}{\partial z^2}+\epsilon-\frac{\partial}{\partial z}Q_N$$

may be simplified to

$$\frac{\partial}{\partial t}(\rho c_p T)+w\frac{\partial}{\partial z}(\rho c_p T)=k\frac{\partial}{\partial z}(\frac{\partial T}{\partial z})+\epsilon-\frac{\partial}{\partial z}Q_N$$

or

$$c_p[\rho\frac{\partial T}{\partial t}+T\frac{\partial \rho}{\partial t}]+wc_p[\rho\frac{\partial T}{\partial z}+T\frac{\partial \rho}{\partial z}] =k\frac{\partial}{\partial z}(\frac{\partial T}{\partial z})+\epsilon-\frac{\partial}{\partial z}Q_N$$

or

$$\rho c_p[\frac{\partial T}{\partial t}+w\frac{\partial T}{\partial z}]+c_pT(\frac{\partial \rho}{\partial t}+w\frac{\partial \rho}{\partial z})=k\frac{\partial}{\partial z}(\frac{\partial T}{\partial z})+\epsilon-\frac{\partial}{\partial z}Q_N$$

Conservation of mass ($\frac{\partial \rho}{\partial t}+\frac{\partial \rho w}{\partial z}=0$) and the continuity equation ($\nabla.v=0$) lead to:

$$\rho c_p[\frac{\partial T}{\partial t}+w\frac{\partial T}{\partial z}]=k\frac{\partial^2 T}{\partial z^2}+\epsilon-\frac{\partial}{\partial z}Q_N$$

or

$$\frac{T}{\theta}[\frac{\partial \theta}{\partial t}+w\frac{\partial \theta}{\partial z}]-w\frac{g}{c_p}=\frac{k}{\rho c_p}\frac{\partial^2 T}{\partial z^2}+\frac{\epsilon}{\rho c_p}-\frac{1}{\rho c_p}\frac{\partial}{\partial z}Q_N,\quad w=\frac{dz}{dt}$$

and

$$\frac{g}{c_p}w=\frac{g}{c_p}\frac{dz}{dt}=-\frac{1}{\rho c_p}(\frac{dp}{dt})=0$$

Also assume that molecular conductivity is negligible above the surface layer, and

$$\frac{\partial \theta}{\partial t}+w\frac{\partial \theta}{\partial z}=\frac{\theta}{\rho c_p T}(\epsilon-\frac{\partial}{\partial z}Q_N)$$

or, by applying Reynold's equations, and averaging:

$$\frac{\partial\bar{\theta}}{\partial t}+\bar{w}\frac{\partial\bar{\theta}}{\partial z}=-\overline{w'\frac{\partial\theta'}{\partial z}}+\overline{\frac{\theta}{\rho c_p T}\left(\epsilon-\frac{\partial}{\partial z}Q_N\right)} \qquad (2\text{-}16)$$

where $\theta=\bar{\theta}+\theta'$

We may replace $\frac{\theta}{T}$ by $\frac{\bar{\theta}}{\bar{T}}$ approximately, assuming that $\frac{R}{c_p}\left|\frac{p'}{p}\right|<<\frac{T'}{\bar{T}}$ or $\frac{\theta'}{\bar{\theta}}=\frac{T'}{\bar{T}}$ (Deardorff, 1960)

and

$$\frac{\theta}{T}=\frac{\bar{\theta}(1+\theta'/\bar{\theta})}{\bar{T}(1+T'/\bar{T})}\simeq\frac{\bar{\theta}}{\bar{T}}.$$

Hence (2-16) becomes

$$\frac{\partial\bar{\theta}}{\partial t}+\bar{w}\frac{\partial\bar{\theta}}{\partial z}=-\frac{\partial}{\partial z}(\overline{w'\theta'})+\frac{1}{\rho c_p}\frac{\bar{\theta}}{\bar{T}}\left(\epsilon-\frac{\partial}{\partial z}\bar{Q}_N\right) \qquad (2\text{-}17)$$

since ϵ is already the average energy dissipation.

2.3.2 The mixed layer model

The literature on convective penetration of stable layers extends back at least to the 1940's. Since 1955 it has been known that a non turbulent fluid is pulled and eventually mixed with a turbulent layer as a result of the differential motion of the interfacial layer between the quiet and turbulent layers (Deardorff, 1980). The study of the growth of a turbulent atmospheric boundary layer at the expense of the nonturbulent overlying stratified atmospheric layer attracted boundary layer scientists and meteorologists in particular commencing in the 1960's (Ball, 1960). Convective instability by heating from below describes most appropriately the dynamics of the process for the

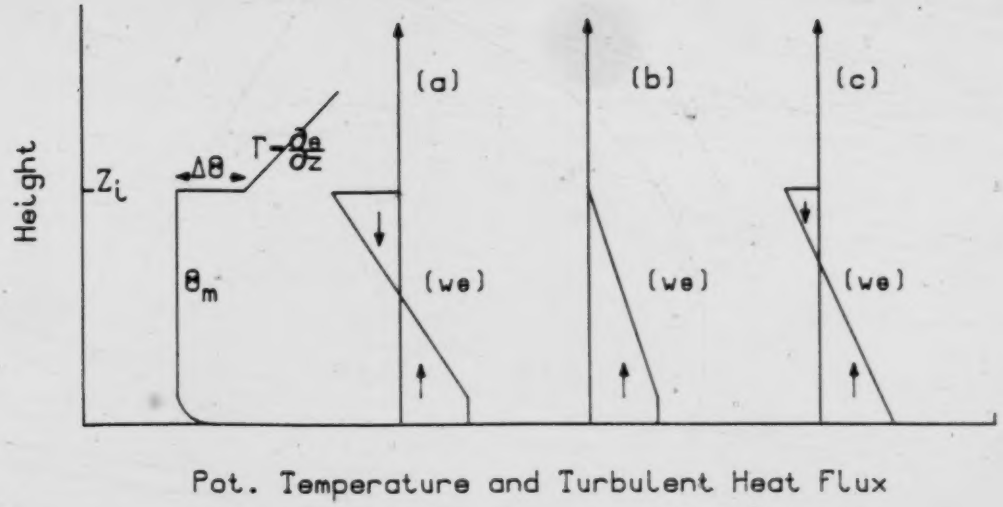

Fig. 2.3 Distribution of potential temperature and turbulent heat flux according to (a) Ball, (b)Lilly and (c)Betts and Carson

development of the mixed layer during the daytime period, under fair weather conditions. These weather conditions (cloudless and windless) lead to simple theoretical models, the most advanced of which is the entrainment model of general structure (Deardorff,1979). The basic concept for the development of a mixed layer by convection is a layer characterized by near constancy of a passive scalar. Henceforth potential temperature will be the only scalar quantity considered, however moisture and concentration of pollutants may be considered as well. This layer is considered to be fully turbulent throughout. The surface layer is assumed thin compared to the mixed layer and all

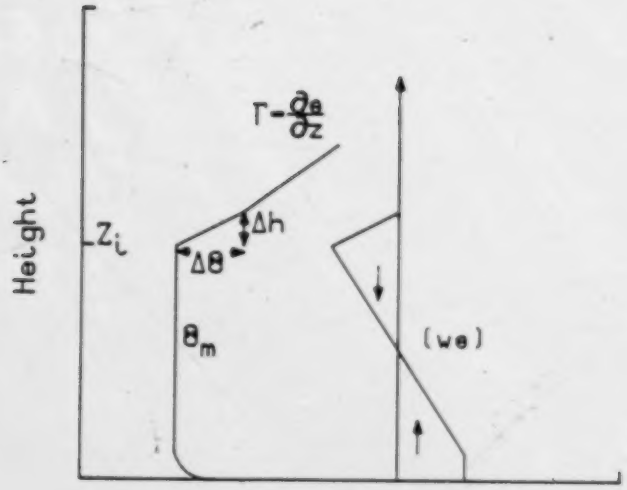

Fig. 2.4 Distribution of potential temperature and turbulent heat flux according to Betts(1974)

relevant variables are assumed horizontally homogeneous. The models developed by Ball(1960), Betts(1973) and Deardorff(1979) differ in the way they analyze the conditions in the interfacial layer. Fig. 2.3 proposed by Ball and elaborated by Lilly(1968) and others assumes the interfacial layer to be very thin with a potential temperature change $\Delta\theta$ occuring at the same level. Fig. 2.4 describes a first order entrainment model with a constant positive lapse rate in the interfacial layer. Fig. 2.5 corresponds to the entrainment model with the potential temperature being a nonlinear function of z (Deardorff, 1979). In the absence of viscous dissipation and radiative transfer eq. (2-17) becomes:

$$\frac{\partial \bar{\theta}}{\partial t} + \bar{w}\frac{\partial \bar{\theta}}{\partial z} = \frac{\partial}{\partial z}(\overline{w'\theta'}) \qquad (2\text{-}17a)$$

Conventionally,an idealized mixed layer is called a "well

mixed layer". The properties of a "well mixed layer" are assumed to be:

1. The vertical gradient of potential temperature (in case of a dry unstable boundary layer) or virtual potential temperature is negligibly small.
2. The sensible eddy (or turbulence potential) heat flux is assumed constant or sinusoidal at the surface (Carson, 1973) and linearly decreasing with height becoming zero between $z_i/2$ and z_i (Lenschow, 1970,1973,1974).
3. The negative heat flux $(\overline{w\theta})_i$ at the bottom of the inversion interfacial layer, where $z=z_i$, is due to the entrainment of the capping stable air into the boundary layer which may vary within a range from zero to the amount produced at the surface $(\overline{w\theta})_o$. There is no accurate and

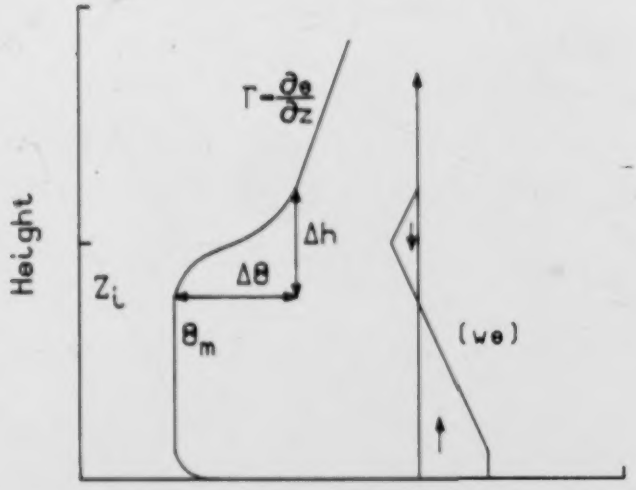

Fig. 2.5 Distribution of potential temperature and turbulent heat flux according to Deardorff (1979).

specific relation between $(\overline{w'\theta'})_i$ and $(\overline{w'\theta'})_o$. Depending on the model different ratios are assumed. Ball(1960) assumes that the eddy heat flux at the top of the convective layer is as much as the surface eddy heat flux. Lilly(1968) considers no entrainment at all with $(\overline{w'\theta'})_i=0$. Deardorff, et al(1974) made a distinction between actual measurement of the downward eddy heat flux below an inversion and that eddy heat flux which is implied when the potential temperature of the "well mixed layer" is assumed constant. The actual is small whereas the "effective" eddy heat flux consists of 25% of the surface eddy heat flux. Betts(1973) adopted

$$\frac{(\overline{w'\theta'})_i}{(\overline{w'\theta'})_o}=0.3$$

Deardorff(1979) took as the height of the mixed layer the height up to which the eddy heat flux decreases to zero. At the height z_o, $(\overline{w'\theta'})_{z_o}=0$.

The two major aspects considered in the study of the convection layer are:

1. The production of heat and how it is distributed throughout the mixed layer and above it.
2. The role of the turbulent kinetic energy either in the mixed layer or at the inversion height. There are two different theoretical approaches (Nieustadt, 1981).

In general it is assumed that in the surface layer the fluxes remain constant and that this layer is thin compared

with the mixed layer. Due to the low conductivity, the surface layer is characterized by a superadiabatic temperature profile as well. The heat flux increases as the surface temperature increases and for small periods of time may be taken as constant or, for long periods, approximated by a sinusoidal function. It may also be approximated as a linear function for the early morning hours

$$(\overline{w'\theta'})_o(t)=(\overline{w'\theta'})_{o\,max}\pi\frac{t}{t_d},\quad t<<t_d,$$

where t_d is the interval between sunrise and sunset, and $(\overline{w'\theta'})_{o\,max}$ is the eddy heat flux value near the local noon hour.The dependence of the turbulent heat flux on height is assumed to be linear. Ball(1960) approached the problem theoretically deriving the equation $(\overline{w'\theta'})_z=(\overline{w'\theta'})_o(1-\frac{2z}{z_i})$. Deardorff(1967) derived a linearly decreasing heat flux with height. Inclusion of radiation may increase the total heat flux by 10% (Elliot, 1964) without affecting, or rather, by improving the approximately linear relation between height and heat flux. Some scientists use a slightly curved heat flux profile (Lenschow,1970; Deardorff, 1972b). Lilly(1968) assumed minimum entrainment $(\overline{w'\theta'})_i$ and

$$\frac{(\overline{w'\theta'})_i}{(\overline{w'\theta'})_o}=1-\frac{z}{z_i}.$$

Lenschow and Johnson (Betts,1973) consider $E=\frac{(\overline{w'\theta'})_i}{(\overline{w'\theta'})_o}=0.25$. Laboratory experiments support a value of E in the range of 0.2-0.3. These values, however, can not be considered as real but rather as apparent, for the simplified models

(Deardorff et al, 1974). The parameter E seems to depend on the turbulent activity in the mixed layer, reaching 0.5 after the time of maximum heating at the surface, for a few hours(Carson and Smith, 1974).Figures 2.3-2.5 show the three simplified entrainment models.

The heat budget equation for the mixed layer can be written for the three models, following Ball's(1960) assumption of conservation of potential heat:

$$\frac{\partial}{\partial z}Q_\theta \equiv \rho c_p \frac{d\theta_m}{dt} \equiv \rho c_p \left(\frac{\partial \theta_m}{\partial t} + w\frac{\partial \theta_m}{\partial z}\right)$$

i.e. the rate of increase of potential heat is equal to the convergence of the turbulent flux of potential heat. And from (2-17a)

$$\bar{\rho} c_p \frac{d\theta_m}{dt} = \bar{\rho} c_p \left(\frac{\partial \theta_m}{\partial t} + w\frac{\partial \theta_m}{\partial z}\right) = -\frac{\partial}{\partial z}\left[\bar{\rho} c_p (\overline{w'\theta'})\right] = -\left[\bar{\rho} c_p \frac{\partial}{\partial z}(\overline{w'\theta'})\right]$$

or

$$\frac{d\theta_m}{dt} = -\frac{\partial}{\partial z}(\overline{w'\theta'}) \qquad (2\text{-}18)$$

where Q_θ is the potential heat. Due to the mixing, θ_m remains constant with height and by integration:

$$\frac{d\theta_m}{dt} \int_0^{z_i} dz = -(\overline{w'\theta'})_s \int^{(\overline{w'\theta'})_i} d(\overline{w'\theta'})$$

or

$$\frac{d\theta_m}{dt} = \frac{1}{z_i}\left[(\overline{w'\theta'})_s - (\overline{w'\theta'})_i\right] \qquad (2\text{-}18a).$$

For Deardorff's model

$$\frac{d\theta_m}{dt} = \frac{1}{z_o}(\overline{w'\theta'})_s \qquad (2\text{-}18b)$$

These equations assume that longwave radiation and viscous dissipation are negligible sources of potential heat. Since viscous dissipation destroys small scale eddies, the turbulent kinetic energy created by buoyancy is not affected by viscous dissipation and it may be neglected in the "well mixed layer" (Ball, 1960; Lilly, 1968). Following Townsend's analysis the radiative transfer is considered quite small and neglected (Nieuwstadt ,1984). However, doubts have been raised about the magnitude of the radiational contribution even for the daytime periods, leading to the argument that radiation should not be considered negligible (Brutsaert, 1972).

Near the inversion, the potential temperature increases as a result of mixing of stable air from above into the convectively developing unstable boundary layer (entrainment process). When weak thermal activity is eroding a strong inversion but cannot create a significant interfacial layer then $\Delta\theta \to 0$ and $(\overline{w'\theta'})_i \to 0$. This is possible in the laboratory (Deardorff et al 1969) but rare in nature. The process is called encroachment of the stable layer by the unstable layer below. The magnitude of the temperature change $\Delta\theta$ (Fig. 2.3) decreases with time as θ_m increases and

increases (as long as $\Gamma_1>0$) as the inversion height increases (Tennekes and Driendonks, 1980):

$$\frac{d\Delta\theta}{dt}=\frac{\partial\theta}{\partial z}\frac{dz_i}{dt}-\frac{d\theta_s}{dt}$$

or

$$\frac{d\Delta\theta}{dt}=\Gamma_1\frac{dz_i}{dt}-\frac{d\theta_s}{dt} \qquad (2\text{-}19a)$$

Assuming $\frac{(\overline{w'\theta'})_i}{(\overline{w'\theta'})_s}=-E$, $\quad 1\geq E\geq 0$ from (2-18a) and (2-18b) we get

$$\frac{d\Delta\theta}{dt}=\Gamma_1\frac{dz_i}{dt}-\frac{1}{z_i}(1+E)(\overline{w'\theta'})_s$$

or

$$z_i\frac{d\Delta\theta}{dt}=\Gamma_1 z_i\frac{dz_i}{dt}-(1+E)(\overline{w'\theta'})_s$$

or

$$\frac{d}{dt}(z_i\Delta\theta)=\Gamma_1 z_i\frac{dz_i}{dt}+\Delta\theta\frac{dz_i}{dt}-(1+E)(\overline{w'\theta'})_s.$$

But $\Delta\theta\frac{dz_i}{dt}$ is the amount of heat entrained when the inversion height changes by dz_i. Therefore $\Delta\theta\frac{dz_i}{dt}=-(\overline{w'\theta'})_i$ and since

$(\overline{w'\theta'})_i=-E(\overline{w'\theta'})_s$ then $\Delta\theta\frac{dz_i}{dt}=E(\overline{w'\theta'})_s$

Therefore

$$\frac{d}{dt}(z_i\Delta\theta)=\Gamma_1\frac{d(z_i^2/2)}{dt}-(\overline{w'\theta'})_s$$

or

$$(z_i\Delta\theta)_t-(z_i\Delta\theta)_0=\frac{\Gamma_1}{2}z_i^2(t)-\int_0^t(\overline{w'\theta'})_s dt'$$

Assuming $(z_i)_t=0$ when $t=0$, i.e. the nocturnal inversion starts at the surface, when convection, during the daytime

first develops:

$$(z_i\Delta\theta)_t=\frac{\Gamma_1}{2}z_i^2(t)-\int_0^t(\overline{w'\theta'})_s\,dt' \qquad (2\text{-}20)$$

Let $w_e(t)=-\frac{dz_i}{dt}$ be the entrainment rate, and assume that the mean, synoptically induced vertical velocity $w(z)=0$. In general $w(z)+w_e(t)=\frac{dz_i}{dt}$. In the case of encroachment $\Delta\theta=0$ for every $t\geq 0$ and

$$z_i^2(t)=\frac{2}{\Gamma_1}\int_0^t(\overline{w'\theta'})_s\,dt' \qquad (2\text{-}21)$$

When $\Delta\theta(t)\neq 0$, (2-20) becomes

$$z_i(t)=\frac{2}{\Gamma_1}\left\{\frac{\Delta\theta(t)}{2}+\frac{1}{2}\sqrt{[\Delta\theta^2(t)-2\Gamma_1\int_0^t(\overline{w'\theta'})_s\,dt']}\right\},\ z_i(0)=0 \qquad (2\text{-}22)$$

Following Carson(1973) $\Delta\theta(t)=\Gamma_1 z_i(t)\frac{E}{1+2E}$ and (2-20) becomes:

$$z_i^2(t)\Gamma_1\frac{E}{1+2E}=\frac{\Gamma_1}{2}z_i^2(t)-\int_0^t(\overline{w'\theta'})_s\,dt'$$

or

$$\Gamma_1 z_i^2(t)\frac{E}{1+2E}-\frac{\Gamma_1}{2}z_i^2(t)=-\int_0^t(\overline{w'\theta'})_s\,dt'$$

or

$$z_i^2(t)=\frac{2}{\Gamma_1}(1+2E)\int_0^t(\overline{w'\theta'})_s\,dt' \qquad (2\text{-}23)$$

Usually Γ_1 is assumed to be constant or $\Gamma_1(t)=\Gamma_1(0)\exp(\beta t)$, $w(z)=\beta t$ in the stable layer.

In order to determine the mixing height by applying the

zero-order entrainment model we need to be able to derive the analytical functions for Γ_1, $(\overline{w\theta})_s$, and the value of $E=-\frac{(\overline{w\theta})_i}{(\overline{w\theta})_s}$

The first-order entrainment model was developed by Betts(1973). A simplified description is shown in Fig. 2.4. The "entrainment zone" has a thickness Δh with the potential temperature linearly increasing with height up to z_τ above which the stable lapse rate of the free atmosphere Γ_2 takes over. The height z_τ is determined by $(\overline{w\theta})_\tau=0$. The heat budget equations for the mixed layer and the entrainment zone are presented here based on Bett's(1974) equations:

Mixing layer:

$$\frac{d}{dt}(z_i\theta_m)=[(\overline{w\theta})_s-(\overline{w\theta})_i]+\frac{dz_i}{dt}\theta_m$$

Entrainment Layer:

$$\frac{d}{dt}\int_{z_i}^{z_\tau}\theta dz=(\overline{w\theta})_i+\theta_\tau(t)\frac{dz_\tau}{dt}-\theta_m(t)\frac{dz_i}{dt}-\int_{z_i}^{z_\tau}\frac{\Delta\theta}{\Delta h}\tilde{w}dz$$

If $\int_{z_i}^{z_\tau}\theta dz=\Delta z\bar{\theta}$ then

$$\frac{d}{dt}[(z_\tau-z_i)\frac{\theta_m+\theta_\tau}{2}]=(\overline{w\theta})_i+\theta_\tau\frac{dz_\tau}{dt}-\theta_m\frac{dz_i}{dt}-\int_{(z_i)}^{(z_\tau)}\frac{\Delta\theta}{\Delta h}\tilde{w}dz$$

where $\tilde{w}$ is the areal average vertical air velocity assumed constant.

If $\bar{\theta}-\theta_m=\frac{1}{2}\frac{\Delta\theta}{\Delta h}\Delta z$ and $\theta_\tau-\bar{\theta}=\frac{1}{2}\frac{\Delta\theta}{\Delta h}\Delta z$, $\quad\frac{\Delta\theta}{\Delta h}=\gamma=$constant

then

$$\frac{d}{dt}[\Delta z\bar{\theta}]=(\overline{w\theta})_i+[\bar{\theta}+\frac{1}{2}\gamma\Delta z]\frac{dz_\tau}{dt}-[\bar{\theta}-\frac{1}{2}\gamma\Delta z]\frac{dz_i}{dt}-\tilde{w}\gamma\Delta z$$

or

$$(\overline{w\theta})_i=\Delta z\frac{d\bar{\theta}}{dt}+\bar{\theta}\frac{d\Delta z}{dt}-\gamma\Delta z\frac{dz_i}{dt}+\tilde{w}\gamma\Delta z$$

or

$$\frac{dz_i}{dt}=\frac{1}{\gamma}[\frac{d\bar{\theta}}{dt}+\bar{\theta}\frac{1}{\Delta z}\frac{d\Delta z}{dt}-\frac{1}{\Delta z}(\overline{w'\theta'})_i]+\tilde{w}$$

or

$$\frac{dz_i}{dt}=\frac{1}{\gamma}[\frac{d}{dt}(\theta_\tau-\frac{\Delta\theta}{2})+\bar{\theta}\frac{1}{\Delta z}\frac{d\Delta z}{dt}-\frac{1}{\Delta z}(\overline{w'\theta'})_i]+\tilde{w}$$

$$=\frac{1}{\gamma}[\frac{d\theta_\tau}{dt}-\frac{d}{dt}(\frac{\Delta\theta}{2}+\bar{\theta}\frac{d\ln\Delta z}{dt}-\frac{1}{\Delta z}(\overline{w'\theta'})_i]+\tilde{w}$$

$$=\frac{1}{\gamma}[(\frac{dz_\tau}{dt}-\tilde{w})\Gamma_2+\bar{\theta}\frac{d\ln\Delta z}{dt}-\frac{1}{\Delta z}(\overline{w'\theta'})_i]+\tilde{w}$$

$$=\frac{1}{\gamma}[(\frac{dz_i}{dt}+\frac{d\Delta z}{dt}-\tilde{w})\Gamma_2-(\overline{w'\theta'})_i]+\tilde{w}$$

or

$$\frac{dz_i}{dt}-\frac{\Gamma_2}{\gamma}\frac{dz_i}{dt}=-\tilde{w}\frac{\Gamma_2}{\gamma}-\frac{(\overline{w'\theta'})_i}{\gamma\Delta z}+\tilde{w}+\frac{\Gamma_2}{\gamma}\frac{d\Delta z}{dt}+\frac{\bar{\theta}}{\gamma}\frac{d\ln\Delta z}{dt}$$

if

$C=\tilde{w}(1-\frac{\Gamma_2}{\gamma})$, then

$$\frac{\gamma-\Gamma_2}{\gamma}\frac{dz_i}{dt}=\frac{E}{\gamma\Delta z}(\overline{w'\theta'})_s+C+\frac{1}{\gamma}(\Gamma_2\frac{d\Delta z}{dt}+\frac{d\ln\Delta z}{dt})$$

or

$$\frac{dz_i}{dt}=\frac{E}{\Delta z(\gamma-\Gamma_2)}(\overline{w'\theta'})_s+C'+\frac{1}{\gamma-\Gamma_2}(\Gamma_2\frac{d\Delta z}{dt}+\frac{d\ln\Delta z}{dt}),\quad C'=\frac{C\gamma}{(\gamma-\Gamma_2)}$$

By integrating dz_i and assuming that Δz is constant and equals to Δh we get

$$z_i(t)-z_i(0)=E'\int_0^t(\overline{w'\theta'})_s dt+C't,\quad E'=\frac{E}{\Delta z(\gamma-\Gamma_2)}$$

Assume $z_i(0)=0$ at $t=0$ and we get

$$z_i(t)=E'\int_0^t(\overline{w'\theta'})_s dt+C't \qquad (2\text{-}24)$$

with $\tilde{w}$, $\Delta\theta$, Δz, E, γ and Γ_2 assumed constants.
To derive the mixing height by the first-order model we have to determine the parameters E', C', which may be assumed constants as long as $\tilde{w}, \Delta\theta, \Delta z, \gamma, \Gamma_2, E$ are constants.

The second-order entrainment model was developed by Deardorff(1979) and was illustrated in Fig. 2.5.
For the mixed layer

$$\frac{d\theta_m}{dt}=\frac{1}{z_0}(\overline{w'\theta'})_s \qquad (2\text{-}25)$$

since $(\overline{w'\theta'})_s=0$ at z_0. As in the first-order model, the assumption is made that $(\overline{w'\theta'})_T=0$. If we include the entrainment zone we may describe the potential temperature in the range $\theta_T\geq\bar{\theta}\geq\theta_m$ by $\bar{\theta}=\theta_m+f(z,t)\Delta\theta$, $1\geq f\geq 0$
For the entrainment zone, assuming no other heat sources or sinks but the turbulent heat flux,

$$\frac{D\bar{\theta}}{Dt}=-\frac{\partial(\overline{w'\theta'})}{\partial z} \qquad (2\text{-}26)$$

and

$$\frac{d\Delta\theta}{dt}=\Gamma_2\left(\frac{dz_0}{dt}-\bar{w}_0+\frac{d\Delta h}{dt}\Delta w\right)-\frac{(\overline{w'\theta'})_s}{z_0}$$

The vertical velocity $\bar{w}$ is assumed to vary linearly with height:

$$\bar{w}(z)=\bar{w}(z_0)+[\bar{w}(z_T)-\bar{w}(z_0)]\frac{z-z_0}{z_T-z_0}$$

According to the other models: $\Delta\theta=\theta_T-\theta_m$, $\Delta h=z_T-z_0$,

$\Delta w=\bar{w}(z_\tau)-\bar{w}(z_0)$ and $Y=\frac{1}{\Delta h_{(z_0)}}\int^{(z_\tau)} f(z,t)dz$

Recall the Leibnitz rule for differentiation of an integral:

$$\frac{d}{ds}\left[\int_{a(s)}^{b(s)} f(x,s)dx\right]=\int_{a(s)}^{b(s)}\frac{\partial}{\partial s}f(x,s)dx-f(a,s)\frac{da}{ds}+f(b,s)\frac{db}{ds}$$

and apply it in (2-26) i.e. $\frac{\partial\bar{\theta}}{\partial t}+\bar{w}\frac{\partial\bar{\theta}}{\partial z}=-\frac{\partial}{\partial z}(\overline{w'\theta'})$:

$$\int_{z_0}^{z_\tau}\frac{\partial\bar{\theta}}{\partial t}dz=\frac{d}{dt}\left(\int_{z_0}^{z_\tau}\bar{\theta}dz\right)+\theta_*\frac{dz_0}{dt}-\theta_\tau\frac{dz_\tau}{dt}$$

After rearrangement we get

$$\int_{z_0}^{z_\tau}\frac{\partial\bar{\theta}}{\partial t}dz=\frac{\Delta h}{z_0}(\overline{w'\theta'})_*+Y\Delta h\frac{d\Delta\theta}{dt}-(1-Y)\Delta\theta\frac{d\Delta h}{dt}+\Delta\theta\Delta h\frac{dY}{dt}-\Delta\theta\frac{dz_0}{dt} \quad (2\text{-}27)$$

Also after some substitutions we get

$$\int_{z_0}^{z_\tau}\bar{w}\frac{\partial\bar{\theta}}{\partial t}dz=\bar{w}_0\Delta\theta+\frac{\Delta w}{\Delta h}[\Delta h\Delta\theta-\Delta\theta\Delta hY]=\bar{w}_0\Delta\theta+\Delta w(1-Y)\Delta\theta \quad (2\text{-}28)$$

Finally

$$-\int_{(z_0)}^{(z_\tau)}\frac{\partial(\overline{w'\theta'})}{\partial z}dz=(\overline{w'\theta'})_0-(\overline{w'\theta'})_T=0$$

Therefore by integrating (2-26) and substituting (2-27) and (2-28) we get:

$$\Delta\theta\frac{dz_0}{dt}-\Delta\theta\bar{w}_0=\frac{\Delta h}{z_0}(\overline{w'\theta'})_*+Y\Delta h\frac{d}{dt}(\Delta\theta)-(1-Y)\Delta\theta\left(\frac{d\Delta h}{dt}-\Delta w\right)+\Delta\theta\Delta h\frac{dY}{dt}$$

Deardorff's(1979) experiments indicate that $z_0\Delta\theta\frac{dY}{dt}=0.05(\overline{w'\theta'})_*$ and the term $\frac{dY}{dt}$ may be neglected since

imperfections of the model count for an error of ≈20%

By substituting $\frac{d\Delta\theta}{dt}$ and replacing $\frac{\Gamma_\theta}{\Delta\theta/\Delta h}=G$ we get:

$$(1-YG)\Delta\theta\left(\frac{dz_o}{dt}-\bar{w}_o\right)=\frac{\Delta h}{z_o}(1-Y)\left(\overline{w'\theta'}\right)_s-(1-Y-YG)\Delta\theta\left(\frac{d\Delta h}{dt}-\Delta w\right) \quad (2\text{-}29)$$

Assuming as an approximation that $Y=0.55\exp(-0.27G)$ with G varying within the limits $3.7\geq G\geq 0$ (Deardorff, 1979) we get for G=0, Y=0.55 and for G=3.7, Y=0.20 [Deardorff(1979) reports 0.40] and $0.75\geq GY\geq 0$

For the minimum and maximum relative stratification G we get the following values:

G	Y	GY	1-GY	1-Y	1-Y-GY
0	0.55	0	1	0.45	0.45
3.7	0.20	0.75	0.25	0.80	0.05

and (2-29) becomes:

for G=0

$$\Delta\theta\left(\frac{dz_o}{dt}-\bar{w}_o\right)=\frac{\Delta h}{z_o}0.45\left(\overline{w'\theta'}\right)_s-0.45\Delta\theta\left(\frac{d\Delta h}{dt}-\Delta w\right) \quad (2\text{-}30a)$$

and for G=3.7

$$0.25\Delta\theta\left(\frac{dz_o}{dt}-\bar{w}_o\right)=\frac{\Delta h}{z_o}0.8\left(\overline{w'\theta'}\right)_s-0.05\Delta\theta\left(\frac{d\Delta h}{dt}-\Delta w\right) \quad (2\text{-}30b)$$

By using the convective velocity scale w_*, and $\alpha=\frac{\Delta h}{z_o}$ and

rearranging (2-29) we get

$$\frac{\frac{dz_o}{dt}-\bar{w}_o}{w_*}=\alpha\frac{1-\gamma}{1-\gamma G}\frac{(\overline{w'\theta'})_s}{w_*\Delta\theta}-\frac{1-\gamma-\gamma G}{1-\gamma G}\frac{\frac{d\Delta h}{dt}-\Delta w}{w_*} \qquad (2\text{-}31)$$

By employing a turbulence Richardson number $R\equiv\frac{g}{\theta}\frac{\Delta\theta z_o}{w_*^2}$

we find: $R^{-1}=\frac{(\overline{w'\theta'})_s}{w_*\Delta\theta}$ and (2-31)becomes:

$$\frac{\frac{dz_o}{dt}-\bar{w}_o}{w_*}=\alpha\frac{1-\gamma}{1-\gamma G}R^{-1}-\frac{1-\gamma-\gamma G}{1-\gamma G}\frac{\frac{d\Delta h}{dt}-\Delta w}{w_*}$$

We need also to parameterize $\frac{d\Delta h}{dt}=\Delta w+w_*Q\alpha R^{-1}$ (Deardorff,1979) where $Q=[(\frac{1-\gamma}{1-G\gamma})^{0.4}-(\frac{1-\gamma}{1-G\gamma})]\frac{1-G\gamma}{\gamma}$ which ultimately depends on the relative stratification G. Furthermore, αR^{-1} is related to the relative stratification as follows: $G\equiv\alpha R^{-1}S$ where S is the ratio of the convective time scale with respect the Brunt-Vaisala time scale:

$$S=\frac{g}{\theta}\Gamma_3\frac{z_*^2}{w_*^2}=\frac{z_o^2/w_*^2}{\theta/g\Gamma_3}$$

Therefore

$$\frac{\frac{dz_o}{dt}-\bar{w}_o}{w_*}=\frac{G}{S}\{\frac{1-\gamma}{1-G\gamma}-\frac{(1-\gamma-G\gamma)}{\gamma}[(\frac{1-\gamma}{1-G\gamma})^{0.4}-\frac{1-\gamma}{1-G\gamma}]\} \qquad (2\text{-}32)$$

and for the minimum and maximum stratification we get the following equations:

for G=0 $\frac{dz_o}{dt}=\bar{w}_o$ and for G=3.7 $\frac{dz_o}{dt}-\bar{w}_o=w_*\frac{26.27}{S}$

or

$$z_o\Gamma_3[\frac{dz_o}{dt}-\bar{w}_o]=26.27(\overline{w'\theta'})_s$$

Assuming Γ_3=constant we integrate and get

$$[\frac{z_0^2}{2}]_0^t = {}_0\int^t \bar{w}_0 z_0 dt + \frac{26.27}{\Gamma_3}\,{}_0\int^t (\overline{w\,\theta})_s dt \qquad (2\text{-}33)$$

If $z_0(0)=0$ and taking the mean vertical velocity $\bar{w}_0=0$, then

$$z_0^2(t) = \frac{52.54}{\Gamma_3}\,{}_0\int^t (\overline{w\,\theta})_s dt \qquad (2\text{-}34)$$

To derive the mixed height through (2-34) it is necessary to know Γ_3 and $(\overline{w\,\theta})_s$ for a maximum relative stratification. For an intermediate relative stratification, with no mean vertical velocity, and for a nocturnal inversion $z_0(0)=0$, (2-32) may be written as:

$$z_0^2(t) = \frac{2}{\Gamma_3}\{\frac{G(1-Y)}{1-GY} - \frac{G}{Y}[(1-Y-GY)[(\frac{1-Y}{1-GY})^{0.4} - \frac{1-Y}{1-GY}]]\}\,{}_0\int^t (\overline{w\,\theta})_s dt \qquad (2\text{-}35)$$

assuming Γ_3 is constant and that G,Y are specific parameters.

3. Experiment

3.1 Introduction

The purpose of the experiment was to compare field measurements with model predictions. Effort was made to ensure that proper weather conditions (clear skies and light winds) prevailed throughout the experimental period. Minisondes were used to take sequential observations of temperature at a series of heights in the lower atmospheric boundary layer during the morning erosion of the nocturnal inversion.

The focal area of our experimental program was a block of land (0.1km^2) located in the outskirts, some twelve kilometers south-west of the city of Edmonton, Alberta. This site was made available to the author through the kindness of the Air Pollution Division of Alberta Environment.
Site geophysical information follows:

Latitude and Longitude: 53° 25′ 35″N, 113° 34′ 37″ W

Elevation : 687.3m

Mean solar time : MST minus 34.4min

3.2 Topography of the area

The general disposition of the observing group is shown in Fig. 3.1 Most of the observations were made under surface wind conditions with westerly components. The location with respect the city of Edmonton is shown in Fig. 3.2. The area at large is devoid of trees. At the eastern border of the

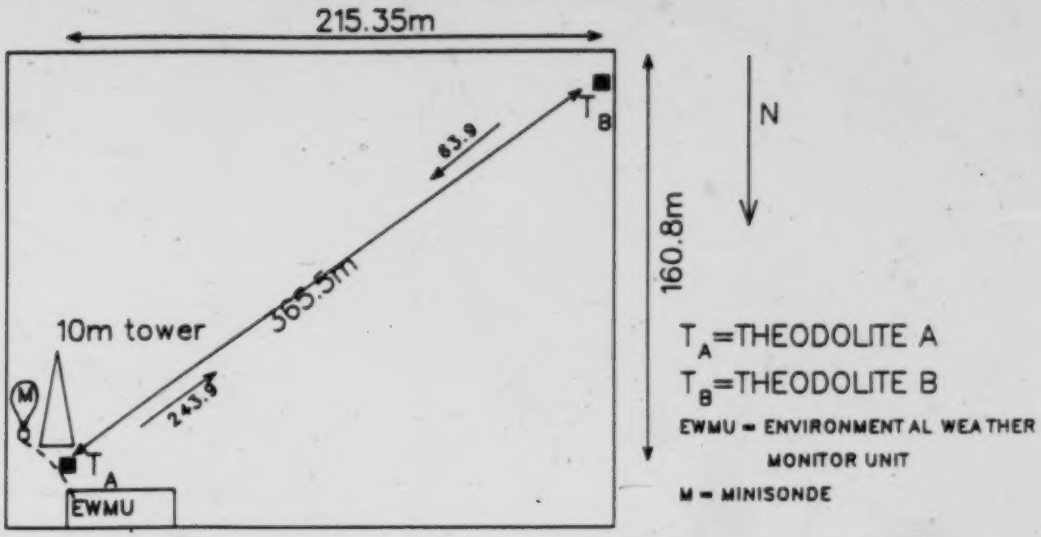

Fig. 3.1 Array of surface and air sampling equipments at the field site.

section a line of trees separates our area from the next farmland. Their height did not exceed 3-4m. Above this line of trees, power lines exist in a north-south direction. To the north and west the area is devoid of trees for a distance greater than 500m. To the south, a road separates our site from a country house (brothel) protected by wooden fences and low trees near the roadside. In general, within a circle of 500m (Fig. 3.3) the relief changes by no more than ±5m except in the southeastern region that encompasses the west bank of Whitemud creek.

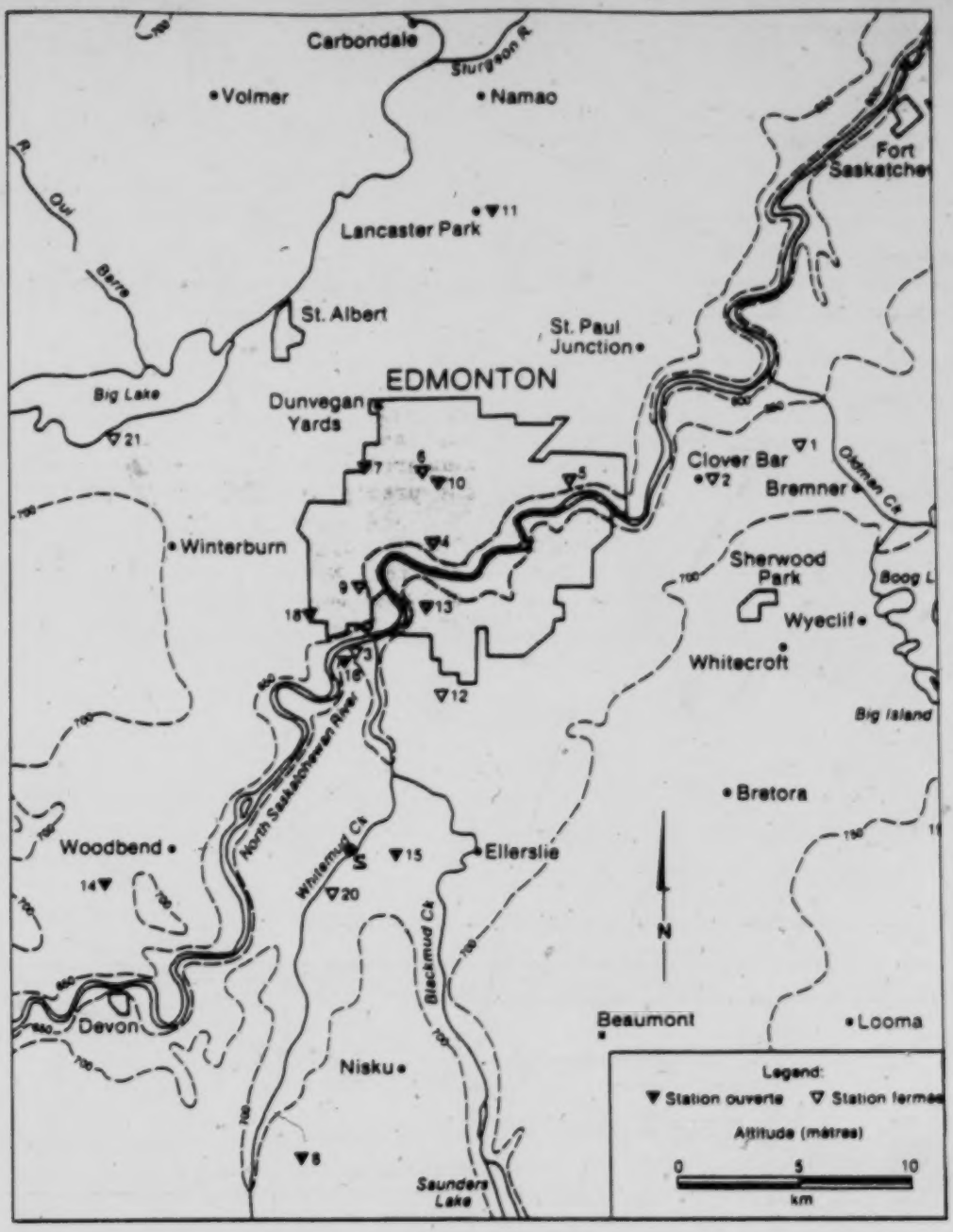

Fig. 3.2 Topographical and physical features and location of climatological stations in the Edmonton area. The area where the experiment was executed is depicted by the letter S, Olsen(1985).

3.3 Climatology of Edmonton

The climate of Edmonton is continental, typical for the interior of large continents in middle latitudes. The Edmonton area is subject to large contrasts in temperatures and rainfall. This is mainly due to the physical barrier of the Western Cordillera, to the westerly flow of air. The main air masses determining the climate of Edmonton are: the cool moist Pacific, the cold, dry Arctic and the warm, dry American continental. Climatologically speaking, spring and autumn are defined as transitional periods with mean daily temperatures ranging between 0°C and 18°C. Autumn is sunny with frequent intense nocturnal radiational inversions. Frost may occur within the two middle weeks of October and in fact was observed during the first hour of some experimental days. On the average, October has sixteen days with frost. October is the driest month of the season with 50% of the Octobers (Olson, 1985) having less than six days with precipitation. Following the normal rainfall decrease in September, October is the transition month to snow precipitation in November. Mean daily freezing temperatures occur near the last ten days of October, well beyond our last experimental days. October has the highest percentage of hours with clear skies. On the average, clear to partly cloudy skies are reported on 50% of all days. Relatively high wind speeds (averaging 14.3km/h) occur in the early fall. October falls in this range, well within our ideal conditions. Figures 3.4 and 3.5 depict surface temperatures

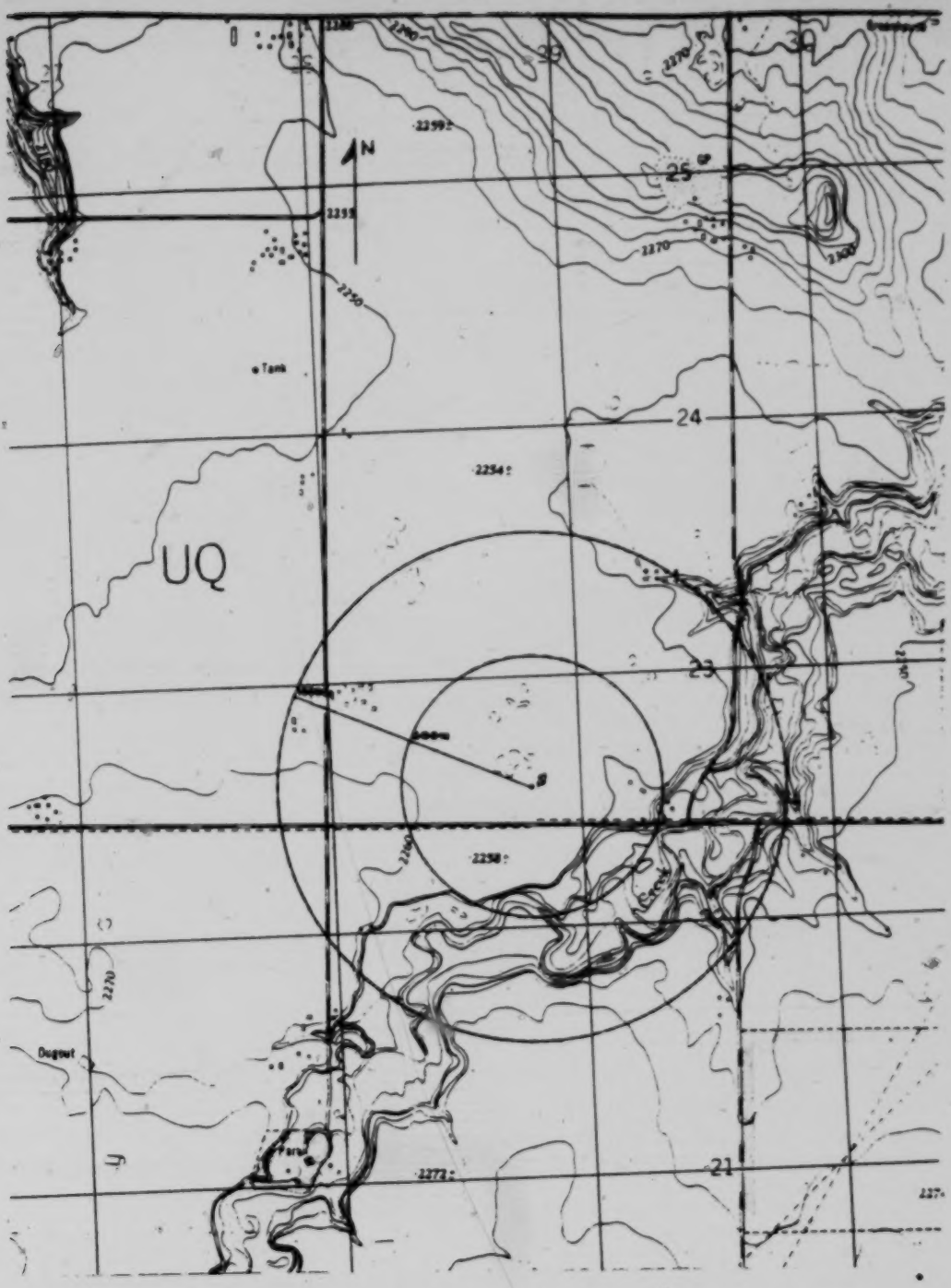

Fig. 3.3 A more detailed description of the area where the experiment was executed. S is the location of the station.

and winds for autumn. The data used were for the climatic period 1971-1980 recorded by Atmospheric Environment Service, Environment Canada.

3.4 Scheduling of observations. Experimental program.

From a theoretical point of view weather conditions should be such as to justify the simple radiational model presented by Brunt for nighttime and the convection model during the day, described in Chapter 2. In addition an ideal observation period should be characterized by a large diurnal variation of the heat fluxes at the earth-air interface. As noted in Chapter 2, ideal conditions are described as (a) clear skies (b) calm winds. In practice, emphasis was given to these two conditions. However,

	Speed	Freq%
N	17.4	4.7
NNE	14.1	2.2
NE	13.1	2.9
ENE	13.1	2.5
E	12.5	3.0
ESE	13.9	2.8
SE	15.0	4.1
SSE	16.3	5.9
S	12.9	14.8
SSW	10.5	8.9
SW	9.9	7.2
WSW	12.1	4.8
W	14.3	8.9
WNW	20.2	9.6
NW	19.6	8.3
NNW	20.5	5.6
CALM	—	4.6

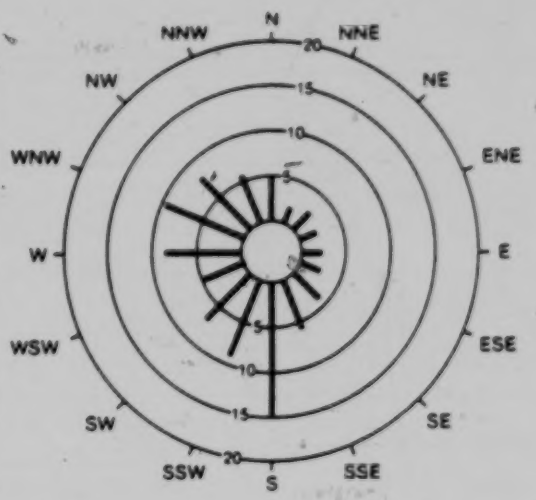

Fig. 3.4 Autumn winds (From "The climate of Edmonton" Olsen (1985))

periodically scattered clouds were present during the experiments. The wind was always below 4msec^{-1} (about 15km/h) at 10m height.

Table 3.1 Instruments and priority of measured quantities

Instrument	Priority	Quantity measured
Minisonde	1	Temperature vs. height.
Double Theodolite	1	Azimuth and elevation of minisonde
Acoustic Sounder	2	Altitude, mean horizontal wind speed, mean vertical wind speed. Averaging interval 15min.
Net radiometer, Funk type	1	Net radiation, incoming solar radiation.
Sonic Anemometer, Thermometer	1	Turbulent heat flux (Tower data, 10m)
Mercury thermometer	1	Surface temperature at screen height.
Hygrometer	1	Relative humidity at screen height
Propellor anemometer	2	Wind components. Averaging time 30min (Tower data)
Thermohygrograph	1	Temperature, relative humidity in Stevenson's Screen.
Assman Psychrometer	2	Dry bulb, wet bulb temperatures near surface
Barometer	2	preasure
Ventilated thermometer	2	Temperature at 8m

The observations were scheduled to start before sunrise in order to aquire a nocturnal inversion profile and to continue approximately till noon or earlier if the inversion base were lifted up to or greater than 500m. I employed two sets of data to test my model. One set was provided by the Atmosphric Environment Service. The data were from the rural area around Edmonton during the month of November 1974. The second set consists of a total of four observation days. The experiments were prepared and executed with the assistance of Mr J. Godin, technician of the Air Pollution Division,

Alberta Environment and responsible for this environment weather monitor unit. The last two observation days were executed by the author. Minisonde observations were taken every 45 minutes. Table 3.1 presents a description of the experimental program as far as instruments is concerned. Table 3.2 presents a summary of the measurements and data. "A" indicates that the instrument was active and tabulated data are complete or nearly complete, "a" indicates that instrument was active during less than half of the period, and "O" indicates that the instrument was on the site but

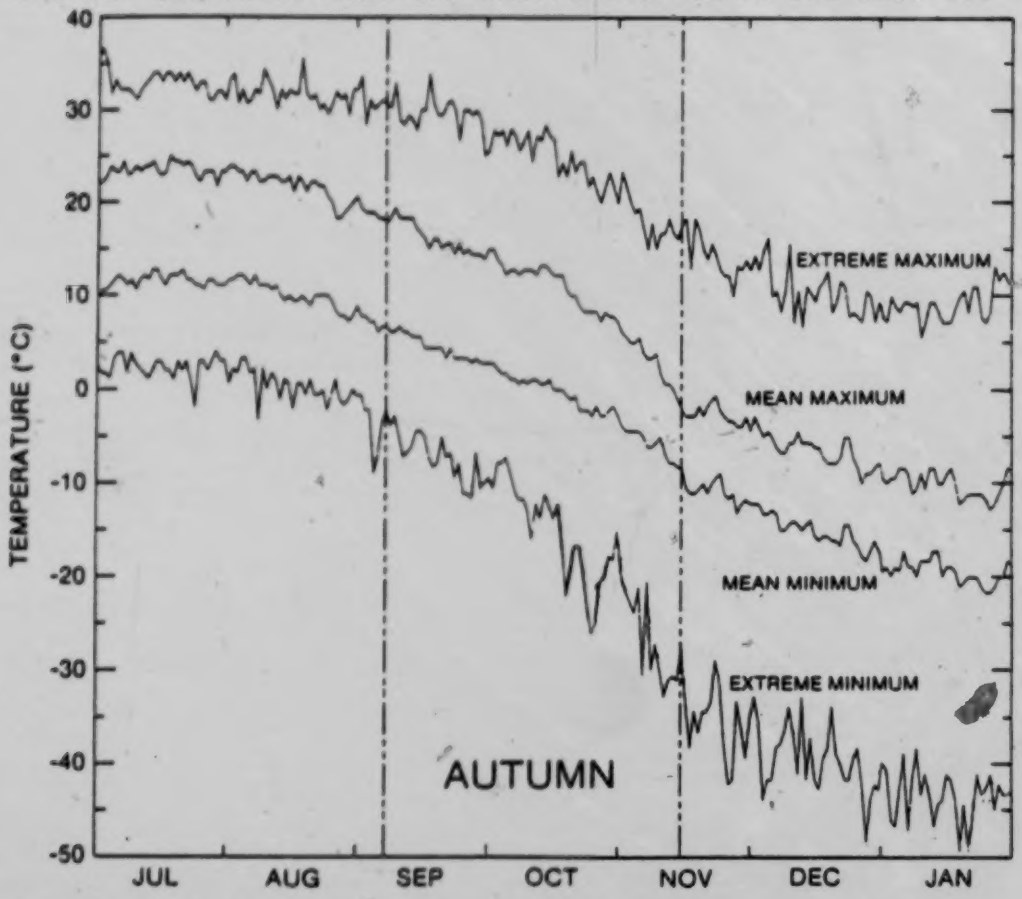

Fig. 3.5 Autumn Temperatures (From "The climate of Edmonton"; Olsen (1985))

inactive, or no data are available due to failure or other reasons.

3.5 Observation periods

3.5.1 First general observation period

Date :October 2, 1987

Sunrise (MST) :0637

Apparent noon (MST):1250

3.5.1.1 Summary of synoptic conditions

During the first general observation period, central Alberta was under the influence of a maritime polar air mass. The circulation was dominated by a low pressure center located over Great Bear Lake in the Northwest Territories and a high pressure cell located over central North Dakota. At 0600 MST, a cold front oriented north-south was situated in British Columbia, moving southeast. The sky conditions were clear for the entire period. The small pressure gradient provided light SSW winds. The relative humidity decreased from ≃100% to ≃40% near the end of the period (see Fig. 3.6 and 3.7)

3.5.1.2 Relevant data

a) Direction (deg from North) and speed (m/sec) of the surface wind from a propellor anemometer at 10m height are listed in Table 3.3

Table 3.2 Summary of measurements and data

Table No	Instrument and type of data	GENERAL OBSERVATION PERIOD/ CUMMULATIVE MINISONDE RELEASE NUMBER																							
		October 2,1987							October 3,1987						October 6,1987						October 12,1987				
		1	2	3	4	5	6	7	8	9	10	11	12	13	14	15	16	17	18	19	20	21	22	23	24	26
A.1	Minisonde temperature data	A	A	A	A	A	A	A	A	A	A	A	A	A	A	A	A	A	A	A	A	A	A	A	A	A
A.2	Double Theodolite Azimouth & Elevation	A	A	A	A	A	A	A	a	o	o	o	o	o	o	o	o	o	o	o	o	o	o	o	o	o
A.3	Single Theodolite	A	A	A	A	A	A	A	A	A	A	A	A	A	A	A	A	A	A	A	A	A	A	A	A	A
A.4	Net radiometer	A	A	A	A	A	A	A	A	A	A	A	A	A	A	A	A	A	A	A	A	A	A	A	A	A
A.5	Sonic anemometer thermometer	o	o	o	o	o	o	o	o	o	o	o	o	o	o	o	o	o	o	o	o	o	o	o	o	o
A.6	Thermometer Screen temperature	A	A	A	A	A	A	A	A	A	A	A	A	A	A	A	A	A	A	A	A	A	A	A	A	A
A.7	Hygrometer Relative Humidity	A	A	A	A	A	A	A	A	A	A	A	A	A	A	A	A	A	A	A	A	A	A	A	A	A
A.8	Thermohygrograph screen temperature	A	A	A	A	A	A	A	A	A	A	A	A	A	A	A	A	A	A	A	A	A	A	A	A	A
A.9	Thermohygrograph screen rel. humidity	A	A	A	A	A	A	A	A	A	A	A	A	A	A	A	A	A	A	A	A	A	A	A	A	A
A.10	Pressure	A	A	A	A	A	A	A	A	A	A	A	A	A	A	A	A	A	A	A	A	A	A	A	A	A
A.11	Ventilated temperature at 8m	A	A	A	A	A	A	A	A	A	A	A	A	A	A	A	A	A	A	A	A	A	A	A	A	A
A.12	Ashman Psychrometer Td near surface	o	o	o	o	o	o	o	o	o	o	o	o	o	A	A	A	A	A	A	A	A	A	A	A	A
A.13	Ashman Psychrometer Tw near surface	o	o	o	o	o	o	o	o	o	o	o	o	o	A	A	A	A	A	A	A	A	A	A	A	A
A.14	Propellor anemometer wind components	A	A	A	A	A	A	A	A	A	A	A	A	A	A	A	A	A	A	A	A	A	A	A	A	A

This page has been removed
due to poor print quality

Fig. 3.6 Synoptic surface conditions on October 2, 1987 at 1200Z.

Table 3.3 Wind measurements at 10m

TIME(MST):	0617	0700	0745	0830	0915	1000	1045
DIRECTION:	187	189	181	191	193	213	251
SPEED :	2.3	2.9	2.1	2.6	1.7	2.3	2.4

b) Double theodolite minisonde temperature at indicated height (m), for the first approximately 4 min. of ascent are listed in Table 3.4

Table 3.4 Minisonde temperature data based on an assumed rate of ascent of 3m/s

H m	T_{0617} °C	T_{0700} °C	T_{0745} °C	T_{0830} °C	T_{0915} °C	T_{1000} °C	T_{1045} °C
SFC	5.0	5.9	8.1	10.5	12.9	16.8	20.1
30	6.2	6.4	8.2	10.5	12.9	16.6	19.7
60	9.0	8.9	9.4	11.1	14.3	16.0	19.2
90	11.2	11.7	11.4	14.0	15.1	15.8	18.8
120	12.8	13.8	13.0	16.2	15.3	15.8	18.7
150	13.7	15.2	14.4	17.4	15.4	16.0	18.7
180	14.5	16.6	15.6	18.7	16.2	18.3	18.7
210	15.6	17.9	16.5	19.5	17.3	20.7	18.7
240	16.9	18.5	17.3	19.9	18.7	21.7	18.7
270	17.8	18.9	18.0	20.3	19.4	21.9	18.8
300	18.4	19.5	18.6	20.5	19.8	22.0	20.0
330	18.7	20.0	19.0	20.4	19.9	22.0	21.6
360	19.5	20.1	19.3	20.3	19.9	22.0	22.1
390	19.7	20.2	19.4	20.2	20.1	22.0	22.2
420	19.7	20.4	19.4	20.5	20.1	22.0	22.2
450	19.7	20.5	19.4	21.1	20.0	22.0	22.2
480	19.7	20.5	19.5	21.3	19.9	21.8	22.1
510	19.6	20.4	19.7	21.6	19.9	21.9	22.1
540	19.6	20.3	19.9	21.7	19.8	22.1	22.0
570	19.6	20.2	20.0	21.8	19.7	22.1	19.8
600	19.6	20.3	20.2	21.7	19.6	22.0	19.7
630	19.6	20.7	20.2	21.7	19.6	21.7	19.7
660	19.6	20.9	20.2	21.6	19.5	21.3	19.7
690	19.5	20.9	20.1	21.5	19.3	21.3	19.6

c)Table 3.5 presents measurements of standard shelter

This page has been removed
due to poor print quality

Fig. 3.7 Radiosonde of Stony Plain (WSE) on October 2, 1987 at 1200Z (temperature history T_H is valid at 0000Z)

temperature(°C), wet bulb temperature(°C) relative humidity(%) from Feuchte type hygrometer, station surface pressure(kpa), ventilated temperature at 8m(°C)

Table 3.5 Temperature, humidity and pressure at the surface at the onset of the minisonde releases

MST	Temp. °C	T_w °C	T_s °C	R.H. %	Pressure kpa
0617	5.0	5.2	6.4	100	93.13
0700	5.2	5.3	5.9	100	93.13
0745	6.2	6.0	8.3	96	93.12
0830	9.1	7.6	9.4	81	93.12
0915	15.4	10.3	-	43	93.12
1013	17.8	11.8	-	38	93.11
1046	19.7	12.4	20.0	34.5	-
1100	21.2	12.4	-	33	-

3.5.2 Second general observation period

Date :October 3, 1987

Sunrise (MST) :0639

Apparent noon (MST):1249

3.5.2.1 Summary of synoptic conditions.

During the second general observation period, central Alberta remained under the influence of the maritime polar air mass modified considerably during the previous 24 hours. It became warmer and drier. The circulation was dominated by a series of low pressure centers to the north and a series of high pressure centers to the south. A low pressure center was located near the border of Manitoba and the Northwest Territories west of the coast of Hudson Bay. Another low pressure center was located northwest of Great

This page has been removed
due to poor print quality

Fig. 3.8 Synoptic surface conditions on October 3, 1987 at 1200Z.

Slave Lake, in the midway from the border of the Northwest Territory and Yukon Territory. A frontal line connecting the two low centers extended south through Eastern British Columbia and through Eastern Manitoba. To the south a high pressure center was situated just west of the coast of Washington and another main high pressure center was situated over Iowa. Central Alberta was influenced by a northwesterly flow with light winds. The sky conditions in central Alberta were overcast clearing to the south. Throughout the province of Alberta convective activity was reported as a result of an approaching upper cold front (Fig. 3.8,3.9). At the site, the experiment was initiated with less of 1/10 sky cover and ended with overcast conditions. The relative humidity decreased from 91% to 55% at the end of the second general observation period.

3.5.2.2 Relevant data

a) Table 3.6 presents information on the direction (deg from North) and speed (m/s) of the surface wind from a propellor anemometer at 10m height.

Table 3.6 Wind data at 10m height

TIME(MST):	0630	0700	0803	0837	0915	1001
DIRECTION:	212	220	149	270	090	090
SPEED:	1.3	1.2	1.3	0.4	0.1	0.4

b) Double theodolite minisonde temperatures at indicated heights (m), for the first approximately 4 min. of ascent

This page has been removed
due to poor print quality

Fig. 3.9 Radiosonde of Stony Plain (WSE) on October 3, 1987 at 1200Z (temperature history T_H is valid at 0000Z)

are listed in Table 3.7

Table 3.7 Minisonde data based on an assumed rate of ascent of 3 m/s

H m	T_{0615} °C	T_{0700} °C	T_{0803} °C	T_{0837} °C	T_{0915} °C	T_{1001} °C
SFC	7.2	5.3	7.3	10.2	16.4	17.9
30	12.4	10.8	7.4	8.8	16.0	17.2
60	16.8	14.8	9.0	9.2	15.9	16.7
90	19.0	16.8	10.0	10.5	17.1	16.8
120	20.4	17.8	12.3	11.8	17.8	16.9
150	21.2	18.4	13.6	12.5	18.2	17.0
180	22.2	18.8	14.5	12.9	18.5	17.2
210	22.8	19.3	14.9	13.2	18.7	17.3
240	23.0	19.4	15.2	13.5	19.0	17.3
270	23.0	19.4	15.5	13.9	19.2	17.2
300	22.9	19.3	15.7	14.0	19.4	17.2
330	22.7	19.2	15.8	14.0	19.5	17.1
360	22.4	19.1	15.6	13.8	19.5	17.1
390	22.2	19.0	15.4	13.7	19.4	17.0
420	22.0	18.8	15.2	13.5	19.3	16.8
450	21.8	18.6	15.0	13.2	19.2	16.6
480	21.5	18.4	14.9	13.0	18.9	16.3
510	21.3	18.1	14.7	12.9	18.7	16.1
540	21.0	17.9	14.5	12.8	18.6	15.8
570	20.8	17.7	14.3	12.7	18.3	15.6
600	20.6	17.5	14.1	12.5	18.1	15.4
630	20.4	17.3	14.0	12.3	17.9	15.3
660	20.2	17.2	13.8	12.1	17.9	15.3
690	20.2	17.2	13.8	12.1	17.6	15.1

c)Table 3.8 presents measurements of standard shelter temperature(°C), wet bulb temperature(°C), relative humidity(%) from Feuchte type hygrometer, station surface pressure(kpa), ventilated temperature at 8m(°C)

Table 3.8 Surface temperature, relative humidity and pressure during the minisonde releases

MST	Td °C	Tw °C	T_s °C	R.H. %	Pressure Kpa
0615	4.2	3.2	8.1	91	93.09
0700	5.3	4.0	7.4	93	93.08
0741	5.6	4.7	-	-	-
0803	-	-	-	-	-
0824	9.8	7.5	9.8	81	93.08
0928	16.0	10.2	13.5	56	93.08
1000	17.0	11.5	14.8	54	93.06

3.5.3 Third general observation period

Date :October 6, 1987

Sunrise (MST) : 0644

Apparent noon (MST): 1248

3.5.3.1 Summary of synoptic coditions.

During the third general observation period, central Alberta was under the influence of a maritime polar air mass. The circulation was dominated by a high pressure center north of Calgary. A near stationary front was oriented from northwest to southeast across Northern Alberta (Fig. 3.10) An upper warm front was situated along a line connecting Jasper with Rocky Mountain House and extending north of Calgary. The winds remained light and the sky was half covered with cirrus and altocumulus. Nocturnal radiation had resulted in an inversion up to about 170m topped by a nearly pseudoadiabatic lapse rate (Fig. 3.11). The relative humidity decreased from 90% to

This page has been removed
due to poor print quality

Fig. 3.10 Synoptic surface conditions on October 6, 1987 at 1200Z.

47% near the end of the experimental period.

3.5.3.2 Relevant data

a)Table 3.9 presents data on the direction (deg from North) and speed (m/s) of the surface wind from a propellor anemometer at 10m height.

Table 3.9 Wind measurements at 10m

TIME(MST):	0615	0700	0746	0830	0915	1000
DIRECTION:	273	273	236	223	270	310
SPEED:	2.7	1.5	1.2	0.2	0.2	1.3

b) Table 3.10 contains data on standard shelter temperature (°C), wet bulb temperature (°C), relative humidity (%) from Feuchte type hygrometer, station surface (kpa), ventilated temperature at 8m (°C)

Table 3.10 Temperature, humidity and pressure at the surface on the onset of the minisonde releases

MST	Temp. °C	T_v °C	T_s °C	R.H. %	Pressure kpa
0615	0.7	0.4	2.3	89	94.24
0700	0.7	-0.2	1.7	83.5	94.25
0746	2.5	1.3	2.6	87	94.24
0830	5.0	2.8	4.1	75	94.26
0915	6.6	3.8	5.9	51	94.28
1000	8.1	7.8	8.1	44	94.26

c) Double theodolite minisonde temperatures at indicated heights (m), for first approximately 4min of ascent are listed in Table 3.11

This page has been removed
due to poor print quality

Fig. 3.11 Radiosonde of Stony Plain (WSE) on October 6, 1987 at 1200Z (temperature history T_H is valid at 0000Z)

listed in Table 3.11

Table 3.11 Minisonde temperature data based on an assumed rate of ascent 3 m/s

H m	T_{0815} °C	T_{0700} °C	T_{0745} °C	T_{0830} °C	T_{0815} °C	T_{1000} °C
SFC	8.9	2.2	2.6	4.8	8.9	8.8
30		3.4	2.9	3.8	7.3	8.2
45	9.8					
60		4.8	3.4	3.4	6.3	7.6
90	11.3	5.8	4.2	3.2	6.0	7.0
120		6.9	5.2	3.1	5.7	6.8
135	12.3					
150		7.9	5.5	3.8	5.7	6.6
180	12.4	8.3	6.1	4.4	5.7	6.4
210		8.3	6.2	4.9	5.8	6.2
225	12.2					
240		8.1	6.1	5.0	6.2	5.8
270	11.9	8.0	6.0	4.9	6.2	5.7
300		7.8	5.9	4.8	6.1	5.8
315	11.7					
330		7.7	5.8	4.6	6.0	6.2
360	11.4	7.5	5.7	4.4	5.8	6.3
390		7.3	5.6	4.2	5.6	6.1
405	11.2					
420		7.1	5.5	4.1	5.5	6.0
450	10.9	6.9	5.4	4.0	5.4	5.7
480		6.8	5.3	3.9	5.2	5.5
495	10.7					
510		6.6	5.2	3.9	4.9	5.3
540	10.4	6.6	5.1	3.9	4.6	5.4
570		6.5	5.0	3.6	4.4	5.3
585	10.2					
600		6.4	4.8	3.6	4.2	5.3
630	9.9	6.3	4.3	3.5	4.1	5.3
660		6.2	4.2	3.2	4.0	5.2
675	9.7					
690		6.1	4.2	3.2	3.8	5.1

This page has been removed
due to poor print quality

Fig. 3.12 Synoptic surface conditions on October 12, 1987 at 1200Z.

3.5.4 Fourth general observation period

Date :October 12, 1987

Sunrise (MST) :0655

Apparent noon (MST):1247

3.5.4.1 Summary of synoptic conditions.

The circulation affecting the weather of Alberta on the 12th of October was dominated by a high pressure center situated in the southeast corner of British Columbia and two low pressure centers situated east of Great Slave Lake and north of Fort Nelson, on the border between British Columbia and the Northwest Territory. Alberta was on the warm side of a maritime arctic front situated west of the Alberta-British Columbia border, in a N-S direction. The weak pressure gradient over central Alberta resulted in light winds near the surface. Most of the stations in the region reported clear sky but with up to 2 octants of high clouds over the Edmonton area (Fig. 3.10) The air mass was warm and dry. A nocturnal inversion of magnitude about 10°C was reported at Edmonton Stony Plain (WSE) 80km northwest from our observation site at 1200Z (Fig. 3.11).

3.5.4.2 Relevant data

a) Table 3.12 contains information on the direction (deg from North) and speed (m/s) of the surface wind from a propellor anemometer at 10m height.

This page has been removed
due to poor print quality

Fig. 3.13 Radiosonde of Stony Plain (WSE) on October 12, 1987 at 1200Z (temperature history T_H is valid at 0000Z)

Table 3.12 Wind measurements at 10m.

TIME(MST):	0616	0700	0746	0830	0915	1000
DIRECTION:	180	184	186	208	0915	1000
SPEED:	2.1	2.1	1.8	1.1	1.1	3.1

*These values are 5-min averages.

b)Table 3.13 presents data of the standard shelter temperature(°C), wet bulb temperature(°C), relative humidity(%) from a Feuchte type hygrometer, station surface pressure(kpa),ventilated temperature at 8m(°C).

Table 3.13 Temperature, humidity and pressure at the surface on the onset of the minisonde releases.

MST	Td °C	Tw °C	T_s °C	R.H. %	Pressure Kpa
0615	1.5	-0.7	1.3	88.0	92.48
0700	1.1	-0.6	1.9	84.5	92.39
0745	1.5	-0.3	1.5	86.0	92.35
0830	5.3	2.5	14.3	71.0	92.29
0915	7.8	4.4	17.4	47.0	92.24
1000	13.8	7.0	11.7	42.0	92.21

c) Single theodolite minisonde temperatures at indicated heights (m) for first approximately 4 min of ascent are listed in Table 3.14

Table 3.14 Minisonde temperature data based on an assumed rate of ascent 3 m/s.

H m	T_{0830} °C	T_{0700} °C	T_{0748} °C	T_{0853} °C	T_{0815} °C	T_{1001} °C
SFC	0.4	1.0	1.6	5.7	8.7	13.1
30	3.4	3.6	3.5	4.2	7.4	11.7
60	6.5	7.0	7.1	4.5	7.2	11.0
90	9.8	9.6	10.3	6.8	10.3	10.9
120	12.5	11.7	12.4	10.0	13.3	12.4
150	14.2	13.9	14.2	12.1	15.1	15.0
180	15.2	15.0	15.0	13.5	15.8	15.5
210	16.1	16.1	15.1	14.1	16.0	15.7
240	17.0	17.1	15.4	14.2	16.0	16.1
270	17.9	18.2	16.1	14.3	16.2	16.3
300	18.4	18.9	17.4	14.2	16.7	16.3
330	18.5	19.1	17.9	15.1	16.8	16.4
360	18.6	19.2	18.0	15.3	16.8	16.2
390	18.6	19.6	18.7	15.5	16.8	16.0
420	19.0	20.0	19.0	15.8	16.8	16.0
450	19.2	20.0	18.9	15.9	16.8	16.2
480	19.3	19.9	18.7	15.9	16.8	16.1
510	19.2	19.7	18.5	15.4	16.8	16.0
540	19.0	19.4	18.3	15.3	16.8	16.0
570	18.7	19.2	18.1	15.4	16.5	16.0
600	18.5	19.0	18.1	15.4	16.4	16.0
630	18.3	18.9	17.9	15.1	16.5	16.0
660	18.0	18.8	17.8	15.0	16.5	16.0
690	17.7	18.6	17.6	14.5	16.6	16.0

4. Mixing Height models

4.1 Introduction

A simple analytical diagnostic formula for the height of the mixed layer as it develops on clear mornings over land in response to solar heating is desired.

The basic assumptions are:

1. A radiational nocturnal inversion has developed at the surface under all circumstances justifying the validity of the Anfossi equation presented in Section 2.2
2. The development of the convective turbulent mixed layer follows the principles and assumptions described by the models presented in Section 2.3. Idealized temperature profiles under stable and unstable conditions or before and after sunrise are illustrated in Fig. 4.1

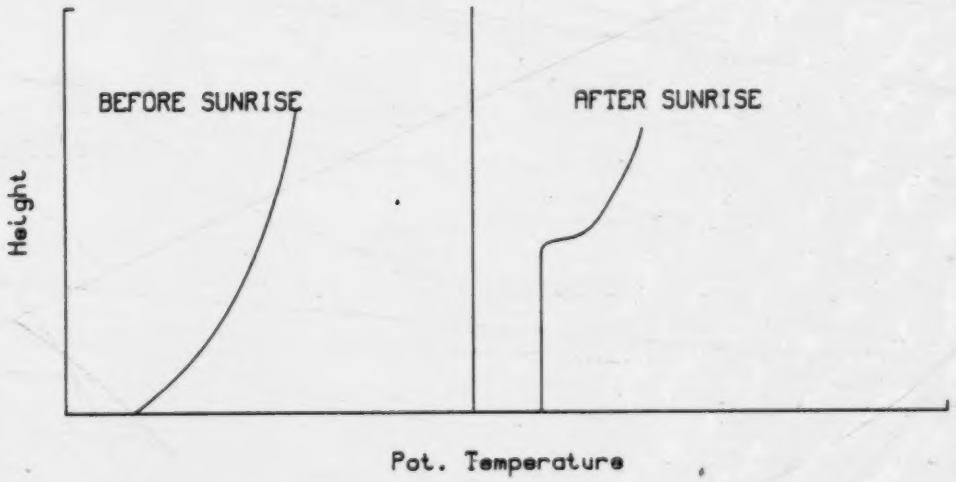

Fig. 4.1 Two ideal temperature profiles before and after sunrise.

4.2 Basic assumptions

1. Following Anfossi, et al (1976) the atmosphere is assumed to be a medium with lower and upper boundaries, the last being variable with time and identified by the condition $\frac{\partial T}{\partial z}=0$.

2. The short wave radiation is assumed unaffected as it passes through the atmosphere. As a result, the effect of the solar radiation is reflected only by the surface temperature.

3. Calm conditions or light winds of speed no more than 15km/hr at approximately 100-150m, are assumed for the validity of the simple solution, in order to avoid advection effects.

4. Clear skies or thin high clouds are assumed in order to justify the use of Brunt's theory which resulted in the equation $\frac{\partial T}{\partial t}=K_R\frac{\partial T}{\partial z}$ (see Section 2.2)

5. Anfossi, et al(1976) suggest the following equation as an appropriate solution to Brunt's equation:

$$T(z,t)=T(0,0)-[T(0,0)-T(0,t)]\{\exp[-(\frac{z}{h_i})^2]-\frac{z}{h_i}\pi^{1/2}\operatorname{erfc}(\frac{z}{h_i})+0.278(\frac{z}{h_i})\}$$

or

$$T(z,t)=T(0,0)-[T(0,0)-T(0,t)]\{\exp[-(\frac{z^2}{4K_Rt})]-\frac{z}{2\sqrt{(K_Rt)}}\pi^{1/2}\operatorname{erfc}(\frac{z}{2\sqrt{(K_Rt)}})+0.278(\frac{z}{2\sqrt{(K_Rt)}})\}\quad(4-1)$$

For a specific height say z_c=100m and $\frac{z_c^2}{4K_R}=t_c$ we get

$$T(z_c,t)=T(0,0)-[T(0,0)-T(0,t)]\{\exp(-\frac{t_c}{t})-\sqrt{(\pi\frac{t_c}{t})}\operatorname{erfc}(\sqrt{\frac{t_c}{t}})+0.278(\sqrt{\frac{t_c}{t}})\}\quad(4\text{-}1a)$$

4.3 No capping inversion-encroachment

Fig. 4.2 illustrates the potential temperature profile during the encroachment stage where z_i is the height of the mixed layer and h_i is the top of the nocturnal inversion. From (2-19a)

$$\frac{d\Delta\theta}{dt}=(\frac{\partial\theta}{\partial z})_{z_i}\frac{dz_i}{dt}-\frac{\partial\theta_m}{\partial t}$$

In the case of encroachment $\Delta\theta=0$ and

$$\frac{dz_i}{dt}(\frac{\partial\theta}{\partial z})_{z_i}=\frac{\partial\theta_m}{\partial t}\qquad(4\text{-}2)$$

where $(\frac{\partial\theta}{\partial z})_{z_i}$ is the lapse rate of the nocturnal stable layer derived from (2-13b) by replacing $q(z,t)=K_R\rho_a c_p\frac{\partial T}{\partial z}$ or

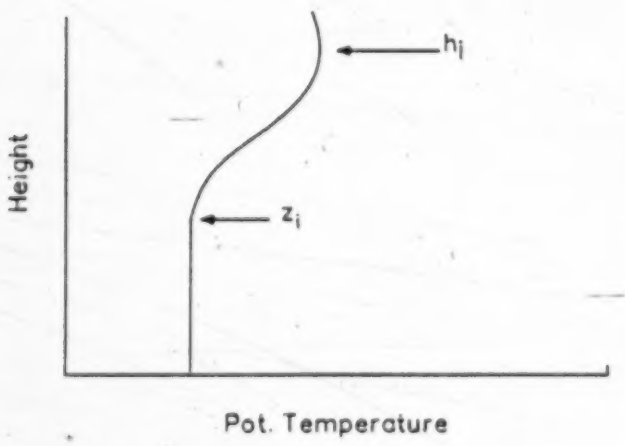

Fig. 4.2 Ideal temperature profile with no capping inversion.

$$\frac{\partial T}{\partial z}=\frac{R_N}{K_R\rho_a c_p[1-\mathrm{erfc}(1)]}[\mathrm{erfc}(z/h_i)-\mathrm{erfc}(1)] \qquad (4\text{-}3)$$

or

$$\left(\frac{\partial T}{\partial z}\right)_{z_i}=C_0\,\mathrm{erfc}(z_i/h_i)-C_1$$

where $C_0=\frac{R_N}{K_R\rho_a c_p[1-\mathrm{erfc}(1)]}$, $C_1=\frac{R_N\,\mathrm{erfc}(1)}{K_R\rho_a c_p[1-\mathrm{erfc}(1)]}$

and $C_1=C_0\,\mathrm{erfc}(1)$

By integrating (4-2) with respect to time:

$$\int_0^{z_i(t)}\left(\frac{\partial\theta}{\partial z}\right)_{z_i}\frac{dz_i}{dt}dt=\int_{\theta_0}^{\theta_m(t)}\frac{\partial\theta_m}{\partial t}dt=\theta_m(t)-\theta_0$$

or

$$\int_0^{z_i(t)}\left(\frac{\partial\theta}{\partial z}\right)_{z_i}dz_i=\theta_m(t)-\theta_0 \qquad (4\text{-}4)$$

From the relation

$$T=\theta\left(\frac{p}{p_0}\right)^{R/c_p}$$

we may derive a relation for the lapse rates

$$\frac{\partial T}{\partial z}=\frac{T}{\theta}\frac{\partial\theta}{\partial z}-\frac{g}{c_p}$$

or

$$\frac{\partial\theta}{\partial z}=\frac{\theta}{T}\left(\frac{\partial T}{\partial z}+\frac{g}{c_p}\right)$$

As a first approximation $\theta\simeq T$ and

$$\frac{\partial\theta}{\partial z}=\frac{\partial T}{\partial z}+\frac{g}{c_p} \qquad (4\text{-}5)$$

We substitute (4-5) in (4-4):

$$\int_0^{z_i(t)} \left(\frac{\partial T}{\partial z}+\frac{q}{c_p}\right)_{z_i} dz_i=\theta_m(t)-\theta_o \qquad (4\text{-}6)$$

We substitute (4-3) in its abbreviated form in (4-6) and get:

$$\int_0^{z_i(t)} C_o \operatorname{erfc}\left(\frac{z_i}{h_i}\right)dz_i-\int_0^{z_i(t)} C_1 dz_i+\frac{q}{c_p}\int_0^{z_i(t)} dz_i =\theta_m(t)-\theta_o$$

or

$$C_o\int_0^{z_i(t)} \operatorname{erfc}\left(\frac{z_i}{h_i}\right)dz_i-C_1 z_i+\frac{q}{c_p}z_i=\theta_m(t)-\theta_o$$

or

$$C_o\int_0^{z_i(t)} \operatorname{erfc}\left(\frac{z_i}{h_i}\right)dz_i+\left(\frac{q}{c_p}-C_1\right)z_i=\theta_m(t)-\theta_o$$

or

$$C_o\left\{\int_0^{\infty} \operatorname{erfc}\left(\frac{z_i}{h_i}\right)dz_i-\int_{z_i(t)}^{\infty} \operatorname{erfc}\left(\frac{z_i}{h_i}\right)dz_i\right\}+\left(\frac{q}{c_p}-C_1\right)z_i=\theta_m(t)-\theta_o$$

or

$$C_o\left[\int_0^{\infty} h_i(t)\operatorname{erfc}\left(\frac{z_i}{h_i}\right)d\left(\frac{z_i}{h_i}\right)-\int_{z_i/h_i}^{\infty} h_i \operatorname{erfc}\left(\frac{z_i}{h_i}\right)d\left(\frac{z_i}{h_i}\right)\right]+\left(\frac{q}{c_p}-C_1\right)z_i(t)$$

$$=\theta_m(t)-\theta_o \qquad (4\text{-}7)$$

Since $h_i=f(K_n,t)$ only, we may rewrite (4-7) as

$$C_0 h_i(t)\left[\int_0^{\infty} \operatorname{erfc}\left(\frac{z_i}{h_i}\right) d\left(\frac{z_i}{h_i}\right) - \left(\frac{z_i}{h_i}\right)\int_{\left(\frac{z_i}{h_i}\right)}^{\infty} \operatorname{erfc}\left(\frac{z_i}{h_i}\right) d\left(\frac{z_i}{h_i}\right)\right] + \left(\frac{q}{c_p} - C_1\right) z_i(t) = \theta_m(t) - \theta_0$$

or

$$C_0 h_i(t)\left[\left(\frac{z_i}{h_i}\right)\operatorname{erfc}\left(\frac{z_i}{h_i}\right) + \frac{1}{\sqrt{\pi}}\left(1 - \exp\left(-\left(\frac{z_i}{h_i}\right)^2\right)\right)\right] + \left(\frac{q}{c_p} - C_1\right) z_i(t) = \theta_m(t) - \theta_0 \quad (4\text{-}8)$$

for $z_i = 0$ $\theta_m(t) \equiv \theta_0$, $\left(\frac{z_i}{h_i}\right) = 0$, $\operatorname{erfc}(0) = 1$, $\exp\left(-\left(\frac{z_i}{h_i}\right)^2\right) = 1$

$$C_0 \equiv \frac{R_N}{K_R \rho_a c_p [1 - \operatorname{erfc}(1)]}, \quad C_1 = C_0 \operatorname{erfc}(1), \quad \delta\theta = \theta_m(t) - \theta_0,$$

$h_i = \sqrt{[4K_R(t - t_s)]}$, where t_s is the time of the previous day at which T is maximum and $z_* \equiv (z_i / h_i)$

Then (4-8) becomes:

$$C_0 h_i(t)\left[z_* \operatorname{erfc}(z_*) + \frac{1}{\sqrt{\pi}}\left(1 - \exp(-z_*^2)\right) - \operatorname{erfc}(1) z_* + \frac{q}{c_p} z_i(t) = \delta\theta\right.$$

or

$$\frac{C_0}{\sqrt{\pi}}\left[1 - \exp(-z_*^2) + z_* \sqrt{\pi} \operatorname{erfc}(z_*)\right] - \sqrt{\pi} \operatorname{erfc}(1) z_* = \frac{\delta\theta}{h_i} \quad (4\text{-}9a)$$

but, according to Anfossi et al(1976) $\frac{C_0}{\sqrt{\pi}} h_i(t_{min}) = T_{max} - T_{min} = \Delta T$ and (4-9a) becomes

$$-\frac{\Delta T}{h_i(t)}\left[\exp(-z_*^2) - \sqrt{\pi} z_* \operatorname{erfc}(z_*) - 1 + 0.278 z_*\right] + \frac{q}{c_p} z_* = \theta_*$$

or

$$0.0098 z_* - \Delta T_*\left[\exp(-z_*^2) - 1.7725 z_* \operatorname{erfc}(z_*) + 0.278 z_* - 1\right] = \theta_* \quad (4\text{-}9b)$$

In our case $h_i(t)$ is considered constant beyond the time at which the temperature is minimum. Therefore $h_i(t)=h_o$ at $\theta_o=T_{min}$.

To allow h_i to increase with time beyond t_{min} we should also allow ΔT to increase with time by allowing T_{min} to continue decreasing with time. This could lead to nonpractical assumptions. Therefore $h_i(t)=h_i(0)$ is estimated from a temperature profile at T_{min}.

The program "encroachment" computes the mixing height z_i

4.4 General structure entrainment model: Steady state case

In this model developed by Deardorff(1979) an entrainment layer is considered (Fig. 4.3). We distinguish three basic layers described by three different processes

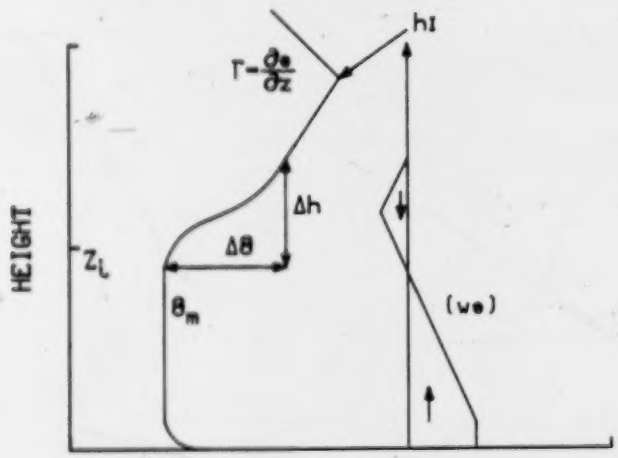

Fig. 4.3 Potential temperature and heat flux vs. height for the General Structure Entrainment model.

and consequently by three different equations.

1. Well mixed layer: θ_m: constant

$$\frac{d\theta_m}{dt}=\frac{1}{z_o}(\overline{w\,\theta})_s \qquad (4\text{-}10a)$$

2. Steady state entrainment layer:

Deardorff(1979) suggests for the steady state entrainment layer, $\Delta\theta$: constant and $0.85<G<0.98$ for meaningful results. For the steady state case

$$\frac{\Delta h}{z_o}=\frac{1-G}{G+Y-1} \qquad (4\text{-}10b)$$

3. Stable Layer:

$$\left(\frac{\partial T}{\partial z}\right)_{z_o+\Delta h}=C_o\,\mathrm{erfc}\left(\frac{z_o+\Delta h}{h_i}\right)-C_1$$

or from (4-5)

$$\Gamma_3=\left(\frac{\partial\theta}{\partial z}\right)_{z_o+\Delta h}=C_o\,\mathrm{erfc}\left(\frac{z_o+\Delta h}{h_i}\right)-C_1+\frac{q}{c_p} \qquad (4\text{-}10c)$$

From (4-10b)

$$\Delta h=\frac{1-G}{G+Y-1}z_o \quad\text{and}\quad \frac{\Delta\theta}{\Delta h}=\frac{\Gamma_3}{G}$$

then

$$\theta_{z_o+\Delta h}=\theta_m+\frac{\Gamma_3}{G}\cdot\frac{1-G}{G+Y-1}z_o=$$

$$\theta_m+\left\{C_o\,\mathrm{erfc}\left(\frac{z_o+\Delta h}{h_i}\right)-C_1+\frac{q}{c_p}\right\}\frac{1-G}{G(G+Y-1)}z_o \qquad (4\text{-}10d)$$

We integrate (4-10c) and get:

$$\theta(z_o+\Delta h,t_{min})=\theta(0,t_{min})-\Delta T\left(\exp(-z_{o*})-1.7725z_{o*}\,\mathrm{erfc}(z_{o*})+0.278z_{o*}-1\right)+\frac{q}{c_p}(z_o+\Delta h)$$

By replacing $\Delta h=\frac{1-G}{G+Y-1}z_o$ and substitute $\frac{1-G}{G+Y-1}\cdot\frac{z_o}{h_i}\equiv G_y z_{o*}$

and $\frac{\gamma}{G+\gamma-1}=\gamma_G$ we get:

$$\theta(z_o+\Delta h,t_{min})=\theta(0,t_{min})-\Delta T[\exp(-(\gamma_G z_{o*})^2) -1.7725\gamma_G z_{o*}\operatorname{erfc}(\gamma_G z_{o*}) +0.278\gamma_G z_{o*}-1]+\frac{q}{c_p}\gamma_G z_{o*} \quad (4\text{-}11)$$

From (4-10d) we get:

$$\theta(z_o+\Delta h,t)=\theta(0,t)-\Delta T+\{C_o[\operatorname{erfc}(\gamma_G z_{o*})-\operatorname{erfc}(1)]+\frac{q}{c_p}\}\frac{G_\gamma}{G}z_o(t) \quad (4\text{-}12)$$

We equate (4-11) with (4-12) by making the assumption that the rate of change of the temperature with time in the stable layer is negligible after sunrise. If $\theta_m(0,t)-\theta(0,t_{min})=\delta\theta$, we finally get:

$$\delta\theta=-\Delta T[\exp(-(\gamma_G z_{o*})^2) -1.7725(\gamma_G-\frac{G_\gamma}{G})z_{o*}\operatorname{erfc}(\gamma_G z_{o*})+0.278(\gamma_G-\frac{G_\gamma}{G})z_{o*}-1]+\frac{q}{c_p}(\gamma_G-\frac{G_\gamma}{G})z_o$$

or

$$\theta_*=0.0098(\gamma_G-\frac{G_\gamma}{G})z_{o*}-\Delta T_*[\exp(-(\gamma_G z_{o*})^2) -1.7725(\gamma_G-\frac{G_\gamma}{G})z_{o*}\operatorname{erfc}(\gamma_G z_{o*})+0.278(\gamma_G-\frac{G_\gamma}{G})z_{o*}-1] \quad (4\text{-}13)$$

if we will divide both sides by h_i, the nocturnal inversion height.

The equation (4-13) is reduced to the "encroachment" equation (4-9b) for G=1.

The program "GSE" computes the mixing height z_o by means of (4-13).

4.5 Input data and results

The data needed are the nocturnal inversion height h_i at the time with minimum surface temperature, the temperature difference between the maximum temperature of the previous day and the minimum temperature of the current day ΔT, the temperature difference of the current hour and the minimum temperature at the surface. This temperature difference is assumed equivalent to the potential difference, $\delta\theta = \theta_m(t) - \theta_0(t)$, where $\theta_0(t) \equiv T_{min}$.
The time and the maximum temperature have been selected from the climatological data of the International Airport of Edmonton because theu were not available on the site. The time and the minimum temperature have been selected from the experimental data collected at Ellerslie.
Table 4.1 depicts the input data. It also contains three additional cases from experiments in the rural area surrounding Edmonton and carried out by the Atmospheric Environment Service. For these three cases the maximum and minimum temperatures were selected from the monthly records of Environment Canada, for the Ellerslie weather station. The times corresponding to the above temperatures was approximated by the time available on the same days in more recent years, where it was available. Figures 4.4 to 4.14 depict the temperature profiles.

In the Ellerslie experiments the observed mixing heights were estimated for the encroachment model and the General Structure Entrainment model (steady state). Fig.

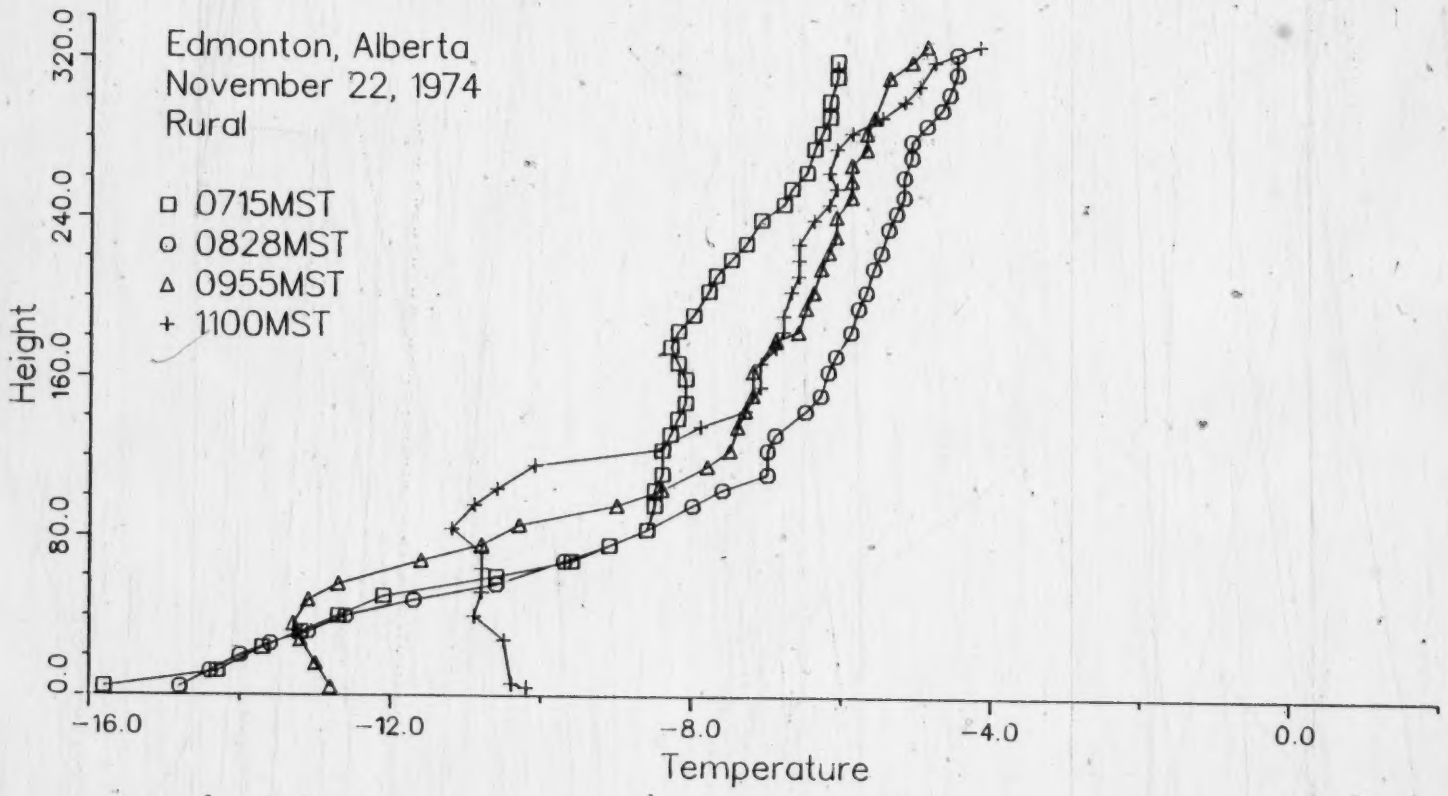

Fig. 4.4 Temperature profiles at indicated times on November 22, 1974, rural area, Edmonton, Alberta

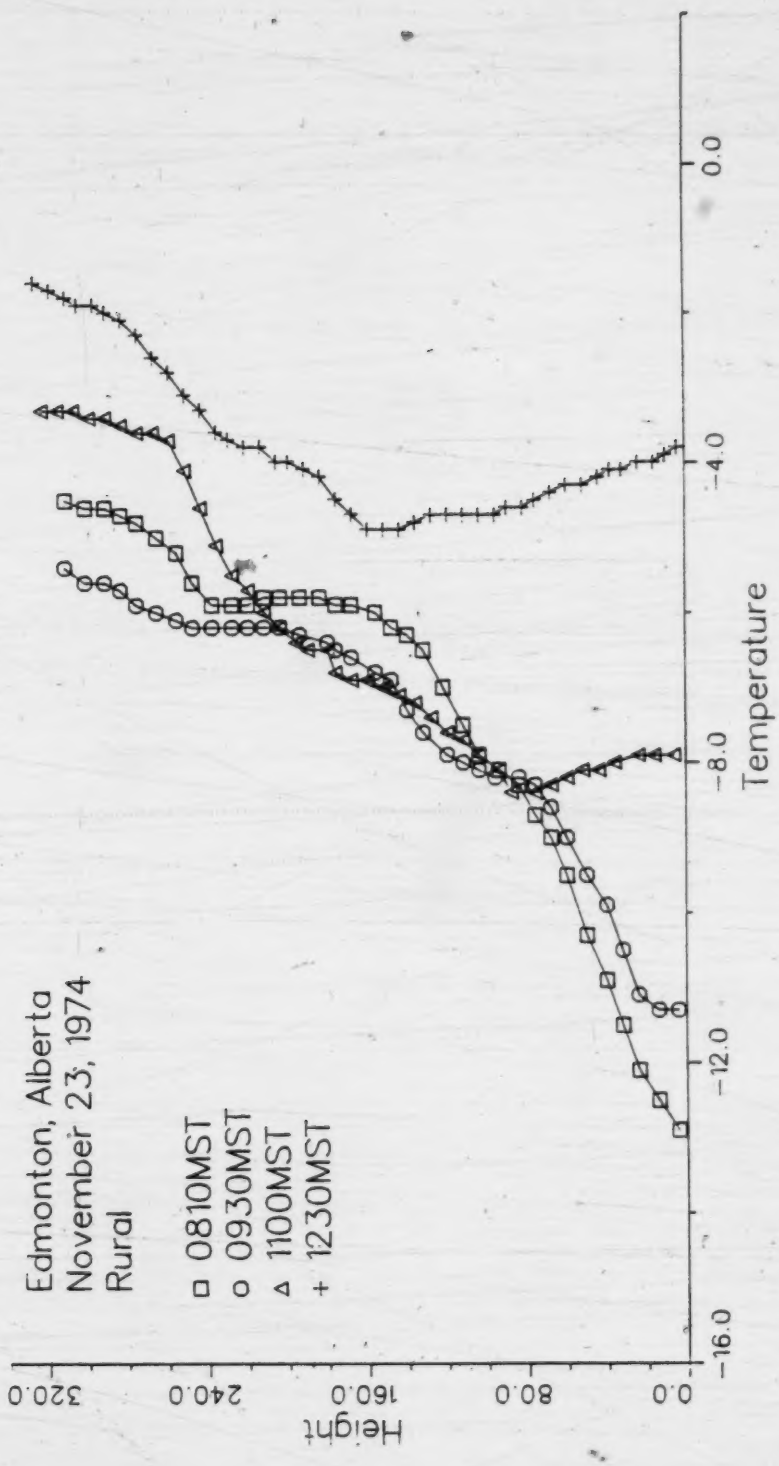

Fig. 4.5 Temperature profiles at indicated times on November 23, 1974, rural area, Edmonton, Alberta

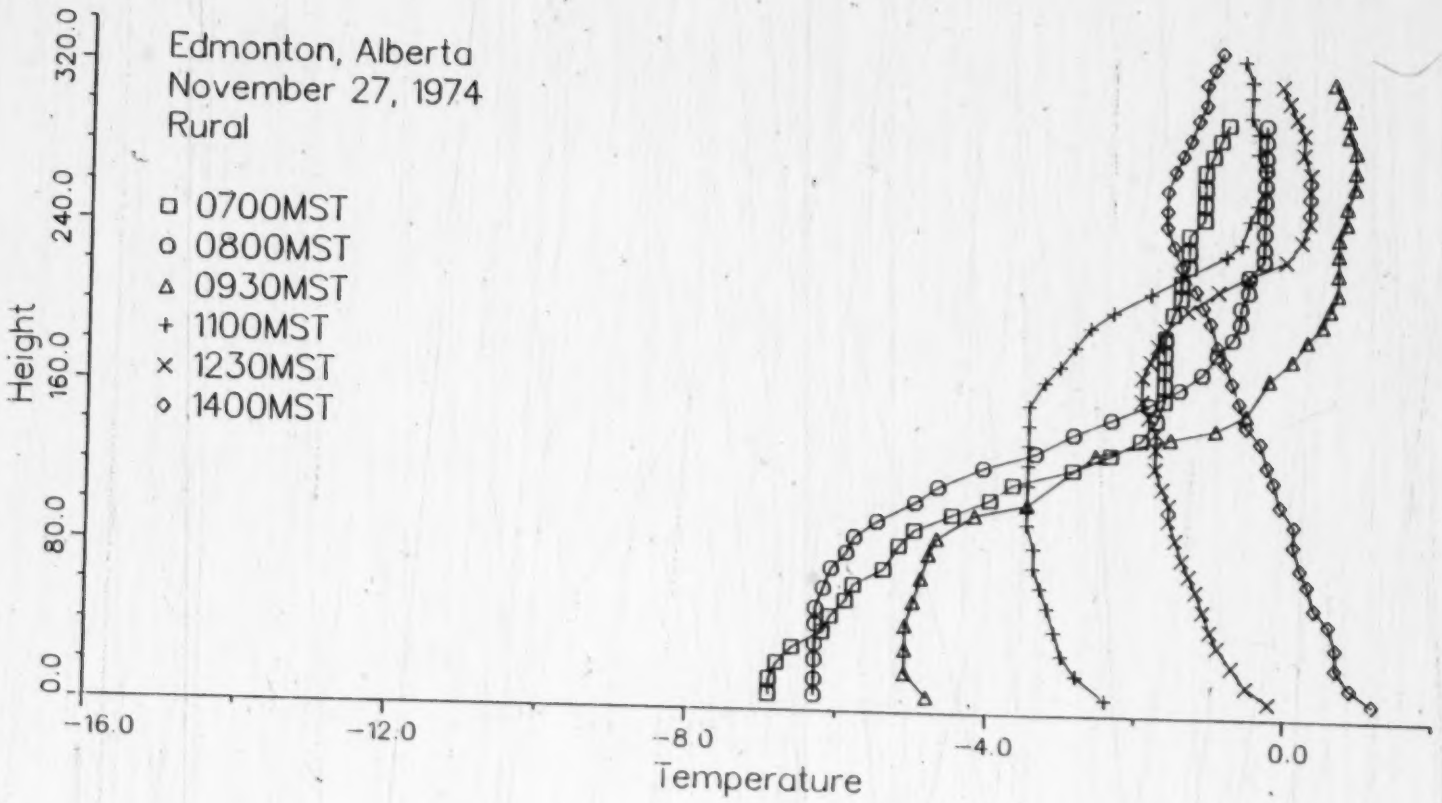

Fig. 4.6 Temperature profiles at indicated times on November 27, 1974, rurar area, Edmonton, Alberta

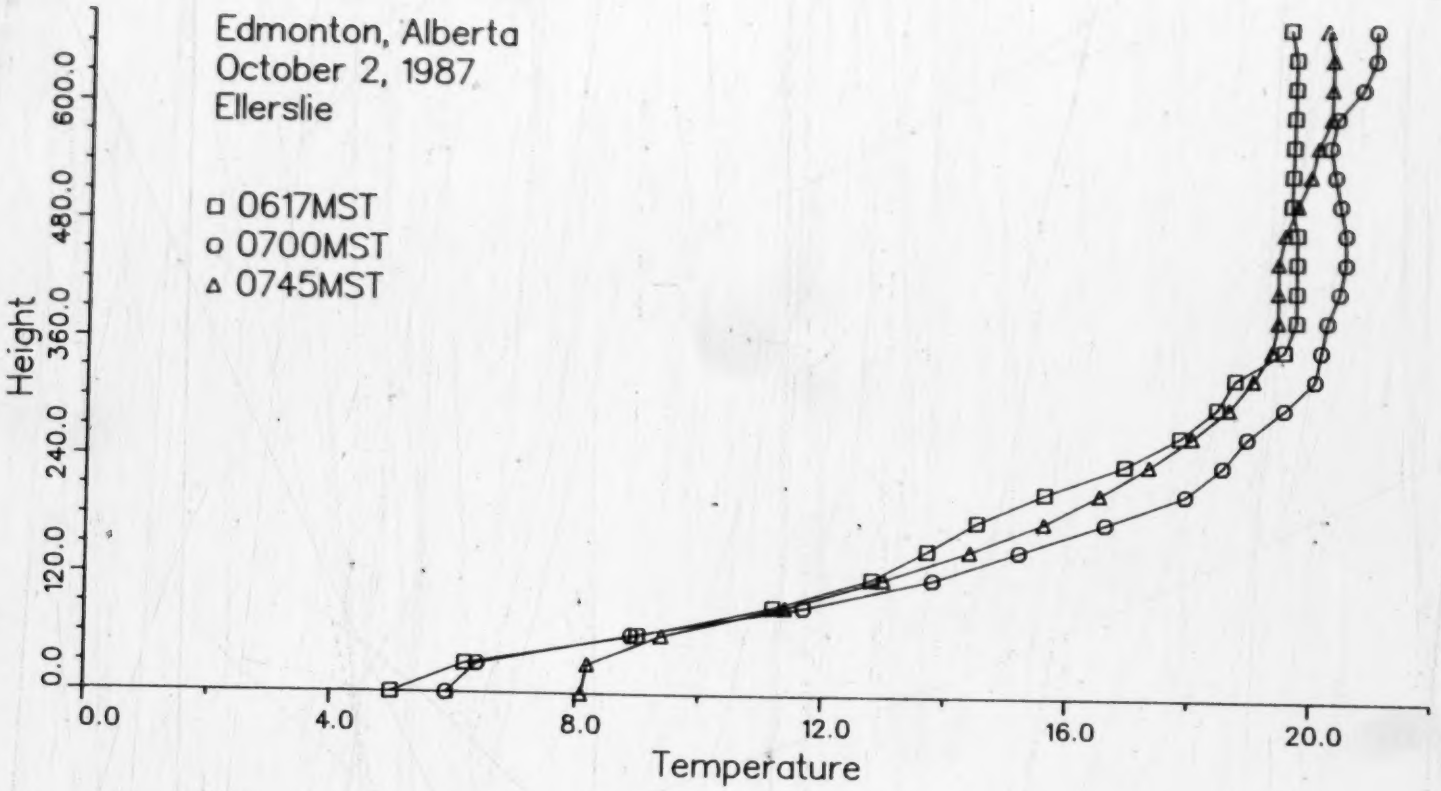

Fig. 4.7 Temperature profiles at indicated times on October 2, 1987 at Ellerslie, Edmonton, Alberta

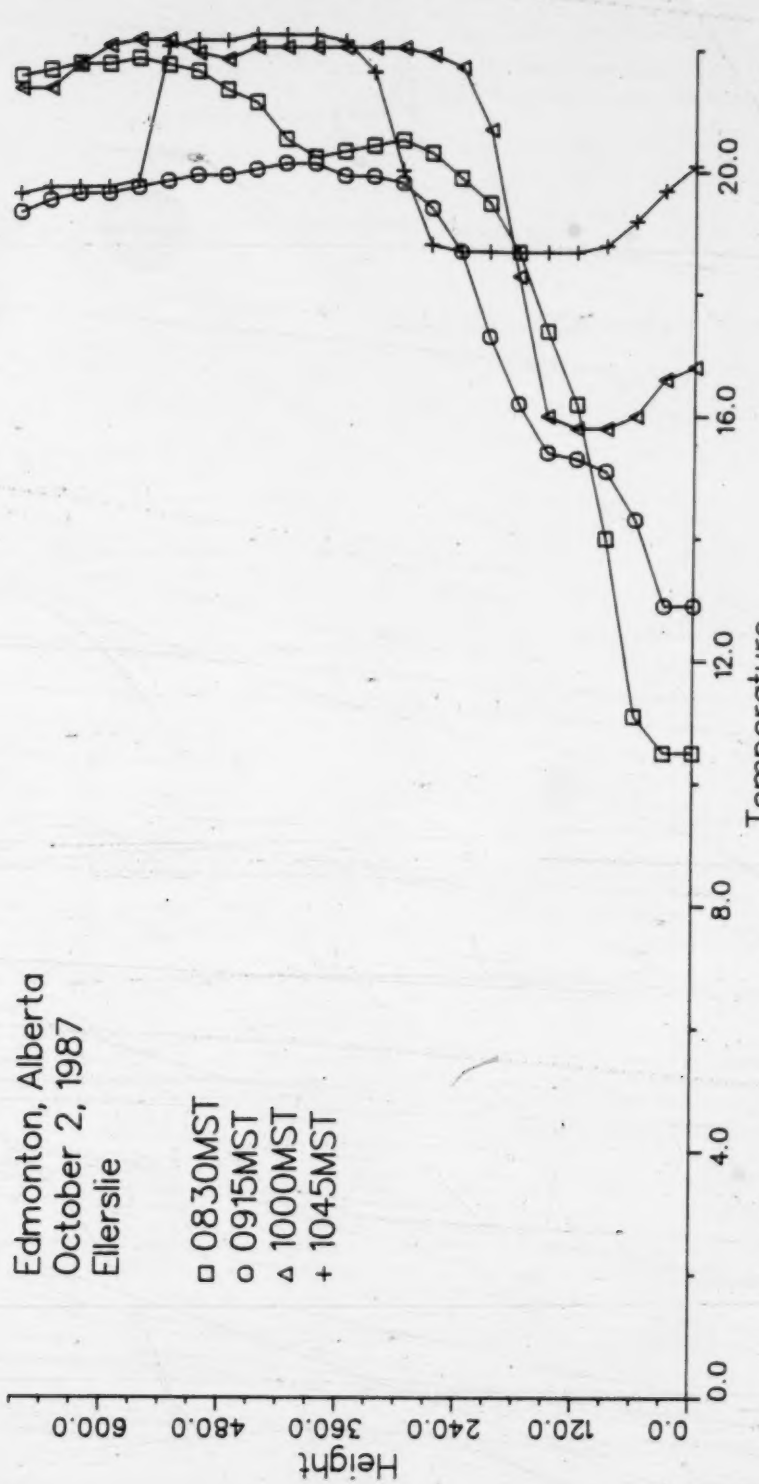

Fig. 4.8 Temperature profiles at indicated times on October 2, 1987 at Ellerslie, Edmonton, Alberta

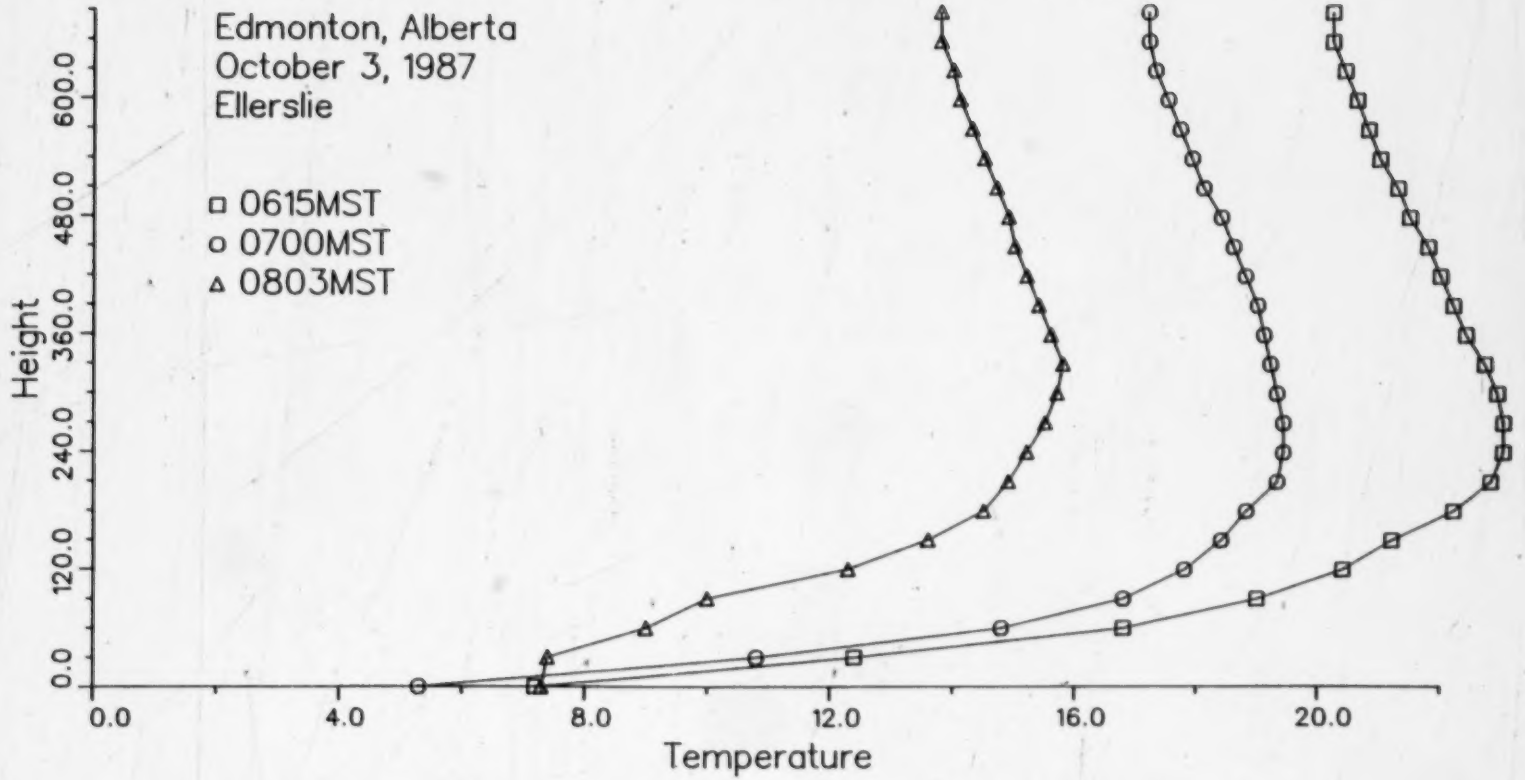

Fig. 4.9 Temperature profiles at idicated times on October 3, 1987 at Ellerslie, Edmonton, Alberta

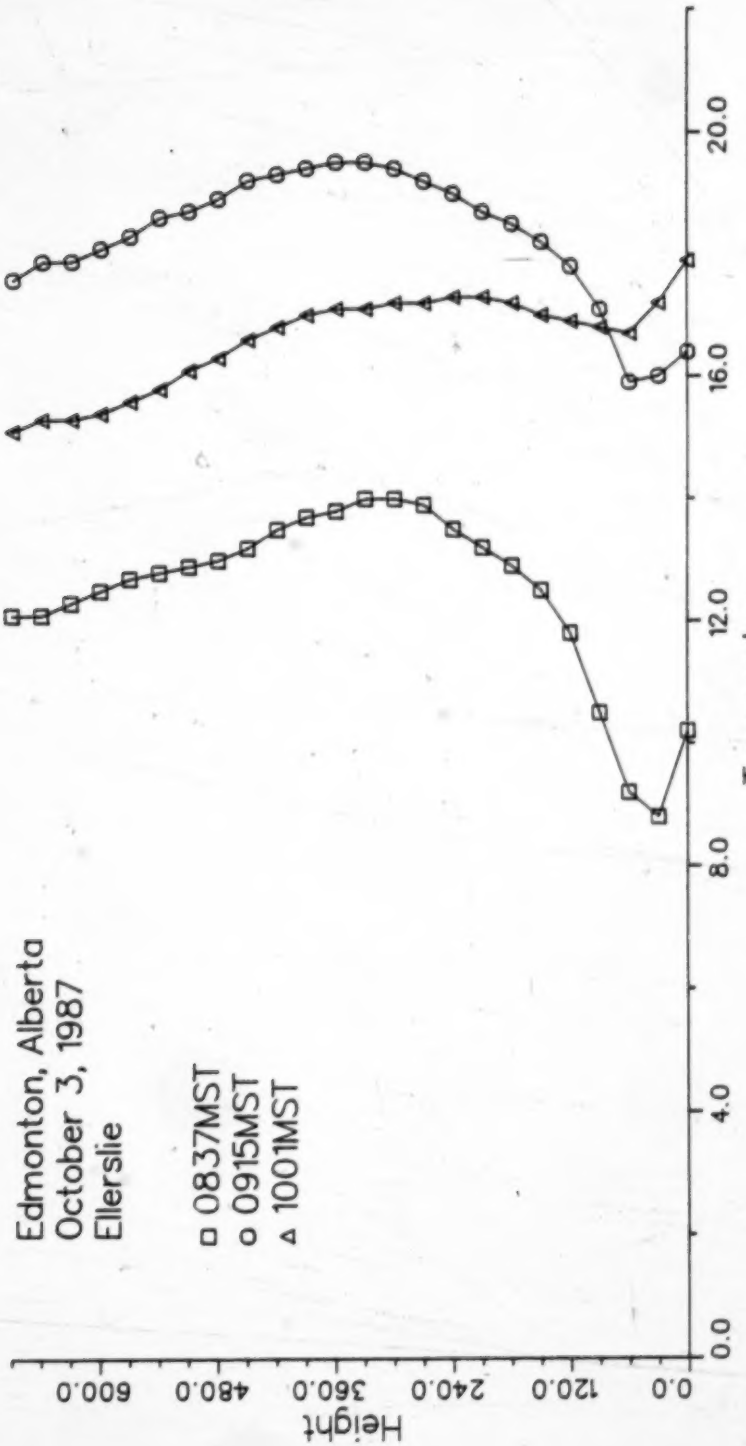

Fig. 4.10 Temperature profiles at indicated times on October 3, 1987 at Ellerslie, Edmonton, Alberta

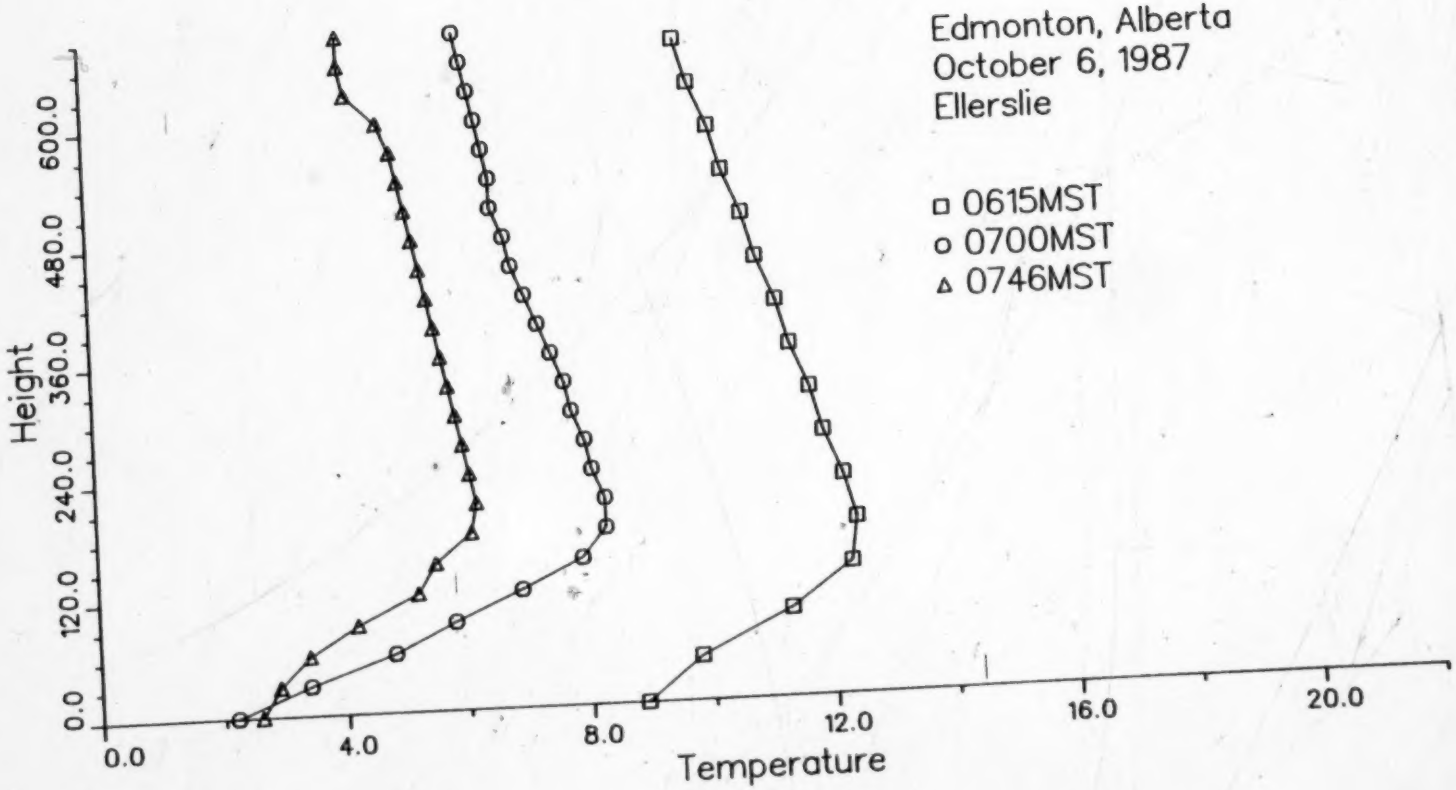

Fig. 4.11 Temperature profiles at indicated times on October 6, 1987 at Ellerslie, Edmonton, Alberta

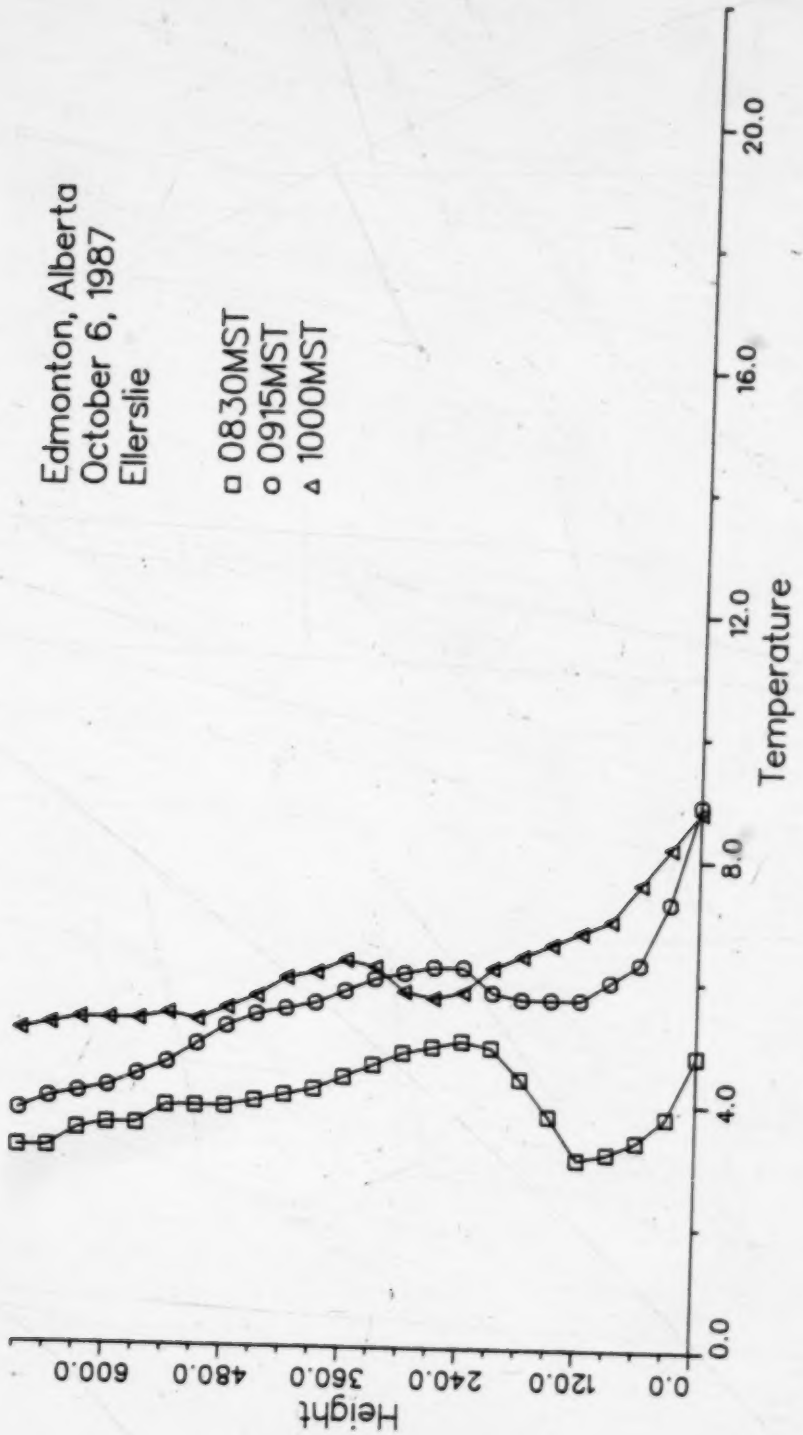

Fig. 4.12 Temperature profiles at indicated times on October 6, 1987 at Ellerslie, Edmonton, Alberta

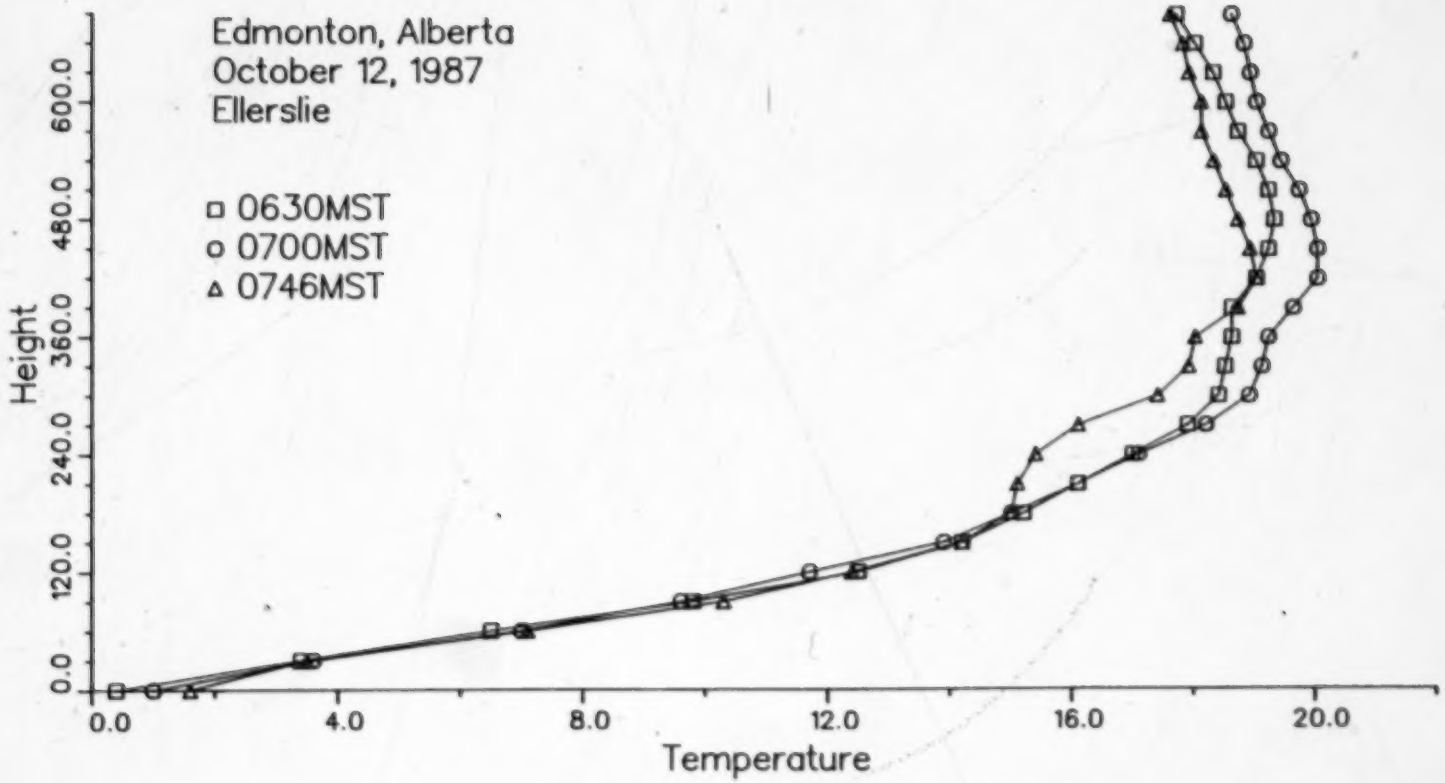

Fig. 4.13 Temperature profiles at indicated times on October 12, 1987 at Ellerslie, Edmonton, Alberta

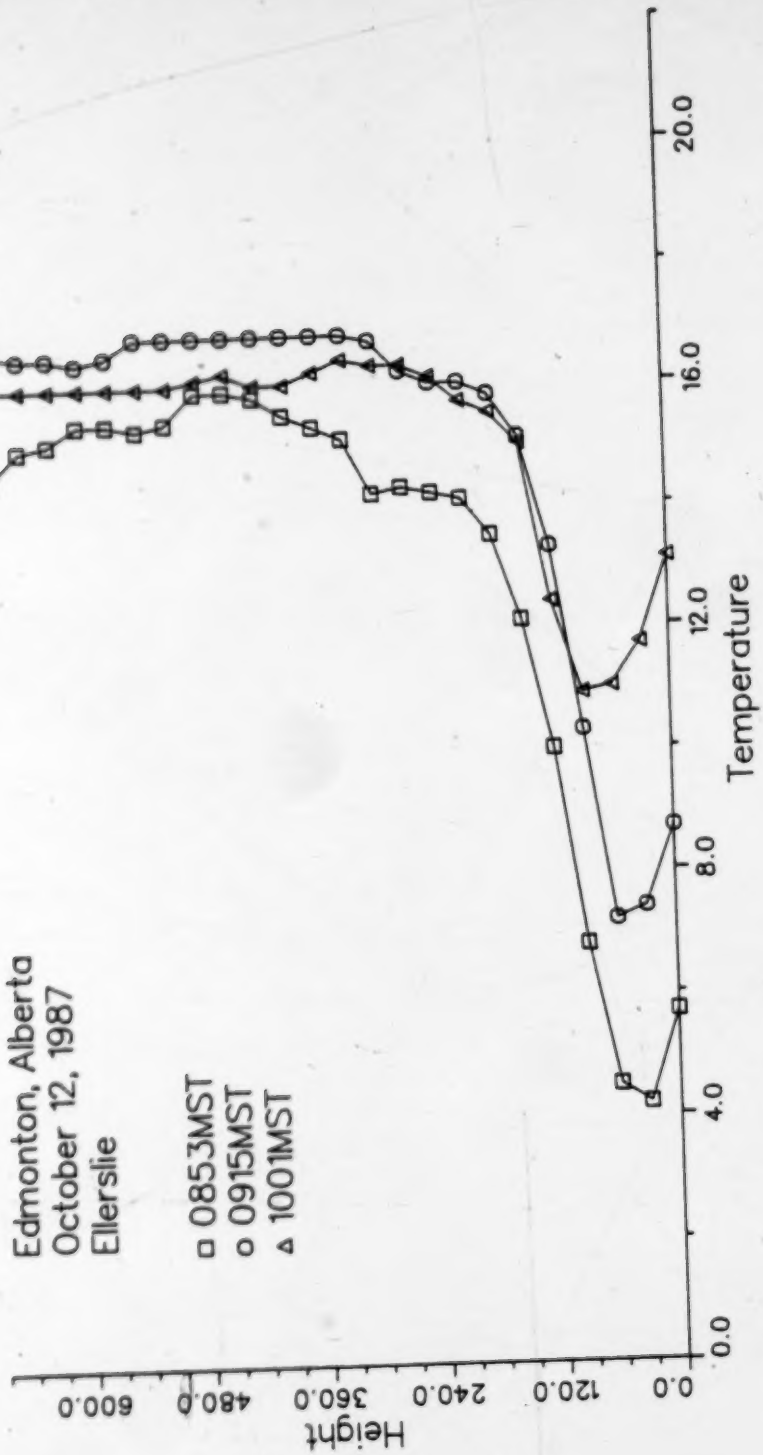

Fig. 4.14 Temperature profiles at indicated times on October 12, 1987 at Ellerslie, Edmonton, Alberta

Table 4.1 Input data to estimate the mixing heights.

Date	T^{max} °C	time MST	T^{min} °C	time MST	ΔT °C	h^i m	$\delta\theta$ at minisonde release 1	2	3	4	5	6
74-11-21	-5.0	13:00										
74-11-22	-2.8	13:00	-17.8	05:00	12.8	720	2.4	3.0	5.0	7.6	14.5	14.6
74-11-23			-14.4	06:00	11.6	291	1.6	3.1	6.5	10.6	13.6	
74-11-26	0.6	14:00	-5.6									
74-11-27	2.2		-10.0	07:00	10.6	378	3.0	3.8	5.2	7.6	9.8	11.2
87-10-01	19.3	16:00										
87-10-02	29.1	14:00	5.9	07:00	13.4	390	0	2.2	4.6	7.0	10.9	14.2
87-10-03	19.6	13:00	5.3	07:00	23.8	270	0	2.0	4.9	11.1	12.6	
87-10-05	17.6	16:00										
87-10-06	13.1	15:00	2.2	07:00	15.4	200	0	0.4	2.6	6.7	6.6	
87-10-11	23.4	15:00										
87-10-12	18.1	13:00	1.0	07:00	22.4	435	0	0.6	4.7	7.7	12.1	

4.15 to 4.25 depict the relation of observed and calculated mixing heights. All heights are in meters.

On November 22, 1974 the model appears to overestimate the mixing height. This overestimate increased with time. The discrepancy increased as higher mixing heights were diagnosed.

On November 23, 1974 the encroachment model demonstrated again a tendency to overestimate the observed mixing height and the discrepancy increased with time.

On November 27, 1974 the pattern followed in the two previous days appeared to change. Although the encroachment model overestimated the observed heights the discrepancy did not increase with time. The highest observed mixing height, actually seems to be underestimated.

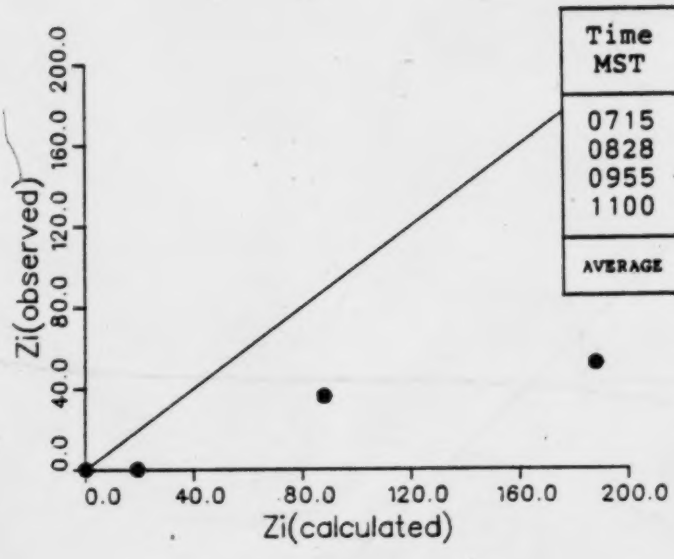

Time MST	Zi OBSERVED	Zi CALCULATED
0715	0 m	0 m
0828	0 m	19m
0955	36m	88m
1100	52m	188m
AVERAGE	22m	74m

Fig. 4.15 Observed vs. calculated mixing heights with the encroachment model valid for November 22, 1974

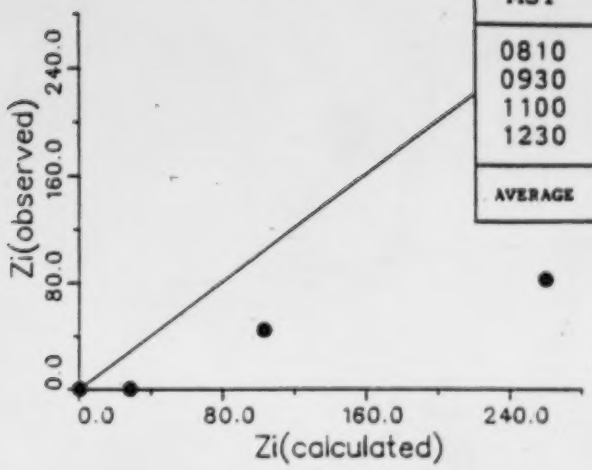

Time MST	z_i OBSERVED	z_i CALCULATED
0810	0 m	0 m
0930	0 m	28m
1100	44m	103m
1230	82m	260m
AVERAGE	31m	98m

Fig. 4.16 Observed vs. calculated mixing heights with the encroachment model valid for November 23,1974

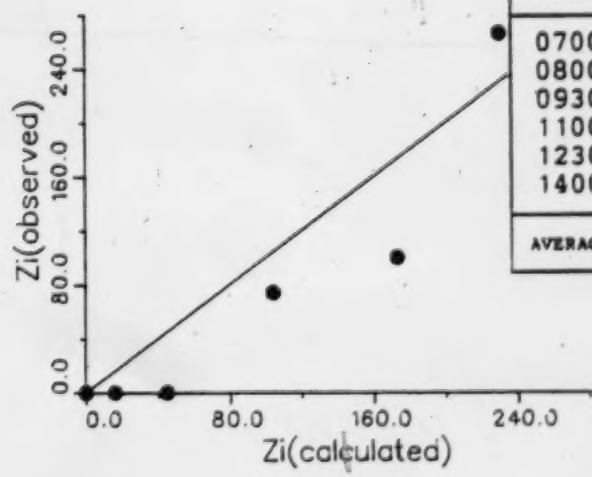

Time MST	z_i OBSERVED	z_i CALCULATED
0700	0 m	0 m
0800	0 m	16m
0930	0 m	45m
1100	74m	104m
1230	100m	173m
1400	266m	230m
AVERAGE	73m	95m

Fig. 4.17 Observed vs. calculated mixing heights with the encroachment model valid for November 27,1974

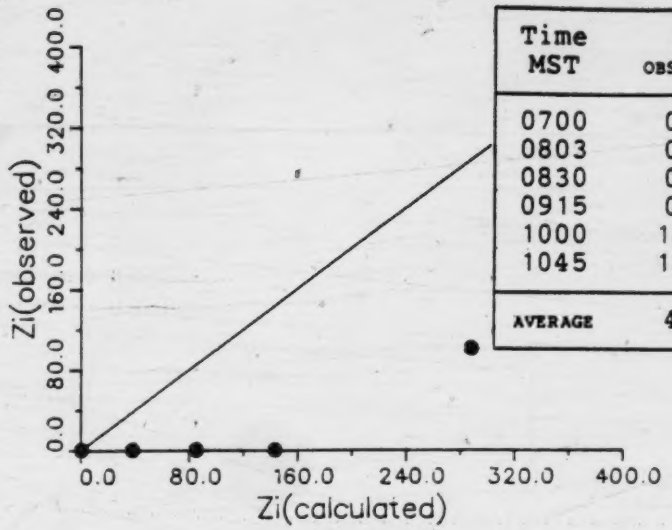

Time MST	Zi OBSERVED	Zi CALCULATED
0700	0 m	0 m
0803	0 m	38m
0830	0 m	85m
0915	0 m	143m
1000	101m	288m
1045	138m	390m
AVERAGE	40m	157m

Fig. 4.18 Observed vs. calculated mixing heights with the encroachment model valid for October 2,1987

On October 2, 1987 the encroachment model again overestimated the observed mixing height and the discrepancy increased with time.

On October 3, 1987 the model overestimated the observed mixing height. However, it appears that the pattern of increasing discrepancy was not followed. The calculated height of 38m was very close to the observed value of 35m, whereas the discrepancy decreased towards the highest observed mixing height.

October 6, 1987 the encroachment model underestimated dramatically the observed mixing heights. As Fig. 4.11 indicates, during that day a cool air advection occurred causing that abnormal behaviour of the model.

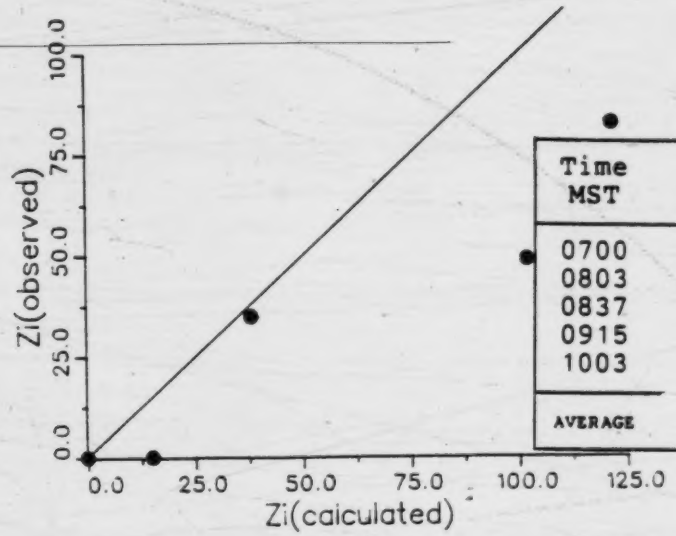

Time MST	Zi OBSERVED	Zi CALCULATED
0700	0 m	0 m
0803	0 m	15m
0837	35m	38m
0915	49m	102m
1003	83m	122m
AVERAGE	33m	55m

Fig. 4.19 Observed vs. calculated mixing heights with the encroachment model valid for October 3,1987

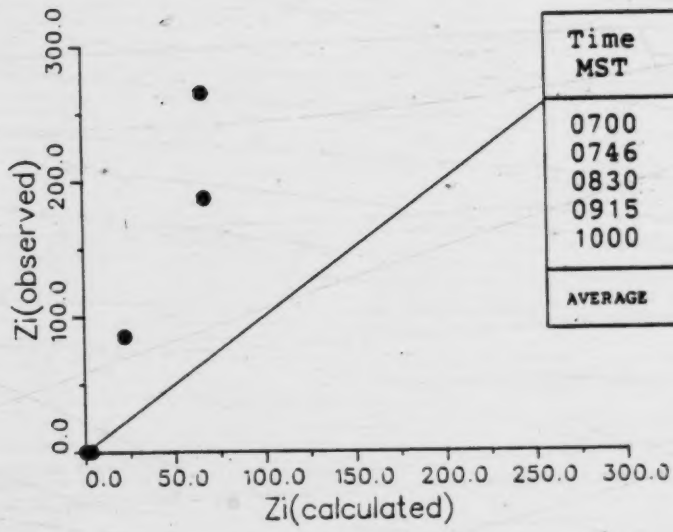

Time MST	Zi OBSERVED	Zi CALCULATED
0700	0 m	0 m
0746	0 m	3 m
0830	85m	22m
0915	187m	67m
1000	265m	66m
AVERAGE	107m	32m

Fig. 4.20 Observed vs. calculated mixing heights with the encroachment model valid for October 6,1987

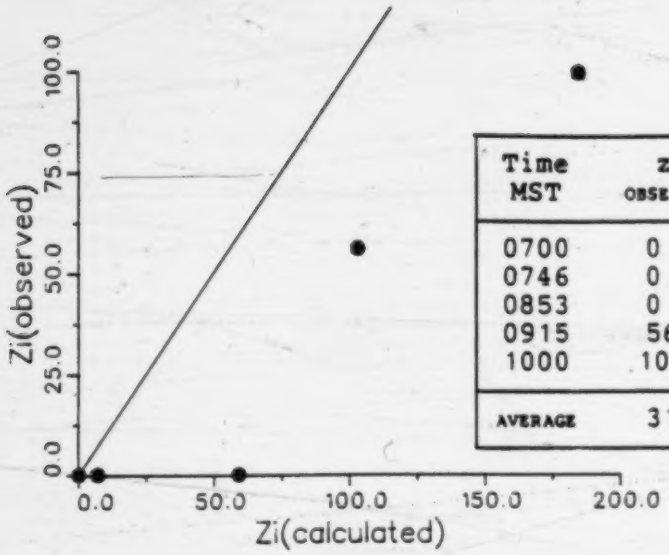

Time MST	zi OBSERVED	zi CALCULATED
0700	0 m	0 m
0746	0 m	7 m
0853	0 m	59m
0915	56m	103m
1000	100m	185m
AVERAGE	31m	71m

Fig. 4.21 Observed vs. calculated mixing heights with the encroachment model valid for October 12,1987

On October 12,1987 the encroachment model overestimated the observed mixing heights. However, the discrepancy appeared to increase with time at a much smaller rate of growth. We could even interpret this growth as negligible, in the average, by viewing the diagram.

On November 22, 1974 the GSE model (Fig. 4.22) overestimated the observed mixing heights and the discrepancy increased with time. This discrepancy appeared to be greater than the one characterizing the encroachment model.

On November 23, 1974 the same pattern was observed. The GSE model overestimated the observed mixing heights with an increasing discrepancy with time. However this discrepancy appeared to be smaller than that observed with the

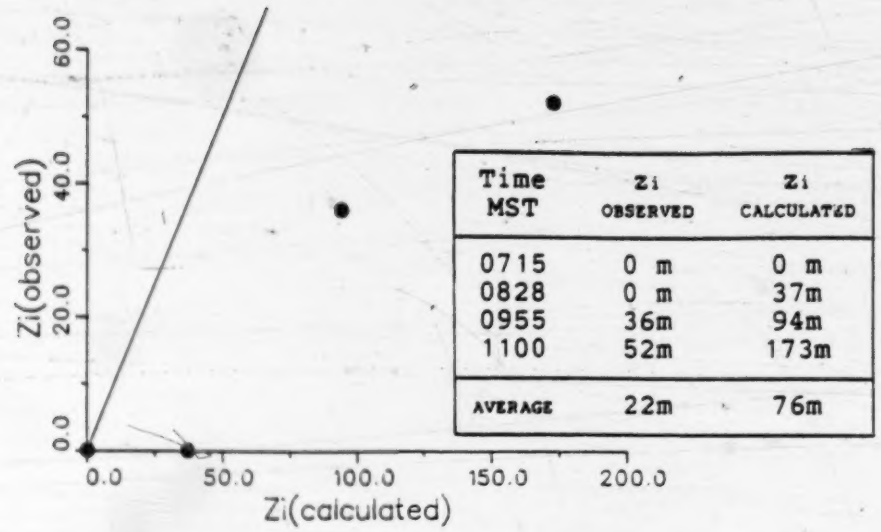

Time MST	z_i OBSERVED	z_i CALCULATED
0715	0 m	0 m
0828	0 m	37m
0955	36m	94m
1100	52m	173m
AVERAGE	22m	76m

Fig. 4.22 Observed vs. calculated mixing heights with the G.S.E.-s.s. model valid for November 22,1974

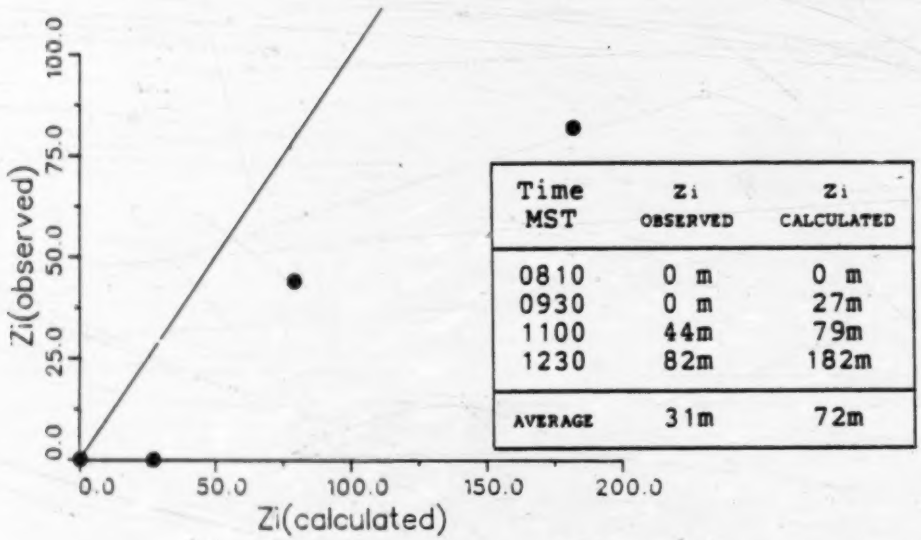

Time MST	z_i OBSERVED	z_i CALCULATED
0810	0 m	0 m
0930	0 m	27m
1100	44m	79m
1230	82m	182m
AVERAGE	31m	72m

Fig. 4.23 Observed vs. calculated mixing heights with the G.S.E.-s.s. model valid for November 23,1974

encroachment model.

On November 27, 1974 the GSE model appeared to make good low mixing height estimates, much better than the estimates made by the encroachment model. However the highest observed mixing height was underestimated and its discrepancy was greater than that found with the encroachment model.

On October 2, 1987 the GSE model overestimated the observed heights and the discrepancy increased with time. However this discrepancy was kept smaller than that found with the encroachment model.

On October 3, 1987 we observe a good estimate of the observed mixing heights made with the GSE model. Although the model overestimated the observed mixing heights the

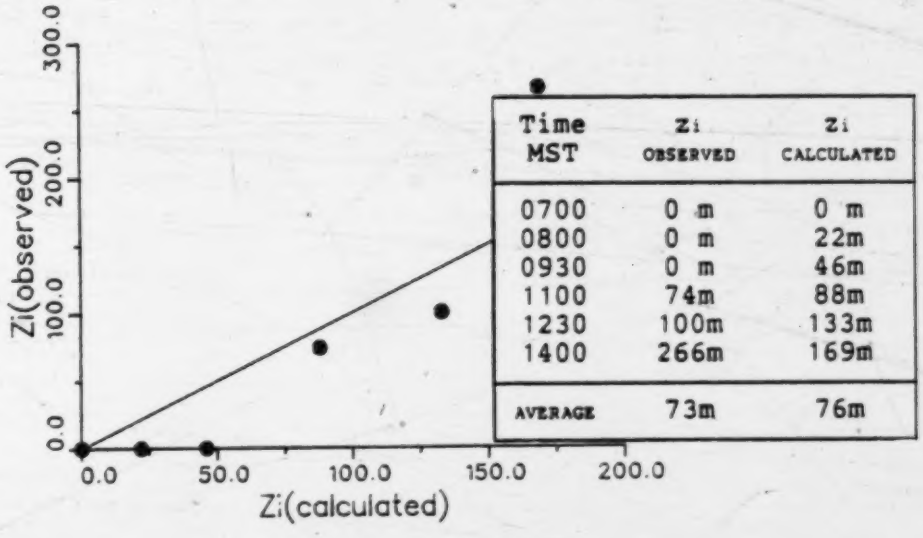

Time MST	Zi OBSERVED	Zi CALCULATED
0700	0 m	0 m
0800	0 m	22m
0930	0 m	46m
1100	74m	88m
1230	100m	133m
1400	266m	169m
AVERAGE	73m	76m

Fig. 4.24 Observed vs. calculated mixing heights with the G.S.E.-s.s. model valid for November 27,1974

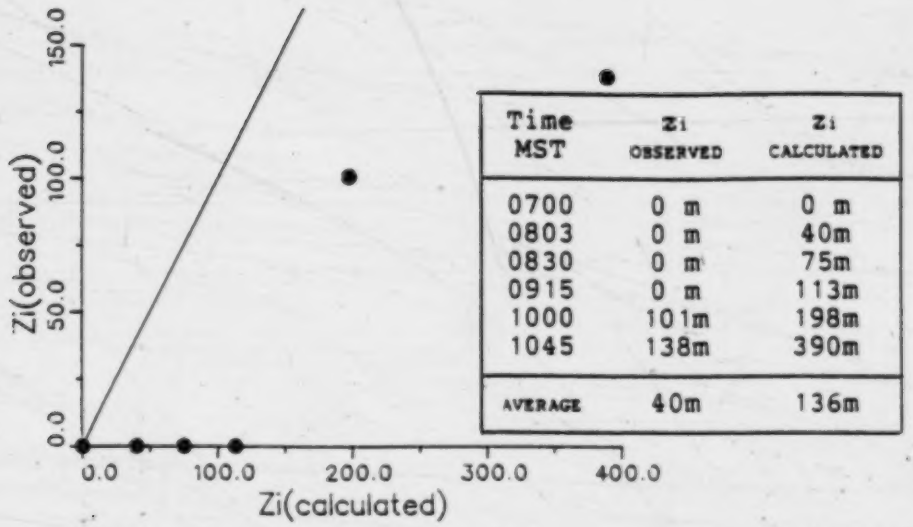

Time MST	z_i OBSERVED	z_i CALCULATED
0700	0 m	0 m
0803	0 m	40m
0830	0 m	75m
0915	0 m	113m
1000	101m	198m
1045	138m	390m
AVERAGE	40m	136m

Fig. 4.25 Observed vs. calculated mixing heights with the G.S.E.-s.s. model valid for October 2,1987

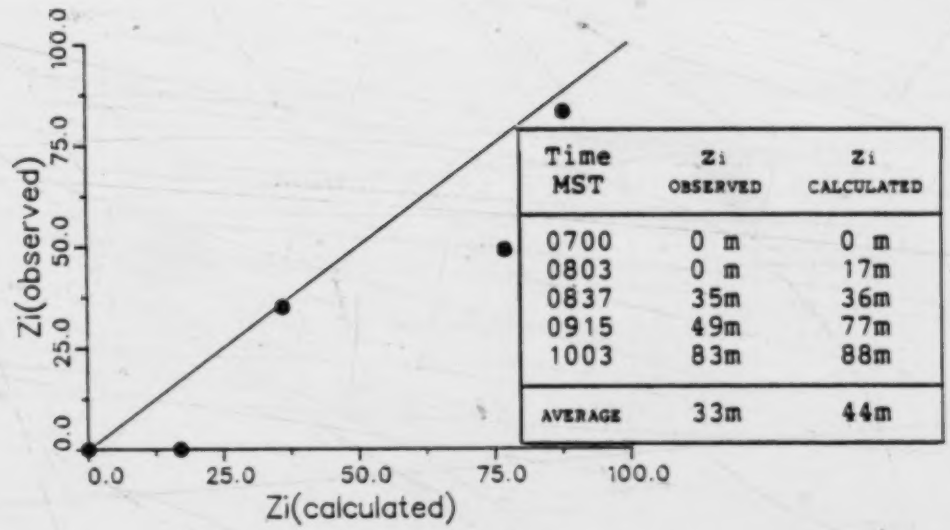

Time MST	z_i OBSERVED	z_i CALCULATED
0700	0 m	0 m
0803	0 m	17m
0837	35m	36m
0915	49m	77m
1003	83m	88m
AVERAGE	33m	44m

Fig. 4.26 Observed vs. calculated mixing heights with the G.S.E.-s.s. model valid for October 3,1987

discrepancy was very small. In fact the estimated mixing height was 33% higher than the observed, compared to 66% higher with the encroachment model.

On October 6, 1987 the GSE model underestimated the observed mixing heights as a result of the cool air advection.

On October 12, 1987 the GSE model overestimated the observed mixing heights. However the discrepancy appeared to increase with time but with a growth rate smaller in magnitude compared with the encroachment model.

Time MST	z_i OBSERVED	z_i CALCULATED
0700	0 m	0 m
0746	0 m	7 m
0830	85m	22m
0915	187m	52m
1000	265m	51m
AVERAGE	107m	26m

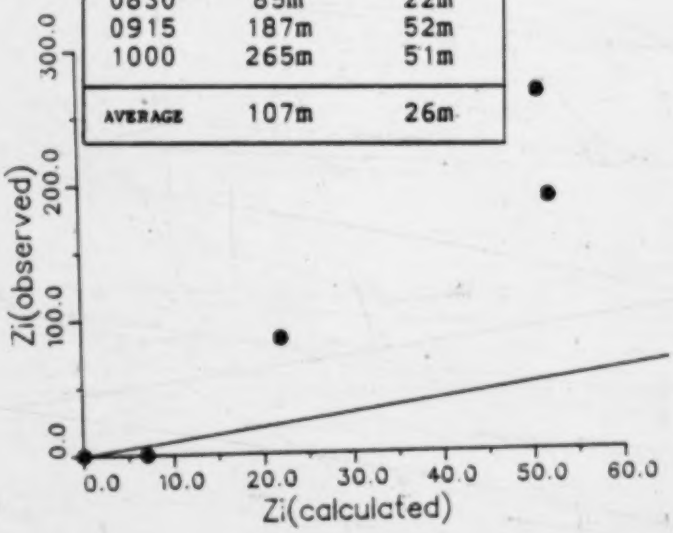

Fig. 4.27 Observed vs. calculated mixing heights with the G.S.E.-s.s. model valid for October 6,1987

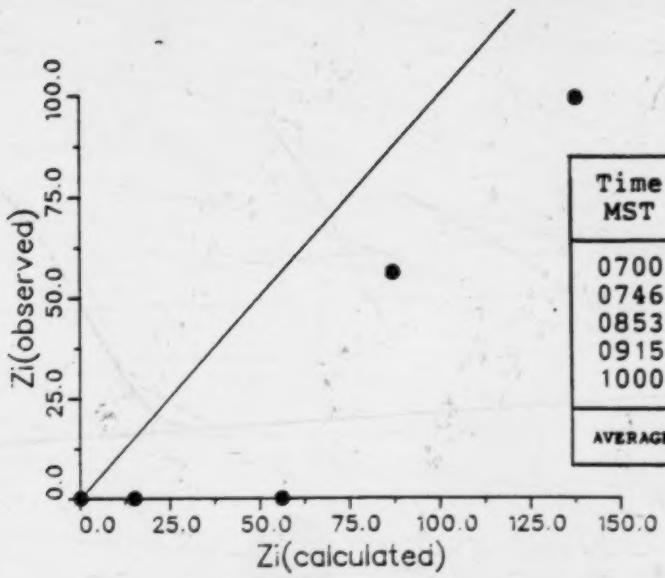

Time MST	Zi OBSERVED	Zi CALCULATED
0700	0 m	0 m
0746	0 m	15m
0853	0 m	56m
0915	56m	87m
1000	100m	138m
AVERAGE	31m	59m

Fig. 4.28 Observed vs. calculated mixing heights with the G.S.E.-s.s. model valid for October 12,1987

4.6 Estimation of the nocturnal inversion height and RMSE of the models.

There are actually three suggested ways to determine the nocturnal inversion height h_i at the time of minimum surface temperature:

a) From the temperature profile corresponding to the minimum surface temperature or for any practical purpose from the upper air weather stations information valid at 1200Z. Of course spatial differences always may incorporate an error, or

b) From the formula $h_i = 2(K_R \Delta t)^{1/2}$ where Δt is the time between the maximum temperature of the previous day and the minimum temperature of the current day. In this case we need also to

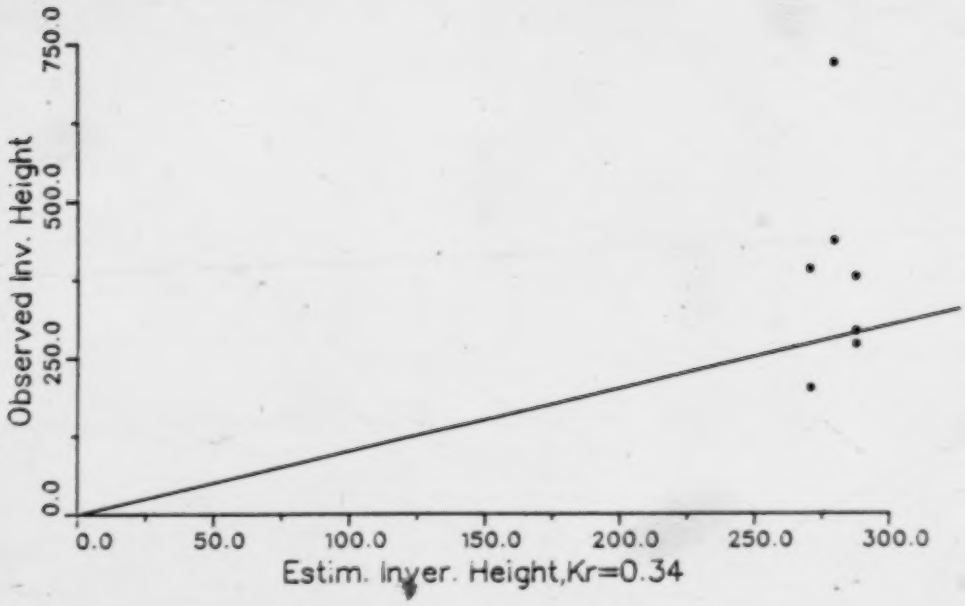

Fig. 4.29 Observed vs. estimated inversion height with K_R=0.34m²/sec

evaluate the radiative diffusivity K_R. Anfossi et al(1976) suggest a value of 0.34m²s⁻¹. The author, based on the collected data from Ellerslie, derived a value of 0.11m²s⁻¹, and

c) From Anfossi's assumption that

$$T(h_i,t)-T_{min}(0,t)\simeq\lambda\ [T(0,0)-T_{min}(0,t)]$$

with λ lying in the range 0.5-0.65. Table 4.2 shows values of h_i estimated by the above methods. Fig. 4.29 shows that the estimated nocturnal inversion height underestimated those observed from the temperature profiles. Fig. 4.30 displays the relation of h_i estimated with the method (b)

Table 4.2 Estimation of the nocturnal inversion height

Date of experiment	h_i (profile)	h_i K_R=0.34	h_i K_R=0.11	h_i $T(h_i,t)$
74-11-22	720m	280m	170m	82m
74-11-23	291m	288m	175m	132m
74-11-27	378m	288m	175m	136m
87-10-02	390m	271m	164m	125m
87-10-03	270m	288m	175m	N/A
87-10-06	200m	271m	164m	N/A
87-10-12	435m	280m	170m	180m

and K_R=0.11m^{2}s^{-1} and with the method (c). Although both (b) and (c) underestimate even more the observed inversion heights, they appear more comparable one with the other.

Tables 4.3 and 4.4 present the calculated root mean square error for the two models,

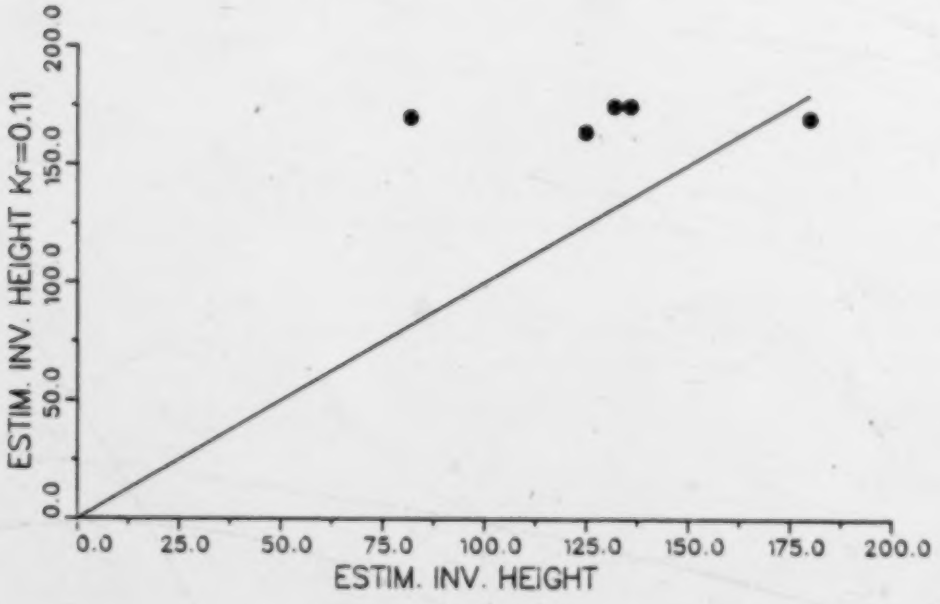

Fig. 4.30 Relation between estimated inversion heights with the methods (b) K_R=0.11m^2/sec and (c)

$A=\Sigma(\Delta z_i)^2$, $B=(\Sigma(\Delta z_i)^2)/N$, $C=[(\Sigma(\Delta z_i)^2)/N\ ]^{1/2}$

The overall RMSE for the encroachment model was 88m whereas for the GSE model it was 78m. The combined RMSE for the complete set of the estimated mixing heights by the models is 83m.

It appears therefore that the GSE-s.s. model had the smallest average error. With respect to the average observed mixing height of 48m both models appear to behave poorly.

Garrett (1981) in his model makes the argument that an initial mixed-layer height of 50m is assumed as a starting height whereas he refers to the literature pointing out that the initial height is difficult to be standarized and defined precisely. Its value may be varied by 100m or more. Under this constraint he tested his model with observed data from four U.S. radiosonde stations for 1978. His annual RMSE was 41% of the mean observed mixing heights. In addition he excluded cases with maximum mixing heights <400m.

In this model the observed mixing height has been determined as the intersection of the environment with a dry adiabat drawn from a 30m height. That was an attempt to minimize the effect of the superadiabatic surface layer. However no attempt was made to consider an initial mixed-layer height.

Two more methods were exploited to determine the observed mixing height. These were the capping inversion and the "kink" method. With the capping inversion method the observed mixing height was determined at the point where an inversion of the potential temperature starts to develop.

Table 4.3 Estimation of the RMSE for the encroachment model

Date	Average Observed mixing height	Average Calculated mixing height	$\Delta z_i = z_{i(observed)} - z_{i(calculated)}$						RMSE		
			1	2	3	4	5	6	A	B	C
74-11-22	22	74	0	-19	-52	-136	N/A	N/A	21201	5300.25	73m
74-11-23	31	98	0	-28	-59	-178	N/A	N/A	35949	8987.25	95m
74-11-27	73	95	0	-16	-45	-30	-73	36	9806	1634.33	40m
87-11-02	40	157	0	-38	-85	-143	-187	-252	127591	21265.17	146m
87-11-03	33	55	0	-15	-3	-53	-39	N/A	4564	912.8	30m
87-11-06	107	32	0	-3	63	120	199	N/A	57979	11595.80	108m
87-11-12	31	71	0	-7	-59	-47	-85	N/A	12964	2592.80	51m

Table 4.4 Estimation of the RMSE for the GSE-s.s. model

Date	Average Observed mixing height	Average Calculated mixing height	$\Delta z_i = z_{i(observed)} - z_{i(calculated)}$						RMSE		
			1	2	3	4	5	6	A	B	C
74-11-22	22	76	0	-37	-58	-121	N/A	N/A	19374	4843.5	70m
74-11-23	31	72	0	-27	-35	-100	N/A	N/A	11954	2988.5	55m
74-11-27	73	76	0	-22	-46	-14	-33	97	13294	2215.67	47m
87-11-02	40	136	0	-40	-75	-113	-97	-253	93412	15568.67	125m
87-11-03	33	44	0	-17	-1	-28	-5	N/A	1099	219.8	15m
87-11-06	107	26	0	-7	63	135	214	N/A	68039	13607.80	117m
87-11-12	31	59	0	-15	-56	-31	-38	N/A	5766	1153.2	34m

With the "kink" method the mixing height was determined up to the point where a "significant" stable layer is established (Myrick, 1987). By "significant" stable layer is meant the layer with a potential gradient greater than 0.5deg/100m by at least 0.2deg/100m. The Holzworth method described in Chapter1 was used, where it was feasible, to determine the morning and afternoon mixing heights. Table 4.5 demonstrates a good correlation between the capping inversion method, the "kink" method and the "30m dry adiabat" method I used.

Table 4.5 Average observed mixing heights estimated by the indicated methods

Date	Holzworth method	Capping inversion	Kink method	30m Dry adiabat	Encroach ment	GSE-s.s.
74-11-22	N/A	30m	19m ,	22m	74m	76m
74-11-23	N/A	66m	31m	31m	98m	72m
74-11-27	N/A	120m	47m	73m	95m	76m
87-10-02	45-315	18m	18m	40m	157m	136m
87-10-03	N/A-135	33m	28m	33m	55m	44m
87-10-06	160-2142	87m	58m	107m	32m	26m
87-10-12	N/A-90	27m	27m	31m	71m	59m

If we attempt to consider only mixing heights greater than 50m, and if we exclude data collected on October 6,1987 when strong thermal advection occurred, we get an overall average of the observed mixing heights of 100m and an RMSE of 100m for the GSE-s.s. model (124m for the encroachment). Given that Anfossi's analytical solution gave good results up to heights of the order of 120m, we may expect the discrepancy

to increase noticeably above that height, something that the figures demonstrated.

5. Summary, Conclusions and Recommendations

Recent progress in the formulation of entrainment models for the morning erosion of nocturnal radiation inversions coupled with recent experimental support for Brunt's simplified model for the temperature profile in a nocturnal radiation inversion, led the author to try to combine these ideas into a model for the height of the mixed layer.

The model is applicable only after the time of minimum surface temperatures on mornings with well developed surface-based inversions. The model assumes that the inversion is purely the result of radiative heat loss from the earth's surface. In other words it was assumed that the skies were clear and that winds were light with no thermal advection. The analytical expression of Anfossi et al (1976) for the nocturnal temperature profile was used to describe the temperature profile of the stable layer during the onset of the convective activity.

Two simple models were employed:

1. The 'ENCROACHMENT' model, assuming no capping inversion ($\Delta\theta=0$).
2. The 'STEADY STATE GENERAL STRUCTURE ENTRAINMENT' model, assuming $\Delta\theta\neq0$, $\Delta h\neq0$ but constant.

Input for the models included the temperature difference between the maximum of the previous day and the morning minimum, current screen height temperatures during the day and the height of the nocturnal inversion at the

time of the minimum temperature. To evaluate the effectiveness of the models, we conducted a series of experiments. The temperature profiles of the lowest 1km were recorded by releasing minisondes into the atmosphere every 45 min. A sonic anemometer installed at 10m height failed to provide reliable data of the turbulent heat fluxes over the period of the experiments. The interface between the theodolite B (see Fig. 3.1) and the computer failed after the first experimental day and forced us to assume an average rate of rise of the minisonde of 3m/s, in order to determine the heights on the temperature records. The experiments lasted four days in early October from 0600MST to 1100MST. Efforts were made to comply with weather conditions comparable to those assumed by the theory, not always successfully.

Other supporting measurements were wind data at 10m height, relative humidity, wet bulb temperature and net and incoming radiation.

The data used were the relative temperatures and the inversion heights. The program estimating the mixing heights was very simple and employed the iteration method. Every mixing height was calculated starting from the initial minimum temperature and not based on the estimated mixing height during the previous release. The program halts the mixed layer growth when the inversion height is reached. Both models provided similar results. Both tended to overestimate the observed mixing heights. However, a

tendency to underestimate the observed mixing heights was found when cool air advection occurred. The similarity of the results, that is overestimates and increased discrepancy with time, may be explained by the fact that the two expressions are reduced to one when the value of the parameter G is 1. G is the ratio of the lapse rates of the stable layer aloft to that of the entrainment layer. Attempts were made to determine G from the temperature profiles. They indicated that G may become as small as 0.1 (sometimes even smaller), depending on the time and the lapse rate of the nocturnal inversion. However, the steady state model for $G<0.6$ implies a negative entrainment height Δh that cannot be justified. The model also appeared to be sensitive to the nocturnal inversion height which was one of the poorly calculated quantities. Ambiguities as to the appropriate radiative diffusivity and the weather conditions overnight existed. A very poor relation between the observed inversion height and that calculated by method (b) existed. The 1200Z radiosonde indicated lower inversion heights comparable to the ones calculated by methods (c) and (b) with a low value of K_R. The model appeared to be sensitive also to the temperature differences. Even the appearance of early morning frost may cause consumption of energy for evaporation and consequent delay of the mixing height growth. As a result the mixing heights would be overestimated.

Some possible reasons for the model's discrepancies are

summarized below:

1. Hour of observation. Early morning observations on October indicated that no mixing layer had developed. This also was confirmed with data taken by Alberta Environment from fall 1977 to fall 1983 (Myrick, 1987). This is because solar radiation cannot provide adequate heat at this hour of the day. Summer periods characterized by high temperatures and significant heat fluxes, should be more representative for our model.

2. Accuracy of temperature differences. In situ measurements of maximum and minimum temperature and their time of ocuurence are needed. These differences enter in the model as independent variables to determine the mixing and the inversion heights. The model incorporates the ratio of the temperature difference and the inversion height. Given that the temperature difference is of the order of 10 and the inversion height of the order of 100 it should not underestimate the importance of its accuracy because the other terms of the analytical expression are equally small. The current temperature measurement at the surface is most likely to be higher than the mean potential temperature of the mixed layer due to the development of the superadiabatic surface layer. Therefore the current surface temperature should contribute to the overestimate of the observed mixing height.

3. The G factor. The steady state model is of limited use. The ratio of the lapse rates in the stable and the

entrainment layer should be reflected more realistically. When the actual G value is small, i.e. a relatively strong lapse rate is present in the entrainment layer, the mixing height growth should be slow since large turbulent heat fluxes from below are needed for effective mixing given that the heat flux from aloft is relatively weak. When G is large the mixing height growth should be faster since the stable layer entrains more heat in the mixed layer and more effective mixing is accomplished. Then if we assume G greater than the actual, an overestimate of the mixing height occurs.

4. Inversion height. The inversion height is another factor for which the model is sensitive. The relation between the mixing height and the inversion height is not obvious from the analytical expression, which appears to be rather complicated. A change of the inversion height with time may have therefore positive or negative results. The fact that the inversion heights that were used were much larger than those estimated by the other methods and the fact that the models overestimated the observed mixing heights leads to the opinion that higher inversion heights enhance the discrepancy between observed and estimated mixing heights. An increase of the inversion height with time may provide better estimates for large mixing heights. Appropriate care should be taken to ensure that the inversion height is the result of radiational cooling with no remaining inversions from previous nights or from thermal advection.

The conclusions of this study are as follows:

(i) The minisonde is an excellent measuring system for this problem.

(ii) Temperatures can be directly applied to mixed height estimations. In situ measurements of the maximum and minimum temperatures should be accurately recorded as well as the weather conditions overnight.

(iii) The model is in its initial stage and needs refinement. However, it is very practical and may be used for quick estimates.

(iv) Given that Garrett(1981) has excluded observed mixing heights <400m from his tests "to remove marginal growth days from the analysis" leads me to the conclusion that the errors of this model are reasonable and the model may be more accurate in low heights which are important for trapping of pollutants.

(v)The General Structure Entrainment (steady state)model is more versatile and can be improved for more accurate estimates.

(vi) It is often very difficult to identify $\Delta\theta$ or Δh with confidence from the observed temperature profiles. The very large temperature gradients in the lower part of the inversions are sensitive to small temperature-height errors.

Factors addressed previously need to be understood for accurate mixing height estimations. Suggested future work to answer some of the problems encountered in this study are summarized below:

1.Inversion height. As mentioned previously the inversion height is very poorly estimated. The relation of the observed inversion heights and the estimated should be established as accurately as possible. Possible additional variables may be needed, e.g. vapor pressure.

2.Entrainment effects. The entrainment process has been discussed by numerous authors as a factor which affects mixing heights. The entrainment layer may represent up to 20% of the mixed-layer height. The unsteady-state General Structure Entrainment model should be explored for better estimates of mixing heights.

3.Temperature difference. Anfossi's assumption $T_{max}-T_{min}=\frac{R_N}{K_R\rho_a c_p(1-\mathrm{erfc}(1))}\cdot\frac{h_i}{\sqrt{\pi}}$ needs to be explored. Anfossi claimed inability to verify this relation as a result of lack of data. An attempt to verify this relation by using overnight net radiation values in the present study revealed discrepancies.

4.Surface temperature error. Systematic errors incorporated in the mixing height due to higher surface temperatures in the superadiabatic layer may contribute in inaccuracies of the model.

Bibliography

Anfossi D., P. Bacci, A. Longetto (1976) Forecasting of vertical temperature profiles in the atmosphere during nocturnal radiational inversions from air temperature trend at screen height, Quart. J. R. Met. Soc. 102: 173-180.

Aron R. (1983) Mixing height-an inconsistent indicator of potential air pollution concentrations, Atmospheric Environment 17: 2193-2197.

Ball F.K. (1960) Control of inversion height by surface heating, Quart. J. R. Met. Soc. 86: 483-494.

Betts A.K. (1973) Non-precipitating cumulus convection and its parameterization, Quart. J. R. Met. Soc. 99: 178-196.

Briggs G.A. (1969) Plume rise, U.S. Atomic Energy Commission, Critical Review Series,TID-25075, U.S. Department of Commerce, 81pp.

Brunt D. (1939) Physical and Dynamical Meteorology, Cambridge at the University Press, 428pp.

Brutsaert W. (1972) Radiation, evaporation and the maintenance of turbulence under stable conditions in the lower atmosphere, Boundary-Layer Meteorology 2: 309-325

Businger J.A. (1972) Remote Sensing of the Troposphere, ch.6, Editor V.E. Derr, U.S. Government Printing Office, Washington, D.C.

Carlslaw S.H. and J.C. Jaeger (1971) Conduction in Solids, 2nd Edition, Oxford at the Clarendon Press, 510pp.

Carson D.J. (1973) The development of a dry inversion-capped convectively unstable boundary layer, Quart. J. R. Met. Soc. 99: 450-467.

Carson D.J., F.B. Smith (1974) Thermodynamic model for the development of a convectively unstable boundary layer, Advances in Geophysics 18A: 111-124.

Chorley L.G., S.J. Caughey, C.J. Readings (1975) The development of the Atmospheric boundary layer: 3 case studies, Met. Magazine 104: 349-360.

Crease B.A., S.J. Caughey, D.T. Tribble (1977) Information on the thermal structure of the Atmospheric Boundary

Layer from acoustic sounding, Met. Magazine 106: 42-52.

Deardorff J.W. (1967) Empirical dependence of the eddy coefficient of heat upon stability above the lowest 50m, J.A.M. 6: 631-643.

Deardorff J.W. (1972b) Numerical investigation of neutral and unstable planetary boundary layers, J.A.S. 29: 91-115.

Deardorff J.W., G.E. Willis, D.K. Lilly (1974) Comment on the paper by A.K. Betts "non-precipitating cumulus convection and its parameterization", Q.J.R.M.S.100: 122-123.

Deardorff J.W. (1976) On the entrainment rate of a stratocumulus topped mixed layer, Q.J.R.M.S. 102: 563-582.

Deardorff J.W. (1979) Prediction of convective mixed layer entrainment for realistic capping inversion structure, J.A.S. 36: 424-436.

Deardorff J.W. (1980) Progress in understanding entrainment at the top of a mixed layer, Workshop on the Planetary Boundary Layer, Proceedings of workshop on the Planetary Boundary Layer, 14-18 Aug., 1978, American Meteorological Society.

Dobbins R. (1979) Atmospheric Motion and Air Pollution, J. Wiley & Son Inc., 323pp.

Elliot W.P. (1964) The height variation of vertical heat flux near the ground, Q.J.R.M.S., 90: 260-265.

Environment Canada Monthly Record, Meteorological Observations in Canada, November 1974.

Garrett A.J. (1981) Comparison of observed mixed layer depths to model estimates using observed temperatures and winds, and MOS Forecasts, J.A.M. 20: 1277-1283

Hanna S.R., G.A. Briggs, J.W. Deardorff, B.A. Egan, F.A. Gifford, F. Pasquill (1977) AMS Workshop on Stability Classification Schemes and σ curves, Bul. of A.M.S. 58: 1305-1309.

Hanna S.R., C.L. Burkhart, R.J. Paine (1980) Mixing height uncertainties, Workshop on the Planetary Boundary Layer, 14-18 August 1978, American Meteorological Society.

Hanna S.R., G.A. Briggs, R.P. Hosker,Jr. (1982) Handbook of Atmospheric Diffusion, U.S. Department of Energy, 102pp.

Hildebrand P.H., B. Ackerman (1984) Urban effects on the convective boundary layer, J.A.S. 41: 76-91

Holzworth G.C. (1967) Mixing depths, wind speeds and Air Pollution for selected locations in the United States, J.A.M. 6: 1039-1044.

Holzworth G.C. (1971) Meteorological Potential for Urban Air Pollution in the Contiguous U.S., in the Proceedings of the 2nd International Clean Air Congress, H.M. England and W.T. Berry, Editors, Academic Press, New York.

Holzworth G.C. (1972) Mixing Heights, Wind speeds and potential for Urban Air pollution throughout the contiguous United States, Office of Air Programs, Publication No AP-101, Environmemntal protection Agency, Research Triangle Park, N.C.

Houghton T. J. (1980) The Physics of Atmospheres, Cambridge University Press, 271pp.

Ingersoll L.R., O.J. Zebel, A.C. Ingersoll (1948) Heat conduction with Engineering and Geological Applications, Mc Graw Hill, New York, 278pp.

Kaimal J.C., J.C. Wyngaard, D.A. Haugen, O.R. Cote, Y. Izumi (1976) Turbulence structure in the convective boundary layer, J.A.S. 33: 2152-2169.

Lenschow D.H. (1970) Airplane measurements of planetary layer structures, J.A.M. 9: 874-884.

Lilly D.K. (1968) Models of cloud-topped mixed layers under a strong inversion, Q.J.R.M.S. 94: 292-309.

Mc Bean G.A. (1979) The Planetary Boundary Layer, WMO Technical Note 165, WMO-No 530, Secretarial of the World Meteorological Organization, Geneva, Switzerland.

Moulsley T.J., D.N. Asimakopoulos, R.S. Cole, B.A. Crease, S.J. Caughey (1981) Measurement of boundary layer structure parameter profiles by acoustic sounding and comparison with direct measurements, Q.J.R.M.S. 107: 203-230.

Myrick R. (1987) Mixing height Climatology of Edmonton, Alberta, Internal Memorandum,Alberta Environment.

Nieuwstadt F.T.M., H. van Dop (1980) (Editors) Atmospheric Turbulence and Air pollution Modelling, D. Reidel Publishing Co., Holland, 358pp.

Nieuwstadt F.T.M., H. Tennekes (1981) A rate equation for the nocturnal boundary layer height,

J.A.S. 38: 1418-1428.

Nieuwstadt F.T.M., (1984) Some aspects of the turbulent stable boundary layer, Boundary Layer Meteorology 30: 31-55.

Olson R. (1985) The climate of Edmonton, Climatological Studies #37, The Climate of Canadian Cities #2, Canadian Publishing Center, Supply and Services, Ottawa, Canada, Cat# En 57-7/37E.

Pasquill F., F.B. Smith (1983) Atmospheric Diffusion, 3rd edition 437pp., Ellis Horwood Ltd.

Plate E.J. (1971) Aerodynamic characteristics of atmospheric boundary layers, Critical Review Series, TID 25465, U.S. Atomic Energy Commission, U.S. Department of Commerce, 198pp.

Plate E.J. (1982) (Editor) Engineering Meteorology, Elsevier Scientific Publishing Co, 740pp.

Portelli R.V. (1977) Mixing heights, wind speeds and ventilation coefficients for Canada. Atmospheric Environment Service, Climatological Studies #31

Reddick H.W., F.H. Miller (1948) Advanced Mathematics for Engineers, John Wiley & Son Inc., 508pp.

Richter J.H., D.R. Jensen, V.R. Noonkester, T.G. Konrad, A. Arnold, J.R. rowland (1974) Clear Air Convection: A close look at its evolution and structures, Geophysical Research Letters 1-2: 173-176.

Sun Wen Yih, Chiao-Zien Chang (1986) Diffusion model for a convective layer. Part II: Plume released from a continuous point source, J. of Climate and Applied Meteorology25: 1454-1463.

Sutton O.G. (1953) Micrometeorology, Mc Graw Hill Co., Inc., London, 333pp.

Tennekes H., A.G.M. Driendonks (1980) Basic Entrainment equations for the atmospheric boundary layer, Bound. Layer Meteorology20: 515-527.

Tennekes H., J.L. Lumley (1972) A First course in Turbulence, M.I.T. Press, Cambridge, Mass., 300pp.

Turner J.S. (1973) Buoyancy effects in fluids, Cambridge, University Press, 367pp.

Whitaker S. (1976) Elementary Heat Transfer Analysis, Pergamon Press Inc., U.S.A., 369pp.

Zdunkowski W.G., F.G. Johnson (1965) Infrared flux divergence calculations with newly constructed radiation tables, J.A.M. 4: 371-377.

Appendix I

```
C     THIS PROGRAM COMPUTES THE MIXING HEIGHT DURING THE ENCRO-
C     ACHMENT STAGE.THE  NOCTURNAL INVERSION HEIGHT IS ESTIMA-
C     TED FROM THE TAYLOR'S FORMULA BY REPLACING THE DIFFUSI-
C     VITY BY THE RADIATIONAL DIFFUSIVITY. THE INITIAL NOCTUR-
C     NAL HEIGHT IS ESTIMATED FROM THE FIRST MINISONDE RELEASE
C     BEFORE SUNRISE. THIS FORMULA INVOLVES THE TIME AT WHICH
C     THE MINIMUM TEMPERATURE WAS REACHED tmin.:
C     NIH=SQRT(4*KR*(t-tmin));t IS THE CURRENT TIME OF TAKING
C     THE SURFACE TEMPERATURE.
C     N IS THE NUMBER OF DAYS.
C     M IS THE NUMBER OF SURFACE TEMPERATURES TAKEN AT DIFFERENT
C     TIMES t, WITH THETAO(I) BEING THE FIRST SURFACE TEMPERATURE
C     MEASURED AND THETAM(I,J) ALL THE SURFACE TEMPERATURES,
C     THETAO(I) INCLUDED. THE THETAM(I,J) CORRESPOND TO THE
C     AVERAGE TEMPERATURES OF THE MIXING LAYER WHEN THAT IS DE-
C     VELOPPED DURING THE MORNING HOURS.
C     THE MIXING HEIGHT IS DETERMINED BY ITERATION, FROM THE FOR-
C     MULA OF THETA(I,J) AND ZMX(I,J).
C     DELT(I) IS THE TEMPERATURE DIFFERENCE BETWEEN THE MAXIMUM
C     TEMPERATURE OF THE PREVIOUS DAY AND THE MINIMUM OF THE CUR-
C     RENT DAY.
C     CP IS THE SPECIFIC HEAT OF DRY AIR 1004 JOULE/KILOG.DEGREE
C     KR IS THE RADIATIONAL DIFFUSIVITY 1224 M2/HR , ACCORDING
C     TO ANFOSSI, OR 450 M2/HR, ACCORDING TO ELLERSLIE'S EXPE-
C     RIMENTAL DATA.
C     DENSA IS THE AIR DENSITY: 1.14Kg/M3
C     CONSTANTS AND ALL DIMENSIONAL VARIABLES ARE IN UNITS OF Kg.m.
C     Hr.Deg.
      READ(5,10)N
      REAL NIH(7,6),KR,NIHO(7)
      DIMENSION THETAO(7),THETAM(7,6),DELT(7),DTH(7,6),THETAH(7,6),
     #ZS(7,6),ZMX(7,6),DT(4,6)
   10 FORMAT(1X,I2)
      DZS=0.0001
C      KR=450
C      KR=1224
      KR=0

      DO 11 I=1,N
      READ(5,30)M,DELT(I),THETAO(I),NIHO(I)
   30 FORMAT(1X,I1,1X,F4.1,1X,F5.1,1X,F5.1)
      DO 77 J=1,M
      READ(5,40)THETAM(I,J),DT(I,J)
   40 FORMAT(1X,F5.1,1X,F4.1)
   77 CONTINUE
      DO 22 J=1,M
      ZS(I,J)=0.0
      NIH(I,J)=NIHO(I)+SQRT(4*KR*DT(I,J))
      DTH(I,J)=(THETAM(I,J)-THETAO(I))/NIH(I,J)
  111 THETAH(I,J)=0.0098*ZS(I,J)-(DELT(I)/NIH(I,J))*
     #(EXP(-ZS(I,J)*ZS(I,J))-1.7725*ZS(I,J)*ERFC(ZS(I,J))+
     #0.278*ZS(I,J)-1)
      IF(THETAH(I,J).GE.DTH(I,J))GO TO 15
      IF(ZS(I,J).GE.1.0) GO TO 15
      ZS(I,J)=ZS(I,J)+DZS
      GO TO 111
   15 ZMX(I,J)=ZS(I,J)*NIH(I,J)
   22 CONTINUE
      DO 44 J=1,M
      WRITE(4,20)I,J,ZMX(I,J),I,J,THETAH(I,J),I,J,DTH(I,J)
   20 FORMAT(' ','ZMX(',I1,',',I1,')=',F8.4,'    THETAH(',I1,',',I1,
     #')=',F8.4,'    DTH(',I1,',',I1,')=',F8.4)
   44 CONTINUE
   11 CONTINUE
      STOP
      END
```

Appendix II

```
C     THIS PROGRAM COMPUTES THE MIXING HEIGHT DURING THE EN-
C     TRAINMENT STAGE UNDER STAEDY STATE CONDITIONS.
C     THE  NOCTURNAL INVERSION HEIGHT IS ESTIMA-
C     TED FROM THE TAYLOR'S FORMULA BY REPLACING THE DIFFUSI-
C     VITY BY THE RADIATIONAL DIFFUSIVITY. THE INITIAL NOCTUR-
C     NAL HEIGHT IS ESTIMATED FROM THE FIRST MINISONDE RELEASE
C     BEFORE SUNRISE. THIS FORMULA INVOLVES THE TIME AT WHICH
C     THE MINIMUM TEMPERATURE WAS REACHED tmin.:
C     NIH=SQRT(4*KR*(t-tmin));t IS THE CURRENT TIME OF TAKING
C     THE SURFACE TEMPERATURE.
C     N IS THE NUMBER OF DAYS.
C     M IS THE NUMBER OF SURFACE TEMPERATURES TAKEN AT DIFFERENT
C     TIMES t, WITH THETAO(I) BEING THE FIRST SURFACE TEMPERATURE
C     MEASURED AND THETAM(I,J) ALL THE SURFACE TEMPERATURES,
C     THETAO(I) INCLUDED. THE THETAM(I,J) CORRESPOND TO THE
C     AVERAGE TEMPERATURES OF THE MIXING LAYER WHEN THAT IS DE-
C     VELOPPED DURING THE MORNING HOURS.
C     THE MIXING HEIGHT IS DETERMINED BY ITERATION, FROM THE FOR-
C     MULA OF THETA(I,J) AND ZMX(I,J).
C     DELT(I) IS THE TEMPERATURE DIFFERENCE BETWEEN THE MAXIMUM
C     TEMPERATURE OF THE PREVIOUS DAY AND THE MINIMUM OF THE CUR-
C     RENT DAY.
C     CP IS THE SPECIFIC HEAT OF DRY AIR 1004 JOULE/KILOG.DEGREE
C     KR IS THE RADIATIONAL DIFFUSIVITY 1224 M2/HR , ACCORDING
C     TO ANFOSSI, OR 450 M2/HR, ACCORDING TO ELLERSLIE'S EXPE-
C     RIMENTAL DATA.
C     DENSA IS THE AIR DENSITY: 1.14Kg/M3
C     CONSTANTS AND ALL DIMENSIONAL VARIABLES ARE IN UNITS OF Kg,m,
C     Hr,Deg.
      READ(5,10)N
      REAL NIH(7,6),KR,NIHO(7)
      DIMENSION THETAO(7),THETAM(7,6),DELT(7),DTH(7,6),THETAH(7,6),
     #ZS(7,6),ZMX(7,6),DT(7,6)
   10 FORMAT(1X,I2)
C     G=0.20
C     G=0.40
C     G=0.60
C     G=0.80
C     G=0.85
C     G=0.90
C     G=0.98
C     G=1.00
C     G=1.20
C     G=1.40
      G=1.50
      Y=0.55*EXP(-0.27*G)
      YG=Y/(G+Y-1)
      GY=(1-G)/(G*(G+Y-1))
      DZS=0.0001
C      KR=450
C      KR=1224
      KR=0
      DO 11 I=1,N
      READ(5,30)M,DELT(I),THETAO(I),NIHO(I)
   30 FORMAT(1X,I1,1X,F4.1,1X,F5.1,1X,F5.1)
      DO 77 J=1,M
      READ(5,40)THETAM(I,J),DT(I,J)
   40 FORMAT(1X,F5.1,1X,F4.1)
   77 CONTINUE
      DO 22 J=1,M
```

(cont'd)

```
      ZS(I,J)=0.0
      NIH(I,J)=NIHO(I)+SQRT(4*KR*DT(I,J))
      DTH(I,J)=(THETAM(I,J)-THETAO(I))/NIH(I,J)
111   THETAH(I,J)=0.0098*(YG-GY)*ZS(I,J)-
     #(DELT(I)/NIH(I,J))*(EXP(-(YG*ZS(I,J))**2)-1.7725*(YG-GY)*
     #ZS(I,J)*ERFC(YG*ZS(I,J))+0.278*(YG-GY)*ZS(I,J)-1)
      IF(THETAH(I,J).GE.DTH(I,J))GO TO 15
      IF(ZS(I,J).GE.1.0)GO TO 15
      ZS(I,J)=ZS(I,J)+DZS
      GO TO 111
   15 ZMX(I,J)=ZS(I,J)*NIH(I,J)
   22 CONTINUE
      DO 44 J=1,M
      WRITE(4,20)I,J,ZMX(I,J),I,J,THETAH(I,J),I,J,DTH(I,J)
   20 FORMAT(' ','ZMX(',I1,',',I1,')=',F8.4,'    THETAH(',I1,',',I1,
     #')=',F8.4,'    DTH(',I1,',',I1,')=',F8.4)
C     WRITE(4,20)I,J,ZMX(I,J),THETA,DT
C  20 FORMAT(' ','ZMX(',I1,',',I1,')=',F8.4,'    THETA=',F8.4,
C     #'    DT=',F8.4)
   44 CONTINUE
   11 CONTINUE
      STOP
      END
```